QCD Parton Fragmentation in Vacuum and Medium with Leading Jet Energy-Loss

Master Thesis in Theoretical Atomic, Nuclear and Particle Physics

by

Kristoffer Skjelanger

June 2022

Department of Physics and Technology

University of Bergen

Abstract

Jets are created in the aftermath of relativistic heavy-ion collisions. While the fragmentation of jets in proton-proton collisions is well known, there is still a lot to learn about jet fragmentation in heavy-ion collisions. Usually, one studies the inclusive fragmentation properties of the shower. However, studying the properties of the leading (or most energetic) particle in the jet might bring a deeper understanding of jet-quenching and the properties of the quark-gluon plasma.

The motivation for the thesis is to investigate the leading parton distribution and describe it analytically. The analytical formalism of the inclusive distribution is presented, for both vacuum and medium, and the evolution equations are solved. In parallel, Monte-Carlo programs are developed for simulating parton showers in both vacuum and medium, and the results are compared with the analytical solutions.

The current formulation of leading parton energy-loss assumes soft radiation and is inaccurate for substantial energy-loss. It would therefore be interesting to formulate evolution equations for the leading parton. The proposed evolution equation is valid for on-branch gluons in vacuum and a solution is obtained in Mellin space.

Contents

Introduction

Shortly after The Big Bang, the universe consisted exclusively of fundamental particles in a primordial soup called quark-gluon plasma (QGP). Quarks and gluons would exist in this matter as free particles, not being bound by the strong nuclear force to form protons and neutrons. Colliders such as the Relativistic Heavy Ion Collider (RHIC) based at the Brookhaven National Laboratory and the Large Hadron Collider (LHC) at CERN, have allowed us to create quark-gluon plasma in the modern world. Heavy ions such as Au and Pb are accelerated to velocities approaching the speed of light and smashed together in relativistic heavy-ion collisions. In the aftermath of these collisions, the temperature and density is large enough for QGP to form, allowing us to model the first moments of the universe.

Measuring the properties of the quark-gluon plasma in colliders is exceedingly difficult. Not only does the QGP exist for just a brief moment ($10^{-24}s$), but how would one go ahead and measure something existing at the center of relativistic heavy-ion collisions? The answer is *jets*. Jets are collimated groups of hadrons generated by successive branchings of a highly energetic parton (quark or gluon), created in relativistic heavy-ion collisions. When this energetic parton traverses the quark-gluon plasma it interacts with the medium, affecting the distribution of final hadrons we observe in the detectors. Therefore, jets provide a way of probing the medium as we know the initial conditions, and can determine the medium impact by measuring the parton showers in the detector. An analogy can be made by considering a game of chess. Imagine you walk into an empty room with a chessboard in the middle of a game. Assuming we know how the pieces were set up at the start of the game, it should be possible to determine which moves were made to get the pieces to where they are now. The challenge is doing this thousands of times, while not being entirely sure what the rules of the game actually are.

This thesis is a study of how energetic partons, created in the aftermath of heavy-ion collisions, split or branch into pairs of new partons, with and without a background medium. Two different fragmentation scenarios will be considered. The first one is the inclusive parton distribution where we are interested in all of the partons accumulated throughout the branching process, such that the total energy is conserved. In the second scenario, we will focus on the leading parton, in which we follow the parton with the highest energy in each branching, and the other partons are considered a loss of energy from the leading parton.

Both an analytical perspective and a numerical perspective will be presented in this thesis. The former relies on known literature and published papers to formulate the current understanding of parton branching for vacuum and medium cascades. The evolution equations for both cascades will be presented, and the most important results will be recreated. The numerical perspective of the thesis is concentrated on developing Monte-Carlo programs which rely on randomly generated numbers, to create parton showers by iterating through the evolution equations. The distributions generated from these programs will be compared to the analytical results, and the properties of the two cascades will be discussed and highlighted using plots.

The thesis is structured in different chapters, with their own purpose. Chapter I is the *Fundamentals*, which will present the fundamental theory and concepts which should be known for truly understanding the content of the thesis. Its primary function is to revive old knowledge, and formal derivations will generally not be given. The first topic to be covered is the foun-

dations of quantum chromodynamics (QCD), which is the theory of the strong nuclear force. Following that, an introduction to jet evolution and jet observables will be given. Finally, we will introduce the most basic quantities of parton branching, which will be used throughout the thesis.

Chapter II is *Analytical*. Here all of the mathematics and formalisms of parton branchings will be discussed, focusing on the inclusive parton distribution. Beginning with parton branching in vacuum, where the DGLAP evolution equations will be presented, alongside the Sudakov form factor, and analytical solution. The same structure is given for parton branching in medium, where the evolution equations are the in-medium kinetic rate equations. The corresponding in-medium Sudakov form factors will also be introduced, and a solution to the evolution equations will be calculated.

Chapter III is *Numerical*. Here the analytical concepts will be used to creating a Monte-Carlo program for simulating parton showers. For vacuum we will be simulating cascades consisting exclusively of gluons, and cascades consisting of both quarks and gluons. When simulating medium cascades, we will be working exclusively with gluons. The results of these programs are then plotted alongside the analytical solutions, and used to discuss and highlight the properties of the different cascades. Chapter II and Chapter III will therefore complement each other.

Chapter IV, *Leading Parton and Energy-Loss*, is dedicated to the leading parton formalism. While the inclusive parton distribution is well known, there is still a lot to learn about the leading parton distribution. The key concepts and obstacles will be presented using current models for the energy-loss. We will then determine how often the leading parton remains on-branch, and will also formulate a new set of evolution equations for the leading parton and attempt to solve them.

The results we are looking for in Chapter IV might be an important step in understanding the leading parton distribution and its energy-loss. A deeper understanding of the leading parton distribution could refine current studies of jet quenching in heavy-ion collisions, and develop new observables sensitive to the properties of QCD.

Chapter I

Fundamentals

This chapter will cover the different topics required for understanding the analytical and numerical aspects of our parton shower formalism. Most of the results given in this chapter will be quoted from known texts, and formal derivations will generally not be recreated. The topics to be covered are quantum chromodynamics, jets, and kinematics of parton branchings. The first of these is a purely theoretical framework for the strong nuclear force, while the second will explore the concepts of jets. Kinematics of parton branchings will be focusing on the mathematics of simple parton branching in vacuum, and will be important when implementing them into Monte-Carlo programs.

Natural units are used throughout the thesis such that $\hbar = c = 1$.

1 Quantum Chromodynamics

Quantum chromodynamics (QCD) is the theory describing the strong interaction, one of the four fundamental forces in nature. It is a quantum field theory and a part of the famous standard model.

Historically there were several problems QCD tried to address. Among them was the ratio of the hadronic cross section to the muon-pair cross section produced by e^+e^- interactions

$$R = \frac{\sigma(e^+e^- \to \text{hadrons})}{\sigma(e^+e^- \to \mu^+\mu^-)} \tag{1.1}$$

which was off by a factor three in the calculation. Another issue yet to be addressed was the existence of the Ω^- particle, consisting of three strange quarks, giving it a symmetrical wavefunction which violates the Pauli principle. It was also unclear at the time why members of the triplet representations of the SU(3) group, with fractional charges ($\frac{2}{3}$ and $-\frac{1}{3}$), were unobserved in experiments [1].

The addition of the color degree of freedom resolved all of these challenges. By allowing three different colors, the R ratio gained a factor of three. The Ω^- could now have an anti-symmetric wavefunction as there was now another quantum number with three different values. The elusive fractionally charged hadrons were also accounted for by assuming that hadrons can only form as colorless states. This will be further explored in the section on confinement. As the name implies, quantum chromodynamics is the theory of color charges, and we will see that it is aptly named.

This section begins by exploring the basics of QCD. Covering how casimirs (color factors) originate from the generators of the SU(3) group, and giving a short overview of the Lagrangian and the first-order Feynman diagrams. Following that, a discussion on confinement will be given. Finally the concept of the running coupling, or asymptotic freedom, which defines how the strength of the strong interactions changes with scale and distance, will be introduced.

1.1 The basics of QCD

Group theory

Formally quantum chromodynamics is a non-abelian gauge theory described by the SU(3) symmetry, which is a Lie group. The generators of the group are defined from the traceless hermitian Gell-Mann matrices λ_a defined as

$$\begin{aligned}
\lambda_1 &= \begin{pmatrix} 0 & 1 & 0 \\ 1 & 0 & 0 \\ 0 & 0 & 0 \end{pmatrix} \quad , \quad \lambda_2 = \begin{pmatrix} 0 & -i & 0 \\ i & 0 & 0 \\ 0 & 0 & 0 \end{pmatrix} \quad , \quad \lambda_3 = \begin{pmatrix} 1 & 0 & 0 \\ 0 & -1 & 0 \\ 0 & 0 & 0 \end{pmatrix}, \\
\lambda_4 &= \begin{pmatrix} 0 & 0 & 1 \\ 0 & 0 & 0 \\ 1 & 0 & 0 \end{pmatrix} \quad , \quad \lambda_5 = \begin{pmatrix} 0 & 0 & -i \\ 0 & 0 & 0 \\ i & 0 & 0 \end{pmatrix} \quad , \\
\lambda_6 &= \begin{pmatrix} 0 & 0 & 0 \\ 0 & 0 & 1 \\ 0 & 1 & 0 \end{pmatrix} \quad , \quad \lambda_7 = \begin{pmatrix} 0 & 0 & 0 \\ 0 & 0 & -i \\ 0 & i & 0 \end{pmatrix} \quad , \quad \lambda_8 = \begin{pmatrix} 1 & 0 & 0 \\ 0 & 1 & 0 \\ 0 & 0 & -2 \end{pmatrix} \frac{1}{\sqrt{3}}.
\end{aligned} \tag{1.2}$$

The generators T^a of QCD satisfy the Lie Algebra of the SU(3) group $\left[T^a, T^b\right] = i\, f^{abc}\, T^c$. Where f^{abc} is the *structure constants*. Physicists generally normalize the structure constants as $\sum_{c,d} f^{acd}\, f^{bcd} = N\delta^{ab}$, where N is the number of colors. The normalization of the generators follows naturally as [2, p.485],

$$T^a = \frac{1}{2}\,\lambda_a \quad , \qquad (a = 1, 2, \cdots, 8). \tag{1.3}$$

The generators are also called *color operators* as they act on the color wavefunctions χ^c. For a single quark the wavefunction is written as a product of the space/spin wavefunction ψ, and the color wavefunction χ^c represented by the color spinors,

$$r = \begin{pmatrix} 1 \\ 0 \\ 0 \end{pmatrix} \quad , \quad g = \begin{pmatrix} 0 \\ 1 \\ 0 \end{pmatrix} \quad , \quad b = \begin{pmatrix} 0 \\ 0 \\ 1 \end{pmatrix}. \tag{1.4}$$

When examining the color operators it can be noted that only two of them commute, T^3 and T^8. The color states $\chi^c = a, b, c$ are therefore eigenstates of both these operators and do not change if acted on by T^3 or T^8. The remainder of the color operators are non-diagonal and can therefore change color states, which means that the interaction can annihilate quarks of one color, and create quarks of a different color. It is therefore implied, by conservation of color, that gluons must have non-zero color charges, and therefore be able to self-interact.

The color operators will inevitably allow us to introduce eight real gauge fields $\mathbf{A}^\mu = A^{\mu a}\,\lambda^a$, where $a = (1, 2, \cdots, 8)$, which corresponds to the octet of vector gauge bosons - the eight gluon fields.

The generators as presented here define the fundamental representation of the SU(3) group, meaning that it is the smallest non-trivial representation of the algebra. It is the most important representation, along with the adjoint representation described by $(T^a_{\text{adj}})^{bc} = -if^{abc}$. Different representations can be characterized in a basis-independent way using *casimirs*. The quadratic

casimir of a representation R is defined, $T_R^a T_R^a = C_2(R)\mathbf{1}$. For evaluating the quadratic casimir, it will be useful to define an inner product for the generators as $\text{tr}\left[T_R^a T_R^b\right] = T(R)\delta^{ab}$. The number $T(R)$ is then known as the index of the representation. For a given SU(N) group the index $T_R \equiv T(R)$ and quadratic casimir $C_R \equiv C_2(R)$ of a given representation R is then given by [2, p.484-489].

$$T_A = C_A = N \quad , \qquad T_F = \frac{1}{2} \quad , \qquad C_F = \frac{N^2-1}{2N}. \tag{1.5}$$

These quantities appear in almost every QCD calculation.

The QCD Lagrangian

Since QCD is a quantum field theory it has a *Lagrangian* which describes the free and interacting parts of the particle fields. We will not do any formal derivation, but will be motivating the relevant results given by standard textbooks. QCD is described by the Yang-Mills Lagrangian [3],

$$\mathcal{L}_{QCD} = \bar{\Psi}^f(x)\left[i\not{D} - m_f\delta_{ij}\right]\Psi^f(x) - \frac{1}{4}G_{i\mu\nu}(x)G_i^{\mu\nu}(x) \tag{1.6}$$

where $f = (1, \cdots, N_f)$ is a flavor index. The gluon term and covariant derivative is defined as

$$G_i^{\mu\nu}(x) = \partial^\nu A_i^\mu(x) - \partial^\mu A_i^\nu(x) + g_s f_{ijk} A_j^\mu(x) A_k^\nu(x) \tag{1.7}$$

$$D^\mu \Psi^f(x) = \left[\partial^\mu + i g_s \lambda_j A_j^\mu(x)/2\right]\Psi^f(x) \tag{1.8}$$

where $i, j = (1, 2, \cdots, 8)$. The gluon term corresponds to free gluons, with an additional interaction term for achieving gauge-invariance. The covariant derivative then ensures invariance under local phase transformations. The Lagrangian of Eqn. (1.6) is therefore gauge invariant, and not suitable for quantization as the path integral formulation gives no methods for selecting among equivalent solutions. This is resolved by the Faadeev-Popov method which fixes the choice of gauge by adding a gauge fixing term to the Lagrangian [4]. We will now explore two of the most common gauges, the *Feynman gauge*, and the *light-cone gauge*.

Feynman gauge

The first type of gauges we will examine are the covariant R_ξ gauges introduced by the gauge fixing

$$\mathcal{L}_{\text{gauge-fix}} = -\frac{1}{2\lambda}\left(\partial_\mu A_i^\mu(x)\right)^2. \tag{1.9}$$

These gauges preserve Lorentz invariance and give simpler calculations than non-covariant gauges. We will be working with the Feynman gauge, commonly used in field theory calculations, which is obtained by setting $\lambda = 1$ in the gauge fixing.

The consequence of choosing covariant gauges is that we are no longer guaranteed that only physical transverse modes of A_μ^a propagate, and we obtain additional kinetic terms which are ghost-like, giving us ghost fields $\eta_i(x)$. These fields correspond to unphysical spin-0 fermions which can only appear as virtual particles in loop corrections [2, 4]. Introducing the gauge-fixing

term of the Feynman gauge and resulting ghost fields gives the following Lagrangian

$$\begin{aligned}\mathcal{L}_{QCD} = \bar{\Psi}^f(x)\left[i\not{D} - m_f\right]\Psi^f(x) - \frac{1}{4}G_{i\mu\nu}(x)G_i^{\mu\nu}(x) \\ - \frac{1}{2\lambda}\left(\partial_\mu A_i^\mu(x)\right)^2 + \partial_\nu\eta_i(x)\left[\partial^\nu\tilde{\eta}_i(x) + g_s f_{ijk}\tilde{\eta}_j(x)A_k^\mu(x)\right].\end{aligned} \tag{1.10}$$

The gluon propagator in the Feynman gauge is given as

$$i\Pi^{\mu\nu ab}_{\text{feynman}} = \frac{-ig^{\mu\nu}}{p^2 + i\epsilon}\delta^{ab}. \tag{1.11}$$

The light-cone gauge

Turning to the light-cone gauge which is a type of axial gauge. Axial gauges violate Lorentz invariance, and makes it such that ghosts decouple from the physical particles, and can be ignored altogether. The gauge fixing of axial gauges is given by

$$\mathcal{L}_{\text{gauge-fix}} = -\frac{1}{2\lambda}\left(n_\mu A_i^\mu(x)\right)^2, \tag{1.12}$$

where n_μ is some vector. The light-cone gauge is then defined from $n^2 = 0$ and $\lambda = 0$, meaning that n_μ is light-like. The gluon propagator in the light-cone gauge is given as

$$i\Pi^{\mu\nu ab}_{\text{light-cone}} = \frac{i}{p^2 + i\epsilon}\left[-g^{\mu\nu} + \frac{n^\mu p^\nu + p^\mu n^\nu}{np}\right]\delta^{ab}. \tag{1.13}$$

There are only two physical polarizations in the light-cone gauge, those transverse to the $n - p$ plane. The numerator of the propagator is the polarization sum of transverse modes in a given basis, since there are only two propagating polarizations, we don't need ghosts to eliminate unphysical polarizations.

Axial gauges are not really useful unless there is some natural direction to choose. It is therefore very applicable in heavy-ion collisions, as we generally have an initial parton travelling in some direction which can define the vector n_μ.

Feynman diagrams

Since we are generally concerned with interactions it is possible to expand the terms of our Lagrangian in the Feynman gauge, Eqn. (1.10), and isolate the interaction parts of the Lagrangian for quarks, gluons, and ghosts, respectively as:

$$\mathcal{L}_{\mathcal{I}\,\text{quark}} = -\frac{1}{2}g_s\bar{\Psi}^f(x)\gamma_\mu\lambda_j\Psi^f(x)A_j^\mu(x) \tag{1.14}$$

$$\begin{aligned}\mathcal{L}_{\mathcal{I}\,\text{gluon}} = g_s f_{ijk}A_{i\mu}(x)A_{j\nu}(x)\partial^\mu A_k^\nu(x) \\ - \frac{1}{4}g_s^2 f_{ijk}f_{ilm}A_j^\mu(x)A_k^\nu(x)A_{l\mu}(x)A_{m\nu}(x)\end{aligned} \tag{1.15}$$

$$\mathcal{L}_{\mathcal{I}\,\text{ghost}} = g_s f_{ijk}(\partial_\mu\eta_i(x))\tilde{\eta}_j(x)A_k^\mu(x). \tag{1.16}$$

From these interaction-terms the famous Feynman diagrams can be obtained. Eqn. (1.14) gives us a single three-point vertex which gives rise to two diagrams (depending on how the contraction is done), with two quarks and one gluon in each. The diagrams are pictured in Figure 1.1. The

gluon contribution to the lagrangian gives us two different terms containing exclusively gluon fields, demonstrating the gluon self-interaction we expected from the color operators. The result is the three-gluon vertex and the four-gluon vertex as pictured in Figure 1.2. The ghost term also gives rise to a Feynman diagram, which we have not printed here, as it can only occur in virtual loops and can be completely neglected in the light-cone gauge.

Figure 1.1: Tree-level Feynman diagrams for the quark contributions in the QCD Lagrangian.

Figure 1.2: Tree-level Feynman diagrams for the gluon contributions in the QCD Lagrangian. Three-gluon vertex (left), and four gluon vertex (right).

These are all of the $\mathcal{O}(g)$ interactions of QCD. There are naturally higher-order diagrams and loop-corrections which may pose challenges when dealing with calculations, but for our purposes the first-order terms are sufficient. This allows us to disregard the four-gluon vertex in later sections as it is $\sim g^2$.

1.2 Confinement

Confinement is the phenomenon that particles with color charge does not exist as isolated particles under normal conditions of temperature and pressure. While it is not clear how it emerges from the Lagrangian of QCD, it remains an experimental fact - quarks and gluons are forced to be bound into color-neutral states called hadrons [5]. The simplest example is mesons which consist of a quark and an anti-quark of the same flavor which is a color-neutral state.

The familiar Coulomb potential of QED is attractive for opposite charges, and repulsive for similar charges. It would therefore be interesting to observe how the QCD potential behaves for $q\bar{q}$-pairs, of similar and different color charge. For large separations the potential increases linearly $V(r) \sim k\,r$, while at small separations a potential similar to the Coulomb will dominate. This calculated in [2, p.512-513], and the QCD potential can then be written as

$$\begin{aligned} V_{\mathrm{QCD}}(r) &= k\,r - \frac{4}{3}\frac{g_s^2}{4\pi r} \quad , \qquad \text{(color singlet)}, \\ V_{\mathrm{QCD}}(r) &= k\,r + \frac{1}{6}\frac{g_s^2}{4\pi r} \quad , \qquad \text{(color octet)}. \end{aligned} \tag{1.17}$$

The color singlet represents the potential for $q\bar{q}$-pairs of the same color charge and is the only one attractive at small separations. This is consistent with our expectations that quarks can

form color-neutral mesons. The color octet, which gives all combinations of $q\bar{q}$-pairs of different color charge, is however repulsive for all r, and mesons with a net color charge does not form.

An interesting part of confinement should become apparent when examining the potential between a $q\bar{q}$-pair of similar color charge. If we were to forcefully separate the quarks, the potential between them would eventually become large enough for it to be energetically favorable to form a new $q\bar{q}$-pair which then combine with the existing pair, giving us two mesons. This property is illustrated by the famous rubber band analogy in Figure 1.3.

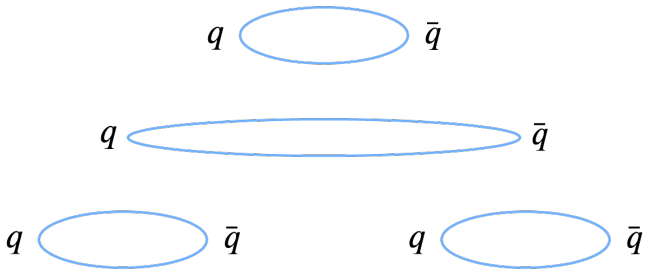

Figure 1.3: When the potential between a $q\bar{q}$-pair becomes too large, it is energetically favorable to create a new $q\bar{q}$-pair. This can be visualized as pulling a rubber band that instead of breaking, spontaneously turns into two new rubber bands.

1.3 The running coupling

Field theories such as QED and QCD, have a coupling constant describing the strength of a given interaction, relative to the free fields. For QED this is the fine-structure constant $\alpha \approx \frac{1}{137}$, which is proportional to the squared electric charge e^2, which we can intuitively associate with how strongly an electrically charged particle interacts with an electric field. The same goes for QCD, where the coupling constant g_s only appears in the interaction-parts of the Lagrangian. higher-order interactions scale with orders of the coupling constant, as is apparent in Eqn. (1.15) where the three-gluon vertex is scaled by g_s, and the four-gluon vertex is scaled by g_s^2.

The QCD Lagrangian given by Eqn. (1.6) contains the bare coupling constant g_s. This is only valid for tree-level in perturbation theory, and needs to be corrected by the method of *renormalization* to account for divergences appearing from higher-order loop corrections. Renormalization will allow us to replace the bare coupling constant with a renormalized coupling constant $g_r(\mu)$, where μ is an scale dependence appearing as a consequence of the renormalization procedure. It is customary to define this new coupling in analogy to the fine-structure constant such that $\alpha_s(\mu) = \frac{g_r^2}{4\pi}$, the new coupling can be written to leading order as

$$\alpha_s(\mu) = \frac{2\pi}{\beta_0 \ln\left(\mu^2/\Lambda_{\text{QCD}}^2\right)}. \tag{1.18}$$

In this coupling β_0 is the leading order expansion of the full β-*function*, which encodes how the coupling changes with scale. The β-function is therefore responsible for the running of the coupling constant. Λ_{QCD} is the scale at which the coupling constant becomes infinite, also called the Landau pole, and for QCD this scale is typically $\Lambda_{\text{QCD}} \sim 0.2$ GeV.

The importance of the running coupling in QCD is that $\alpha_s(\mu) \to 0$ as $\mu \to \infty$. This is known

as *asymptotic freedom*. For processes with a large momentum transfer $Q >> \Lambda_{\text{QCD}}$, such as high energy jets, the process can be described by perturbation theory. The uniqueness of the running coupling in QCD is that the β-function is negative, which gives rise to confinement [5].

1.4 Quark-gluon plasma

In our discussion on confinement we made an explicit statement that particles with color charge can not exist as isolated particles under "normal conditions of temperature and pressure". This naturally sparks the question of what happens under extreme conditions with high temperature and high pressure.

At increasing temperature and/or increasing baryonic chemical potential, a phase transition occurs such that hadrons no longer exist. The resulting matter consisting of free quarks and gluons is commonly called a *quark-gluon plasma* (QGP). While it is commonly called a plasma it is not always clear whether it should be interpreted as a weakly interacting gas or a strongly correlated system such as a fluid. The properties of the quark-gluon plasma is best illustrated using a phase diagram such as the one given in Figure 1.4.

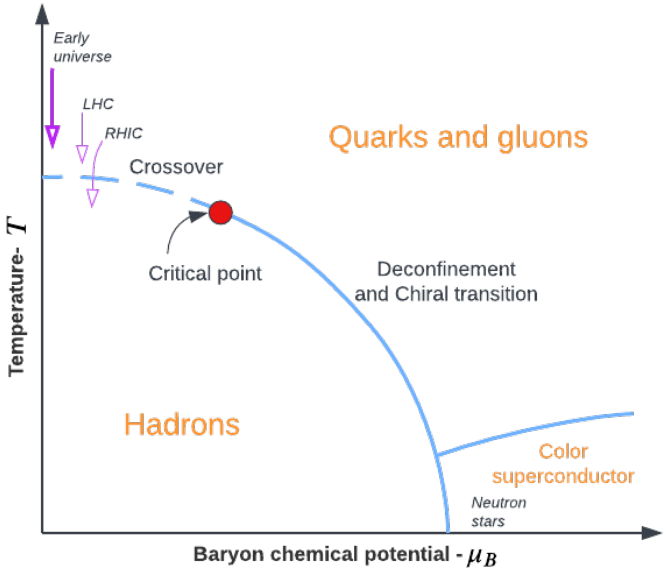

Figure 1.4: Diagram for the phase transition from hadronic matter to quark-gluon plasma. The transition from hadrons to QGP is split into a crossover section, and a phase transition (deconfinement).

There are several points of interest in this phase diagram. The most obvious feature is the phase transition between the hadron gas and the quark-gluon plasma, at finite μ_B, which is an important feature of QGP. However, at the same point, there is also a *chiral phase transition* happening. In short, chiral symmetry is broken in QCD, meaning that the theory acts differently on left and right-handed fields. This symmetry is restored for high pressure and/or temperature, and seemingly coincides with deconfinement when plotting the phase transitions in terms of the baryonic chemical potential. Another important feature is the *crossover*, at high temperature and low baryonic chemical potential, where there is no well defined phase transition and the

hadrons transform smoothly into a QGP, this is the region LHC operates at [6]. In the color superconducting phase the quarks are bound in Cooper pairs and form the SU(3) analogue of superconductivity [7].

Studying the QGP is difficult as it is incredibly short-lived and difficult to measure directly. The main method of probing the quark-gluon plasma is to observe how highly energetic partons interact with the plasma in the immediate aftermath of heavy-ion collisions ($Au + Au$), at colliders such as RHIC and LHC. These high-energy particles lead to *jets*.

2 Jets

A jet is a narrow cone of particles, produced by successive branchings of some initial parton created in the aftermath of particle collisions with extremely large momentum transfer, at colliders such as RHIC and LHC. The quarks and gluons created by parton branchings eventually hadronize and are observed in the detector as parton showers. The jets may propagate with or without a background medium. The former requires relativistic heavy-ion collisions, typically Pb or Au, while the latter may be created by e^+e^--collisions.

This section will discuss the properties of jets in both vacuum and medium, and the terminology associated with them. After that, we will introduce the observables relevant for this thesis.

2.1 Jets in vacuum

Starting with jets in vacuum. Since there is no background medium for the partons to interact with the picture is relatively simple, and we need only concern ourselves with basic parton branching.

Basic parton branching

Parton branching is simply the process of an energetic parton splitting into two new partons. This can happen via all of the basic QCD vertices (Figure 1.1 and Figure 1.2) and allows for the number of partons in a jet to increase, which eventually leads to the parton showers we observe in the detector. When addressing parton branching we will generally mean *soft* and *collinear* branching. In soft branching the emitted parton carry very little transverse momentum z, relative to the parent parton. Collinear branching is when the newly created parton travels in roughly the same direction as the branching parton, implying that the opening angle θ of the branching is very small. Soft and collinear branching will appear as divergences in the branching probability proportional to

$$\mathcal{P}_{\text{branching}} \sim \frac{\alpha_s}{\pi}\frac{d\theta}{\theta}\frac{dz}{z}. \tag{2.1}$$

This will be derived in Section 3. Here the momentum fraction is written as z as we are speaking of the outcome of a branching. When concerned with the final distribution when the shower has terminated, we will be replacing the z with an x. The soft divergence will then frequently be called the small x-limit.

Angular ordering

The parton showers evolving without a background medium will be angular ordered, meaning that any subsequent emission angle is smaller than the previous angle. For simple parton branchings, angular ordering can be obtained by considering the spatial separation of the daughter-partons of the branching.

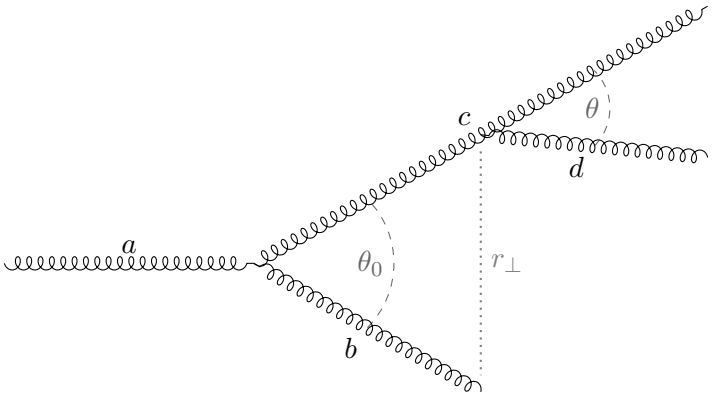

Figure 2.1: Illustration of the opening angles for successive parton branchings. The branching is said to be resolvable if the separation distance $r_\perp$ at the time t_f of the second branching is larger than the wavelength of the emitted gluon d.

Looking at Figure 2.1, we have noted the opening angle as θ_0 for the initial branching, and θ for the successive branching. If the secondary branching parton has a wavelength $\lambda \sim \frac{1}{k_\perp} \sim \frac{1}{\omega\theta}$, with formation time $t_f \sim \omega/k_\perp^2$, then the formation time can be written

$$t_f \sim \frac{\omega}{k_\perp^2} = \frac{1}{\omega\theta^2}. \tag{2.2}$$

The spatial separation of the partons from the initial branching can be given from the same formation time as $r_\perp \sim \theta_0\, t_f = \frac{\theta_0}{\omega\theta^2}$. Demanding that the wavelength λ of the branched parton d must be smaller than the separation distance $r_\perp$ we obtain

$$\begin{aligned} \lambda &< r_\perp \\ \frac{1}{\omega\theta} &< \frac{\theta_0}{\omega\theta^2} \\ \theta &< \theta_0. \end{aligned} \tag{2.3}$$

The criteria $\lambda < r_\perp$ leads us therefore to angular ordering. The reason we are able to impose this criterion originates from our desire to have *resolvable* branchings. This means that the branched parton d should be able to probe whether it branched from c, or from b. This is also called *coherent branching*. If the wavelength of d is too large, then it will not be able to distinguish b and c as individual partons, and it would instead branch from the sum of the color charges, which is equivalent to branching from a [8]. When we are constructing our Monte-Carlo program we will be using the angle θ as our ordering variable, meaning that we start from a large value of θ and branch our way down to smaller angles. Angular ordering follows therefore naturally from the choice of evolution variable.

Coherent branching also imply that color charge is conserved along the parton shower for the

same reasons - if the branching is resolvable each successive branching will conserve the net color charge.

2.2 Jets in medium

Jets traversing a background medium, typically QGP formed in the aftermath of heavy-ion collisions, bring along some more complex phenomena. Highly energetic partons interacting with the medium give rise to the phenomena of *induced gluon radiation*, *broadening*, and *quenching*. All of these properties will be discussed, but first, we must take a closer look at how relativistic heavy-ion collisions evolve.

Evolution of relativistic heavy-ion collisions

The different phases of relativistic heavy-ion collisions is given in Figure 2.2. The units of the diagram is $fm/c \sim 10^{-24}s$. The first stage of the evolution is the pre-equilibrium dynamics where partons (mostly gluons) are quickly freed by the collision, and then start to approach thermal equilibrium. This gives us an initial energy density around $1fm/c$ which is the basis for the quark-gluon plasma phase which evolves until around $10fm/c$. When the pressure and temperature become too small for deconfinement, hadrons are formed in a process called *hadronization*. The hadron gas is treated using relativistic hydrodynamics until it cools enough for the *freeze-out*, which finally leaves us with the free hadrons we can observe in our detector.

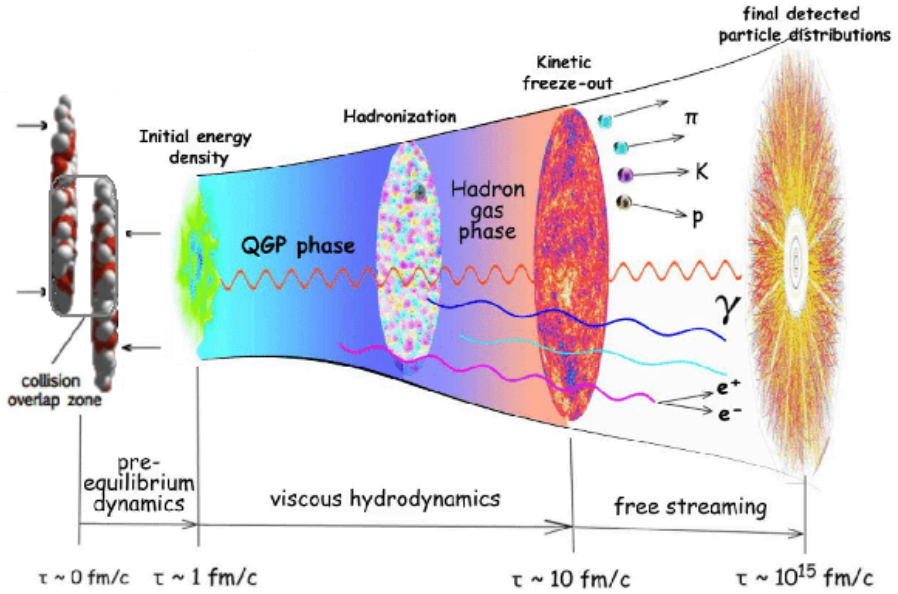

Figure 2.2: Illustration of the evolution of relativistic heavy-ion collisions. Evolution starts at the initial collision and continues until the hadronized particles reach the detector. The bottom axis gives the time scale of the evolution, units $fm/c \sim 10^{-24}s$, and the dynamics governing the system. This thesis concerns itself primarily with the QGP phase, evolving from the initial energy density to the hadronization. Figure from [9] but colors are inverted.

When discussing jets in medium, we are interested in the high-energy partons at the very start of the QGP phase, and how they interact with the medium. These will lead to hadronization and eventually the parton showers we observe in the detector, which will be quite different from the jets evolving without a medium.

Gluon radiation

Induced gluon radiation is very similar to the simple parton branchings discussed for vacuum cascades, but it is created by the jet interacting with the QGP and radiating soft gluons. These soft gluons are produced in abundance when jets move through a background medium. This happens via multiple collisions between the parton and the medium constituents, resulting in induced gluon radiation with a formation time of

$$t_f \sim \omega/k_\perp^2. \tag{2.4}$$

These soft gluons carry very little momentum, and are typically emitted at large angles - the softer the emission, the larger the emission angle. This leads to incoherent branchings, as the newly emitted partons will probe the net color charge. Color is therefore not necessarily conserved along the shower, and angular ordering is no longer the norm [10].

Jet broadening

Broadening takes place during the QGP phase of heavy-ion collisions. The concept is simply gluons exchanging transverse momentum with the medium, resulting in a broader transverse momentum distribution.

During the time-scale of soft gluon emissions, the gluon can experience multiple kicks and gain transverse momentum on the scale of $k_\perp^2 \sim \hat{q}\, t_f$. Here $\hat{q}$ is a diffusion coefficient, called the *jet-quenching parameter*, representing how the partons interact with the medium. ω is the energy of the radiated gluon, and $k_\perp$ is its transverse momentum relative to the parent gluon. If these kicks from the medium are the only source of transverse momentum then the formation time can be written in terms of the jet-quenching parameter

$$t_f = \sqrt{\frac{\omega}{\hat{q}}} \tag{2.5}$$

and can also be called the branching time. When the collisions are soft, and a large number of collisions is needed to change the transverse momentum by a significant amount, the diffusion approximation given by $\hat{q}$ is valid. The total transverse momentum $k_\perp$ gained by a high-energy parton traversing a medium of length L is therefore given From the definition of the diffusion coefficient as

$$\langle k_\perp^2 \rangle = \hat{q}\, L. \tag{2.6}$$

The jet-quenching parameter will generally be set to some constant, even though it is a function of momentum [11]. Quenching is understood as the suppression of high p_T hadrons due to energy-loss from the most energetic parton of a given jet, commonly known as the leading parton. This energy-loss is primarily caused by soft gluon radiation, which is induced by collisions with the medium [10]. The concepts of broadening and quenching are closely connected, and both are consequences of medium interactions.

2.3 Observables

This section will present different observables and quantities which will be particularly important for our treatment of parton showers. Before going into specific observables, it is necessary

to define the transverse momentum p_t of the initial parton in a given jet, by the transverse momentum it has in the lab frame p_T, such that $p_t \equiv p_T$.

The jet radius

The method of grouping different quarks and gluons into the same jet is defined by *jet algorithms*. A recombination algorithm can be made by grouping any quarks or gluons separated by a distance

$$\Delta_{ij}^2 = ((y_i - y_j)^2 + (\phi_i - \phi_j)^2) < R^2 \tag{2.7}$$

into a single jet. Here y_i and ϕ_i is the rapidity and azimuth of particle i, and R is the *jet radius*. The jet radius is not an observable for out showers, but it is an important quantity which must be defined for both numerical and analytical purposes [12].

The inclusive parton distribution

The observable we will encounter most frequently is the inclusive parton distribution. For a jet evolving according to an arbitrary evolution variable t, the inclusive parton distribution is given as

$$f_i(x,t) = \frac{dN_i}{dx} \tag{2.8}$$

where $i = (g, q, \bar{q})$ labels the species of the parton, and x is its transverse momentum relative to the initial parton. The inclusive parton distribution then gives us any partons within a given energy range, at a given time of the evolution, evolving according to some evolution variable. The choice of evolution variable is somewhat arbitrary, common choices are momentum $t = p_t^2$, scale $t \sim \ln \frac{Q^2}{Q_0^2}$, and angle $t \sim \ln \frac{\theta_{\max}^2}{\theta_{\min}^2}$. We will discuss the evolution variable at length in Chapter II.

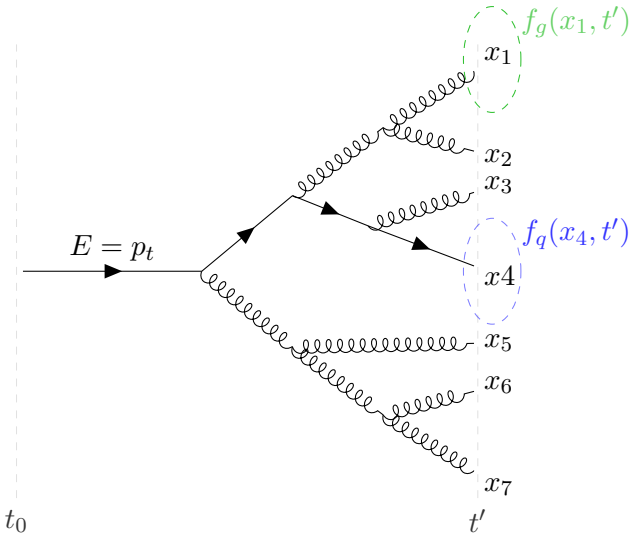

Figure 2.3: Illustration of the inclusive parton distribution $f_i(x,t)$ in a shower with both quarks and gluons, evolving according to an arbitrary evolution variable t. Since the inclusive distribution can give any of the relevant partons in a given energy range at give point t', we have highlighted $f_g(x_1, t')$ and $f_q(x_4, t')$.

The inclusive parton distribution $f_i(x,t)$ is described by the DGLAP evolution equations which will be introduced in Chapter II. Some of the properties of the inclusive distribution are

$$\int_0^1 dx\, f_i(x,t) = \langle N_i \rangle \tag{2.9}$$

$$\int_0^1 dx\, x\, f_i(x,t) = 1. \tag{2.10}$$

Eqn. (2.9) follows from the definition of the inclusive parton distribution, and tells us that the integral over all momentum values in the inclusive parton distribution yields the total number of partons. Since the inclusive distribution gives us the number of partons, it must conserve the total momentum as given by Eqn. (2.10) [13].

When we develop our Monte-Carlo shower program the outcome is a list of all final partons which makes it easy to find the number of particles in a given momentum interval $\frac{dN_i}{dx}$ and the energy density $x\frac{dN_i}{dx}$. The inclusive parton distribution is therefore ideal for comparing analytical and numerical results in our parton showers.

The leading parton distribution

The leading parton distribution $\mathcal{J}_i(x,t)$ contrasts the inclusive distribution as it only concerns itself with the parton with the highest momentum relative to the initial parton, at a given time of the evolution.

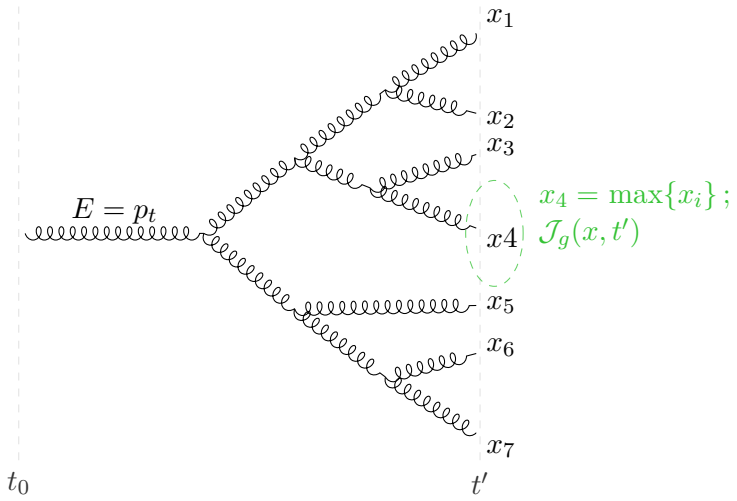

Figure 2.4: Illustration of the leading parton distribution, for a parton shower consisting exclusively of gluons, evolving according to an arbitrary evolution variable t. Here it is assumed that $x_4 = \max\{x_1, x_2, \cdots, x_7\}$ and the leading parton distribution $\mathcal{J}_g(x,t')$ is highlighted accordingly.

In contrast to the inclusive parton distribution, the leading parton distribution $\mathcal{J}(x,t)$ represents a well-defined object which has lost energy due to emissions. The sum rules for the leading

parton distribution are

$$\int_0^1 dx\, \mathcal{J}_i(x,t) = 1 \tag{2.11}$$

$$\int_0^1 dx\, x\, \mathcal{J}_i(x,t) = \langle x \rangle. \tag{2.12}$$

The number of partons is constant in the leading distribution, as can be seen from Eqn. (2.11), and the energy is not conserved as can be seen from Eqn. (2.12). Since we have an expression for the average energy contained in the leading parton, the energy-loss can be calculated from $\langle x_i \rangle_{\text{loss}} = 1 - \langle x_i \rangle$, this will be revisited in Chapter IV [13].

3 Kinematics of Parton Branching in Vacuum

Taking a step back from the concepts of QCD and jets, this section will discuss the actual kinematics of parton branchings in vacuum. Beginning by introducing the basic kinematic variables, before we explore the properties and origin of the Alterelli-Parisi splitting functions by considering the matrix-elements of the different QCD vertices. Finally we will take a look at the branching probability by considering the cross sections of a given process.

Rather than obtaining a precise result to some fixed order in perturbation theory, we will aim for an approximate result by considering the kinematics of parton branchings, which will be valid to all orders, allowing us to introduce a parton shower picture that can be easily implemented into Monte-Carlo programs.

3.1 Kinematic variables

Before doing any calculations the basic kinematic variables must be introduced. Restricting ourselves to the variables which will be used throughout the later sections. We start by considering the branching $a \to b, c$ under the assumption that $p_b^2, p_c^2 << p_a^2$. For now, we will be ordering our showers with respect to the initial parton energy $t \equiv p_a^2$. An illustration of a single branching is given in Figure 3.1.

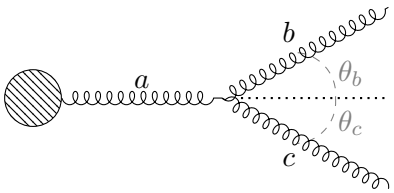

Figure 3.1: Branching of an outgoing gluon a from some initial blob, into two gluons b, c. The opening angle is given as $\theta = \theta_b + \theta_c$.

The opening angle is given as $\theta = \theta_b + \theta_c$, and the energy carried by the branched partons is given relative to the energy of the parent parton such that $E_b = z\, E_a$ and $E_c = (1-z)\, E_a$. The relationships between z and the different energies can therefore be written as

$$z = \frac{E_b}{E_a} = 1 - \frac{E_c}{E_a}. \tag{3.1}$$

Assuming most of our emissions are *collinear*, the opening angle θ is small, and we can use

the small-angle approximations $\cos\theta \approx 1 - \frac{\theta^2}{2}$ and $\sin\theta \approx \theta$. Conservation of four-momentum can be used to derive the following relationships between the kinetic variables - assuming the particles are massless:

$$\begin{aligned} p_a^2 &= 2E_b E_c(1-\cos\theta) \\ &= 2\frac{E_b}{E_a}\frac{E_c}{E_a}(1-\cos\theta)E_a^2 \\ &= z(1-z)E_a^2\theta^2 \end{aligned} \tag{3.2}$$

where the relationships in Eqn. (3.1) has been used to introduce $z(1-z)$. The transverse momentum of the partons in Figure 3.1 is

$$\begin{aligned} p_{b_\perp} &= |\mathbf{p}_b|\sin(\theta_b) = zE_a\sin(\theta_b) \\ p_{c_\perp} &= |\mathbf{p}_c|\sin(\theta_c) = (1-z)E_a\sin(\theta_c). \end{aligned} \tag{3.3}$$

Conservation of transverse momentum can then be used to give a relationship between the opening angle θ and z

$$\begin{aligned} z\,E_a\sin\theta_b &= (1-z)\,E_a\sin\theta_c \\ z\,\theta_b &= (1-z)\,\theta_c \\ \frac{\theta_b}{1-z} &= \frac{\theta_c}{z} = \theta. \end{aligned} \tag{3.4}$$

3.2 Altarelli-Parisi splitting functions

The Altarelli-Parisi splitting functions $P_{ba}(z)$ appear when evaluating the matrix elements of the basic QCD vertices[1]. They have a physical interpretation as the probability density of finding a parton b "inside" of parton a, with a particular momentum fraction z of the parent parton [14]. This distribution changes with the scale due to its dependence on α_s. The splitting functions are valid as long as the coupling constant is sufficiently small, which for QCD is fulfilled at large scales and in the collinear limit [15].

Now we will do a re-derivation of the $P_{gg}(z)$ splitting function by identifying the QCD vertex factors of the three-gluon vertex given in Figure 1.2, and then averaging over incoming and outgoing polarization. The method is outlined in [15, p.159-163]. When taking all the gluon momenta to be incoming, the matrix element $\mathcal{M}_{n+1}$ will be given by the initial matrix element, $\mathcal{M}_n$, the gluon propagator $\Pi^{\mu\nu}$, the vertex factor $V_{\alpha\beta\gamma}$, and the two final gluon polarization vectors $\epsilon_b^\beta \epsilon_c^\gamma$:

$$\mathcal{M}_{n+1} = \left(\epsilon_b^\beta \epsilon_c^\gamma\right)\left(g f_{\alpha\beta\gamma} V_{\alpha\beta\gamma}\right)\, i\Pi^{\mu\nu ij}\delta_{ij}|\mathcal{M}_n| \tag{3.5}$$

where α, β, γ are color indices. We will start by rewriting the gluon propagator in Feynman

[1] The notation for the splitting vertices is such that the first letter gives the parton type with momentum z after the splitting, and the second letter given the initial parton type. The branching $a \to b, c$ is therefore noted as ba.

gauge Eqn. (1.11), in terms of the gluon polarization states, with $p = p_a$,

$$\Pi^{\mu\nu}_{\text{feynman}} = \left(\sum_{\lambda} \epsilon^{\mu}_{\lambda}(p)\, \epsilon^{\nu *}_{\lambda}(p) \right) \frac{-i}{p_a^2 + i\epsilon}, \tag{3.6}$$

where we have neglected off-shell and logitudinal polarizations. One of these gluons will connect to the initial matrix element, while the other will be connected to the vertex element such that

$$\mathcal{M}_{n+1} = \sum_{\lambda} \left(\epsilon^{\alpha}_{a} \epsilon^{\beta}_{b} \epsilon^{\gamma}_{c} \right) \left(g f_{\alpha\beta\gamma} V_{\alpha\beta\gamma} \right) \frac{-i}{p_a^2 + i\epsilon} \left(\epsilon^{\nu *}_{\lambda} | \mathcal{M}_{n,\nu} | \right). \tag{3.7}$$

Squaring the matrix element, taking the limit $\epsilon \to 0$, and using $t = p_a^2$, we obtain the final expression for our vertex element

$$|\mathcal{M}_{n+1}|^2 \sim \frac{g^2}{t^2} C_A V^2_{\alpha\beta\gamma} |\mathcal{M}_n|^2. \tag{3.8}$$

Continuing lets take a closer look at $V_{\alpha\beta\gamma}$, which comes from the vertex factor. Since all momenta are incoming, we can use $p_a + p_b + p_c = 0$, and the condition $\epsilon_i \cdot p_i = 0$ to write

$$\begin{aligned} V_{\alpha\beta\gamma} &= (\epsilon^{\alpha}_{a} \epsilon^{\beta}_{b} g_{\alpha\beta})(\epsilon^{\gamma}_{c}(p_a - p_b)_{\gamma}) + (\epsilon^{\beta}_{b} \epsilon^{\gamma}_{c} g_{\beta\gamma})(\epsilon^{\alpha}_{a}(p_b - p_c)_{\alpha}) + (\epsilon^{\alpha}_{a} \epsilon^{\gamma}_{c} g_{\gamma\alpha})(\epsilon^{\beta}_{b}(p_c - p_a)_{\beta}) \\ &= (\epsilon_a \cdot \epsilon_b)(\epsilon^{\gamma}_{c}(-2p_b - p_c)_{\gamma}) + (\epsilon_b \cdot \epsilon_c)(\epsilon^{\alpha}_{a}(2p_b - p_a)_{\alpha}) + (\epsilon_a \cdot \epsilon_c)(\epsilon^{\beta}_{b}(2p_c - p_b)_{\beta}) \\ &= (\epsilon_a \cdot \epsilon_b)(\epsilon_c \cdot -2p_b) + (\epsilon_b \cdot \epsilon_c)(\epsilon_a \cdot 2p_b) + (\epsilon_a \cdot \epsilon_c)(\epsilon_b \cdot 2p_c) \\ &= -2\left((\epsilon_a \cdot \epsilon_b)(\epsilon_c \cdot p_b) - (\epsilon_b \cdot \epsilon_c)(\epsilon_a \cdot p_b) - (\epsilon_a \cdot \epsilon_c)(\epsilon_b \cdot p_c) \right). \end{aligned} \tag{3.9}$$

We will assume that the polarization vectors of the gluons are purely transverse, either as plane polarization states in the plane of branching ϵ^{in}_i, or normal to the plane of branching ϵ^{out}_i. We can therefore write down the following criteria for the gluon polarizations:

$$\begin{aligned} \epsilon^{\text{in}}_i \cdot \epsilon^{\text{in}}_j &= \epsilon^{\text{out}}_i \cdot \epsilon^{\text{out}}_j = -1 \\ \epsilon^{\text{in}}_i \cdot \epsilon^{\text{out}}_j &= \epsilon^{\text{out}}_i \cdot \ p_j \ = 0. \end{aligned} \tag{3.10}$$

Now we need to relate the individual gluon polarization to the individual gluon momenta, as required by Eqn. (3.9), writing

$$\begin{aligned} p_b &= (E_b, E_b \sin\theta_b, 0, -E_b \cos\theta_b) \\ p_c &= (E_c, E_c \sin\theta_c, 0, E_c \cos\theta_c). \end{aligned} \tag{3.11}$$

From the condition $\epsilon_i \cdot p_i = 0$ we can show that $\epsilon_0 = \epsilon_i$, and the individual polarizations can be written as

$$\begin{aligned} \epsilon^{\text{in}}_a &= (0, 1, 0, 0) \\ \epsilon^{\text{in}}_b &= (0, \cos\theta_b, 0, \sin\theta_b) \\ \epsilon^{\text{in}}_c &= (0, \cos\theta_c, 0, \sin\theta_c). \end{aligned} \tag{3.12}$$

Now we will combine the results in Eqn. (3.11) and Eqn. (3.12) to determine the relations between gluon momenta and polarization, in the small-angle approximation where $\sin\theta \approx \theta$

and $\theta^2 \approx 0$, we obtain the following identities:

$$\begin{aligned}
\epsilon_a^{\text{in}} \cdot p_b &= -E_b \sin\theta_b \\
&\approx -E_b\theta_b \\
\epsilon_b^{\text{in}} \cdot p_c &= E_c \sin\theta_c \cos\theta_b + E_c \sin\theta_b \cos\theta_c \\
&\approx E_c\theta \\
\epsilon_c^{\text{in}} \cdot p_b &= -E_b \sin\theta_b \cos\theta_c - E_b \sin\theta_c \cos\theta_b \\
&\approx -E_b\theta.
\end{aligned} \tag{3.13}$$

Rewriting these results by using the relations given by Eqn. (3.1) and Eqn. (3.4), we obtain our final relations between the polarization and momenta

$$\begin{aligned}
\epsilon_a^{\text{in}} \cdot p_b &= -z(1-z)\, E_a\theta \\
\epsilon_b^{\text{in}} \cdot p_c &= (1-z)\, E_a\theta \\
\epsilon_c^{\text{in}} \cdot p_b &= -z\, E_a\theta.
\end{aligned} \tag{3.14}$$

Now we will use Eqn. (3.10) and Eqn. (3.14) to determine the vertex factor from Eqn. (3.9) for different polarizations

$$\begin{aligned}
V_{\epsilon_a^{\text{in}}\epsilon_b^{\text{in}}\epsilon_c^{\text{in}}} &= -2\left[(\epsilon_a^{\text{in}} \cdot \epsilon_b^{\text{in}})(\epsilon_c^{\text{in}} \cdot p_b) - (\epsilon_b^{\text{in}} \cdot \epsilon_c^{\text{in}})(\epsilon_a^{\text{in}} \cdot p_b) - (\epsilon_a^{\text{in}} \cdot \epsilon_c^{\text{in}})(\epsilon_b^{\text{in}} \cdot p_c)\right] \\
&= -2\left[(-1)(-z\, E_a\theta) - (-1)(-z(1-z)\, E_a\theta) - (-1)((1-z)\, E_a\theta)\right] \\
&= -2\left[z - (z(1-z)) + (1-z))\right]\, E_a\theta \\
&= -2\left[(z-1)z + 1\right]\, E_a\theta.
\end{aligned} \tag{3.15}$$

The square of $V_{\alpha\beta\gamma}$ is

$$V^2_{\epsilon_a^{\text{in}}\epsilon_b^{\text{in}}\epsilon_c^{\text{in}}} = 4t\left(\frac{1-z}{z} + \frac{z}{(1-z)} + z(1-z)\right) = 4t\, F(z;\epsilon_a,\epsilon_b,\epsilon_c) \tag{3.16}$$

and can be inserted into Eqn. (3.8) to obtain the final expression of our matrix element

$$|\mathcal{M}_{n+1}|^2 \sim \frac{4g^2}{t} C_A F(z;\epsilon_a,\epsilon_b,\epsilon_c)|\mathcal{M}_n|^2. \tag{3.17}$$

The function $F(z;\epsilon_a,\epsilon_b,\epsilon_c)$ contains the information unique for this particular vertex, and is therefore all that is required for determining the splitting function. The allowed polarizations are given in Table 3.1 [15].

ϵ_a	ϵ_b	ϵ_c	$F(z;\epsilon_a,\epsilon_b,\epsilon_c)$
in	in	in	$\frac{1-z}{z} + \frac{z}{(1-z)} + z(1-z)$
in	out	out	$z(1-z)$
out	in	out	$\frac{1-z}{z}$
out	out	in	$\frac{z}{(1-z)}$

Table 3.1: Polarization dependence of the $g \to gg$-branching.

Now averaging over initial ϵ_a, and summing over final states ϵ_b, ϵ_c, using the values given in Table 3.1,

$$\begin{aligned}\langle F\rangle &= \frac{(\epsilon_a^{\text{in}}\Sigma\epsilon_b\epsilon_c) + (\epsilon_a^{\text{out}}\Sigma\epsilon_b\epsilon_c)}{2} \\ &= \frac{1}{2}\left(\{\frac{1-z}{z} + \frac{z}{1-z} + z(1-z)\} + \{z(1-z)\}\right) + \frac{1}{2}\left(\{\frac{1-z}{z}\} + \{\frac{z}{1-z}\}\right)\} \\ &= \left(\frac{1-z}{z} + \frac{z}{1-z} + z(1-z)\right) \end{aligned} \tag{3.18}$$

the only remaining part is to define the $P_{gg}(z)$ splitting function[2] as

$$P_{gg}(z) = C_A\langle F\rangle = C_A\left[\frac{1-z}{z} + \frac{z}{1-z} + z(1-z)\right]. \tag{3.19}$$

There are some small enchantments for the matrix element for soft gluon emission in the plane of branching, but we will be using Eqn. (3.19) this precision is sufficient for our purposes [15].

The derivation for the qg and qq splitting functions follow the same procedure, so we will merely quote the results here, and leave the full derivation as an exercise for the interested reader. They are given respectively by Eqn. (3.20) and Eqn. (3.21). The gq splitting function is perfectly symmetrical to the qq splitting function and can be disregarded in our numerical treatments, but for completeness it is given here in Eqn. (3.22).

$$P_{qg}(z) = n_f T_R\left[z^2 + (1-z)^2\right] \tag{3.20}$$

$$P_{qq}(z) = C_F\frac{1+z^2}{1-z} \tag{3.21}$$

$$P_{gq}(z) = P_{qq}(1-z) = C_F\frac{1+(1-z)^2}{z} \tag{3.22}$$

In addition to the color factors, $C_A = 3$, $C_F = 4/3$, and $T_R = 1/2$, there is a factor n_f in the qg splitting function. This factor is the number of active quark flavors, and it represents the probability of a gluon emitting a $q\bar{q}$-pair with equal probability for all flavors $P_{q^ig} = P_{qg}$ We will be operating under the assumption that $n_f = 5$. Similarly, the probability of emitting a gg-pair from a quark is the same for all quark flavors $P_{gq^i} = P_{gq}$. Finally when a quark emits a gluon there is no flavor exchange, $P_{q^iq^j} = \delta_{ij}P_{qq}$. All of this is of course under the assumption that the quarks are massless [14].

3.3 Branching cross sections

The splitting functions give us a way of determining the z values in a given parton branching, but we do not have any foundation for knowing how often these branchings occur. This section will therefore explore the cross sections for the different splitting vertices. The cross section is a measure of the probability of how often a given process happens, so this will be important for developing our Monte-Carlo program. This will be done by following the process outlined in [15, p.164].

For time-like branchings, the cross section $d\sigma_n$ is given from the Matrix-element $\mathcal{M}_n$ of the

[2] Literature warning: Some of the literature includes factors 2 in the splitting functions, but we will make these explicit in the evolution equations.

vertex, initial-state flux factor $\mathcal{F}$, and final state phase space $d\Phi_n$:

$$d\sigma_n = \mathcal{F}|\mathcal{M}_n|^2 \, d\Phi_n. \tag{3.23}$$

When going from a state $d\Phi_n$ to $d\Phi_{n+1}$, which is a branching from one to two partons, the following replacement must be made

$$d\Phi_n = \cdots \frac{d^3\mathbf{p}_a}{2(2\pi)^3 E_a} \quad \Rightarrow \quad d\Phi_{n+1} = \cdots \frac{d^3\mathbf{p}_b}{2(2\pi)^3 E_b} \frac{d^3\mathbf{p}_c}{2(2\pi)^3 E_c}. \tag{3.24}$$

If p_b is fixed, then $d^3\mathbf{p}_c = d^3\mathbf{p}_a$. Using the kinematic relations already derived we can rewrite $d\Phi_{n+1}$ as

$$\begin{aligned} d\Phi_{n+1} &= \frac{d^3\mathbf{p}_b}{2(2\pi)^3 E_b} \frac{d^3\mathbf{p}_c}{2(2\pi)^3 E_c} \\ &= \frac{d^3\mathbf{p}_b}{2(2\pi)^3 E_b} \frac{d^3\mathbf{p}_a}{2(2\pi)^3 E_a} \frac{1}{1-z} \\ &= d\Phi_n \frac{1}{2(2\pi)^3} \frac{d^3\mathbf{p}_b}{E_b} \frac{1}{1-z} \end{aligned} \tag{3.25}$$

and integrate over $d^3\mathbf{p}_b$ by inserting $d^3\mathbf{p}_b = E_b^2 dE_b \, \sin(\theta_b) d\theta_b \, d\phi \approx E_b^2 dE_b \, \theta_b d\theta_b \, d\phi$

$$d\Phi_{n+1} = d\Phi_n \frac{1}{2(2\pi)^3} E_b dE_b \, \theta_b d\theta_b d\phi \frac{1}{1-z}. \tag{3.26}$$

We are however interested in performing a change of variable to write this in terms of $t = p_a^2$ and z, instead of θ_b and E_b. This is done by $dz = dE_b/E_a$, and $dt = 2E_b E_c \theta d\theta = 2E_b E_c \theta_b d\theta_b$ (by keeping θ_c constant)

$$\begin{aligned} d\Phi_{n+1} &= d\Phi_n \frac{1}{2(2\pi)^3} E_b dE_b \, \theta_b d\theta_b d\phi \frac{1}{1-z} \\ &= d\Phi_n \frac{1}{2(2\pi)^3} d\phi \, E_b E_a dz \frac{dt}{2E_b E_c} \frac{1}{1-z} \\ &= d\Phi_n \frac{1}{2(2\pi)^3} d\phi \, E_a dz \frac{dt}{2E_c} \frac{1}{1-z} \\ &= d\Phi_n \frac{1}{4(2\pi)^3} dt \, dz \, d\phi. \end{aligned} \tag{3.27}$$

Using the matrix element in Eqn. (3.17), and the phase space factor in Eqn. (3.27), we can write out the cross section $d\sigma_{n+1}$, relative to $d\sigma_n$ given in Eqn. (3.23),

$$\begin{aligned} d\sigma_{n+1} &= \mathcal{F} \, |\mathcal{M}_{n+1}|^2 \, d\Phi_{n+1} \\ &= \mathcal{F} \left(\frac{2g^2}{t} C_A F |\mathcal{M}_n|^2 \right) \left(d\Phi_n \frac{1}{4(2\pi)^3} \, dt \, dz \, d\phi \right) \\ &= d\sigma_n \left(\frac{g^2}{t} C_A F \right) \left(\frac{1}{2(2\pi)^3} \, dt \, dz \, d\phi \right) \\ &= d\sigma_n \frac{dt}{t} \, dz \, \frac{d\phi}{2\pi} \left(\frac{g^2}{2(2\pi)^2} \right) C_A F \end{aligned} \tag{3.28}$$

Writing the coupling in terms of $\alpha_s = g^2/4\pi$, inserting the splitting function $P_{gg}(z)$, and

integrating over the azimuth we obtain our result,

$$= d\sigma_n \, \frac{dt}{t} \, dz \, \frac{\alpha_s}{2\pi} P_{gg}(z). \tag{3.29}$$

This cross section can be thought of as the splitting probability. It is currently written in terms of the virtuality of the emitting particle $t \equiv p_a^2$. For our parton evolutions, we would rather write his probability in terms of the splitting angle θ. This change is straightforward to execute (at fixed z), as $\frac{dt}{t} = \frac{d\theta^2}{\theta^2} = \frac{2d\theta}{\theta}$. The cross section is therefore

$$d\sigma_{n+1} = d\sigma_n \, \frac{d\theta}{\theta} \, dz \, \frac{\alpha_s}{\pi} P_{gg}(z). \tag{3.30}$$

3.4 Multiplicity of emitted partons

The number of gluons emitted from some initial gluon with transverse momentum p_t can be determined from Eqn. (3.30) by integrating over z and θ, with a step function $\Theta(k_\perp - Q_0)$, where $k_\perp$ is the emitted gluon transverse momentum, in order to keep the branchings resolvable

$$N = \frac{\alpha_s}{\pi} \int_0^1 dz \, P_{gg}(z) \int_0^1 \frac{d\theta}{\theta} \, \Theta(k_\perp - Q_0). \tag{3.31}$$

In the the small x approximation we can write $P_{gg}(z) \sim \frac{2C_A}{z}$, and $k_\perp \sim z \, p_t \, \theta$. Absorbing the step-function into the integration limits by observing that $\theta > Q_0/(z \, p_t)$, and that $z > Q_0/(p_t R)$, we obtain

$$\begin{aligned} N &= \frac{2C_A\alpha_s}{\pi} \int_{Q_0/(p_t R)}^1 \frac{dz}{z} \int_{Q_0/(zp_t)}^1 \frac{d\theta}{\theta} \\ &= \frac{2C_A\alpha_s}{\pi} \int_{Q_0/(p_t R)}^1 \frac{dz}{z} \, \ln^2\left(\frac{zp_t R}{Q_0}\right) \\ &= \frac{2C_A\alpha_s}{\pi} \left[\frac{1}{2}\ln^2\left(\frac{zp_t R}{Q_0}\right)\right]_{Q_0/(p_t R)}^1 \\ &= \frac{2C_A\alpha_s}{\pi} \ln^2\left(\frac{p_t R}{Q_0}\right). \end{aligned} \tag{3.32}$$

Writing $Q = p_t \, R$, this becomes,

$$N \frac{2C_A\alpha_s}{\pi} \ln^2\left(\frac{Q}{Q_0}\right) \tag{3.33}$$

In the leading logarithmic approximation (LLA) we have

$$\alpha_s << 1 \quad , \qquad \alpha_s \, \ln^2\left(\frac{Q}{Q_0}\right) \sim 1 \tag{3.34}$$

then in LLA the multiplicity is $N_{\mathrm{LLA}} \sim 1$. For next-to-leading order expansions the multiplicity calculated becomes $N_{\mathrm{NLO}} > 1$ and we need *resummation* in order to account for the terms in the full perturbation series which are enhanced by large logarithms [5].

Results obtained by perturbation theory can be written as a power series $\left(\alpha_s(Q^2)\ln\left(Q^2/Q_0^2\right)\right)^n$, where Q_0 is some reference scale, introduced to make the observables infrared-and-collinear

(IRC) safe. IRC safe means that the divergences at both $x \to 0$ and $x \to 1$, related to soft and collinear emission respectively, are dealt with such that the observables can be calculated using perturbation theory. When $Q >> Q_0$, the perturbation series may not converge and an all-order resummation is required to account for the terms enhanced by large logarithms. The DGLAP equations, which will be presented shortly, is effectively a resummation of these higher-order terms [16].

Chapter II

Analytical

This chapter will investigate parton cascades in both vacuum and medium, from an analytical standpoint. Properties of the two cascades will be discussed and compared against one another, the evolution equations will be presented alongside the respective splitting functions, and finally we will find a solution to the evolution equations. The most interesting observable in this chapter is the inclusive parton distribution, initiated by a single quark or gluon in the aftermath of some collision.

4 Formalism of Parton Branching in Vacuum

This section will cover the analytical details related to parton showers in vacuum. Beginning by defining an evolution variable that will ensure angular ordering for our showers and simplify the DGLAP evolution equations. After an overview of the DGLAP equations, they will be rewritten in terms of a Sudakov form factor, which will be a key part of creating our parton shower programs. At the end of the chapter, a solution to the DGLAP equation will be presented.

4.1 Properties of vacuum cascades

Evolution variable

Before introducing the evolution equations, we will define an evolution variable in order to simplify the evolution equations, and impose angular ordering in our showers [12]. The cross section for branching from one to two partons was calculated in Eqn. (3.30), and it can be interpreted as a probability. With a fixed coupling $\alpha_s << 1$, the probability of branching can be written as

$$d\mathcal{P}_{1\to 2} = \frac{\alpha_s}{\pi}\frac{d\theta}{\theta}\,P(z)\,dz. \tag{4.1}$$

The probability of branching changes in a given volume element by

$$\frac{d\mathcal{P}}{d\theta dz} = \frac{\alpha_s}{\pi}\frac{1}{\theta}P(z). \tag{4.2}$$

Now we want to replace θ with an evolution variable in order to simplify Eqn. (4.2). This evolution variable will be used for all vacuum cascades from this point forward, and can be written as

$$t = \frac{\alpha_s}{\pi}\int_{\theta_{\min}}^{\theta}\frac{d\theta'}{\theta'}. \tag{4.3}$$

The evolution variable changes with θ like

$$\frac{dt}{d\theta} = \frac{\alpha_s}{\pi}\frac{1}{\theta}. \tag{4.4}$$

and inserting this into Eqn. (4.2) gives

$$\begin{aligned}\frac{d\mathcal{P}}{dtdz} &= \frac{d\mathcal{P}}{d\theta dz}\frac{d\theta}{dt} \\ &= \left(\frac{\alpha_s}{\pi}\frac{1}{\theta}P(z)\right)\left(\frac{\pi}{\alpha_s}\theta\right) \\ &= P(z). \end{aligned} \tag{4.5}$$

The evolution variable will therefore simplify the evolution equations by absorbing both the logarithms and constants which would have otherwise been explicitly written.

Since the shower evolves down to the hadronization scale, we must have that the transverse momenta must be greater than $Q_0 \sim 1GeV >> \Lambda_{\mathrm{QCD}}$. In the soft limit it can be written as,

$$k_\perp = z(1-z)p_t\theta \sim zp_t\theta > Q_0. \tag{4.6}$$

With this evolution variable, the parton showers will evolve in angle from the jet radius $R \sim 0.4$, down to the minimum angle, $\theta_{\mathrm{min}} = Q_0/p_t$, given by the hadronization scale[3]. The limits on the evolution variable t is then,

$$t_{\mathrm{max}} = \frac{\alpha_s}{\pi}\ln\frac{p_t R}{Q_0} \quad , \qquad t_{\mathrm{min}} = 0. \tag{4.7}$$

Therefore, as we increase in values for the evolution variable t we will be reducing our emission angles, which leads to angular ordering being directly implemented into our showers.

The literature often writes the evolution variable as $t \sim \ln\frac{Q}{Q_0}$, which is equivalent to ours when we recognize that $Q = p_t R$ is the transverse jet scale. Since our choice of evolution variable t is dependent on the opening angle θ, angular ordering is native to our parton shower programs.

Vacuum splitting functions

The Altarelli-Parisi splitting functions for vacuum branchings was calculated to leading order $P_{ba}^{(0)}$ in Section 3.2. Higher-order corrections are available on the form

$$P_{ba} = P_{ba}^{(0)} + \left(\frac{\alpha_s}{\pi}\right)P_{ba}^{(1)} + \left(\frac{\alpha_s}{\pi}\right)^2 P_{ba}^{(2)} + \cdots \tag{4.8}$$

and next-to-leading order calculations are performed in [17]. Leading order is however sufficient for our treatment, and we will be using Eqn. (3.19), Eqn. (3.20), and Eqn. (3.21) as our splitting functions in vacuum.

These splitting functions are however too complicated for some of the calculations we want to perform. It will therefore be useful to introduce a simplified splitting function for gg branchings in vacuum

$$P_{gg}^{\mathrm{simple}}(z) = \frac{C_A}{z(1-z)} \tag{4.9}$$

which will be used for some of the analytical calculations.

[3] Splittings may still occur beyond this point as $Q_0 >> m_\pi \sim \Lambda_{\mathrm{QCD}}$, and most of the partons hadronize into pions, but it is a convenient cutoff for our evolution.

4.2 The DGLAP equations

As mentioned in the discussion on observables, the inclusive parton distribution is governed by the Dokshitzer-Gribov-Lipatov-Altarelli-Parisi (DGLAP) evolution equations. They are written as a set of integro-differential equations that describe how the distribution of gluons and quarks evolve, respectively. While the general form of the equations presented is valid beyond leading logarithmic approximation, we will be focusing on the leading behavior, and setting α_s to be constant, such that we are only interested in terms of the order t in our evolution variable (equivalent to order $\alpha_s \ln(p_t R/Q_0)$).

The full DGLAP equations

The DGLAP equations have several conventions, so it is important to be consistent in the way it is presented. The DGLAP equations can be written in terms of the inclusive parton distribution $f_i(x,t)$, as

$$\begin{aligned}\frac{\partial}{\partial t} f_g(x,t) = &\int_x^1 \frac{dz}{z} 2\, P_{gg}(z) f_g\left(\frac{x}{z}, t\right) - \int_0^1 dz\, P_{gg}(z) f_g(x,t) \\ &+ \int_x^1 \frac{dz}{z} P_{gq}(z)\, f_q\left(\frac{x}{z}, t\right) - \int_0^1 dz P_{gq}(z) f_g(x,t)\end{aligned} \tag{4.10}$$

$$\begin{aligned}\frac{\partial}{\partial t} f_q(x,t) = &\int_x^1 \frac{dz}{z} P_{qq}(z) f_q\left(\frac{x}{z}, t\right) - \int_0^1 dz\, P_{qq}(z) f_q(x,t) \\ &+ \int_0^1 dz P_{qg}(z) \frac{1}{z} f_g\left(\frac{x}{z}, t\right)\end{aligned} \tag{4.11}$$

where $P(z)$ is the Altarelli-Parisi splitting functions, and $f_{g/q}(x,t) = dN_{g/q}/dx$ is the inclusive parton distribution for gluons and quarks respectively. The factor 2 comes from the symmetry in the P_{gg} splitting function, as the emitted gluons can carry either the momentum z or $(1-z)$. These functions essentially represent how gluons and quarks can enter and leave a given volume element as illustrated in [15, p.166-168]. In Appendix A we have constructed the DGLAP equation using generating functionals, in a manner similar to [18].

The evolution equations may also be written in terms of the energy distribution $D_i(x,t) = x\, f_i(x,t)$. Adding a step-function $\Theta(z > x)$ we can also gather the integrals to make it more compact, in which case Eqn. (4.10) and Eqn. (4.11) becomes,

$$\begin{aligned}\frac{\partial}{\partial t} D_g(x,t) = &\int_0^1 dz\, P_{gg}(z) \left[2\, D_g\left(\frac{x}{z}, t\right)\, \Theta(z > x) - D_g(x,t)\right] \\ &+ \int_0^1 dz P_{gq}(z) \left[D_q\left(\frac{x}{z}, t\right)\, \Theta(z > x) - D_g(x,t)\right]\end{aligned} \tag{4.12}$$

$$\begin{aligned}\frac{\partial}{\partial t} D_q(x,t) = &\int_0^1 dz\, P_{qq}(z) \left[D_q\left(\frac{x}{z}, t\right)\, \Theta(z > x) - D_q(x,t)\right] \\ &+ \int_x^1 dz P_{qg}(z) D_g\left(\frac{x}{z}, t\right).\end{aligned} \tag{4.13}$$

Both these sets of equations will be used, depending on which observables we are interested in.

The DGLAP presented here is to leading order, but higher-order expansions can also be written as is done in [12].

The DGLAP equation for gluons

We will frequently be focusing on cascades involving exclusively gluons, such that $P_{gg}(z)$ is the only splitting we are considering. The evolution equations is then adjusted by simply disregarding the terms with quarks, such that Eqn. (4.10) takes the form

$$\frac{\partial}{\partial t} f_g(x,t) = \int_x^1 \frac{dz}{z} 2\, P_{gg}(z) f_g\left(\frac{x}{z}, t\right) - \int_0^1 dz\, P_{gg}(z) f_g(x,t). \tag{4.14}$$

It can be shown from the symmetry of the $P_{gg}(z)$ splitting function that

$$\int_0^1 dz\, z\, P_{gg}(z) = \frac{1}{2} \int_0^1 dz\, P_{gg}(z) \tag{4.15}$$

and it is therefore possible to rewrite Eqn. (4.14), to the form

$$\frac{\partial}{\partial t} D(x,t) = \int_x^1 dz\, \tilde{P}_{gg}(z)\, D(x/z,t) - \int_0^1 dz\, z\, \tilde{P}_{gg}(z)\, D(x,t) \tag{4.16}$$

where $\tilde{P}_{gg}(z) \equiv 2\, P_{gg}(z)$. Both Eqn. (4.14) and Eqn. (4.16) will be used when discussing gluon showers.

4.3 The Sudakov form factor in vacuum

Now we will rewrite the DGLAP equation by introducing the Sudakov form factor, which will be important in developing the Monte-Carlo shower program in Chapter III. The Sudakov form factor is denoted as $\Delta(t)$ and is defined using the evolution variable introduced in Eqn. (4.3). For gluon showers the Sudakov form factor is

$$\Delta(t) = \exp\left(-t \int_\epsilon^{1-\epsilon} dz\, P_{gg}(z)\right) \tag{4.17}$$

with the derivatives

$$\begin{aligned} \frac{\partial}{\partial t} \Delta(t) &= \left(-\int_\epsilon^{1-\epsilon} dz\, P_{gg}(z)\right) \Delta(t) \\ \frac{\partial}{\partial t} \frac{1}{\Delta(t)} &= \int_\epsilon^{1-\epsilon} dz\, P_{gg}(z) \frac{1}{\Delta(t)}. \end{aligned} \tag{4.18}$$

It is easy to rewrite the DGLAP equation an integral equation using the Sudakov form factor. Starting by implementing the Sudakov into Eqn. (4.14),

$$\begin{aligned}
\frac{\partial}{\partial t}f(x,t) + \int_0^1 dz\, P_{gg}(z) f(x,t) &= \int_x^1 \frac{dz}{z}\, 2\, P_{gg}(z) f(x/z,t) \\
\frac{\partial}{\partial t}f(x,t) + \Delta(t) f(x,t)\frac{\partial}{\partial t}\frac{1}{\Delta(t)} &= \int_x^1 \frac{dz}{z}\, 2\, P_{gg}(z) f(x/z,t) \\
\frac{1}{\Delta(t)}\frac{\partial}{\partial t}f(x,t) - f(x,t)\frac{\partial}{\partial t}\frac{1}{\Delta(t)} &= \frac{1}{\Delta(t)}\int_x^1 \frac{dz}{z}\, 2\, P_{gg}(z) f(x/z,t) \\
\frac{\partial}{\partial t}\frac{f(x,t)}{\Delta(t)} &= \frac{1}{\Delta(t)}\int_x^1 \frac{dz}{z}\, 2\, P_{gg}(z)\, f(x/z,t).
\end{aligned} \tag{4.19}$$

The Sudakov form factor has now been implemented properly into the evolution equation. Continuing we wish to rewrite from a differential to an integral form,

$$\begin{aligned}
\int_{t_0}^t dt' \frac{\partial}{\partial t}\frac{f(x,t')}{\Delta(t')} &= \int_{t_0}^t \frac{dt'}{t'}\frac{1}{\Delta(t')}\int_x^1 dz\, 2\, P_{gg}(z)\frac{1}{z} f(x/z,t) \\
\frac{f(x,t)}{\Delta(t)} - \frac{f(x,t_0)}{\Delta(t_0)} &= \int_{t_0}^t \frac{dt'}{t'}\frac{1}{\Delta(t')}\int_x^1 dz\, 2\, P_{gg}(z)\frac{1}{z} f(x/z,t) \\
\frac{f(x,t)}{\Delta(t)} - f(x,t_0) &= \int_{t_0}^t \frac{dt'}{t'}\frac{1}{\Delta(t')}\int_x^1 dz\, 2\, P_{gg}(z)\frac{1}{z} f(x/z,t)
\end{aligned} \tag{4.20}$$

and we end up with our desired evolution equation on integral form

$$f(x,t) = \Delta(t) f(x,t_0) + \int_{t_0}^t \frac{dt'}{t'}\frac{\Delta(t)}{\Delta(t')}\int_x^1 \frac{dz}{z}\, 2\, P_{gg}(z)\, f(x/z,t'). \tag{4.21}$$

The physical interpretation of this equation comes from considering the Sudakov form factor as a no-branching probability. This means that the first term on the right-hand side of Eqn. (4.21) is the probability of no branching between t_0 and t (since $\Delta(t_0) = 1$). The second term then represents that some branching has occurred at time t', followed by no branchings between t' and t. The Sudakov form factor is effectively a way of resumming all orders of the DGLAP equation, by absorbing the divergences into the Sudakov form factor [2].

If we are working with both quarks and gluons then the Sudakov form factor will be slightly different, as several different branchings may occur in a given interval. The Sudakovs for showers with both gluons and quarks will be respectively

$$\Delta_g(t) = \exp\left(-t\int_\epsilon^{1-\epsilon} \left[P_{gg}(z) + P_{qg}(z)\right]\, dz\right) \tag{4.22}$$

$$\Delta_q(t) = \exp\left(-t\int_\epsilon^{1-\epsilon} P_{qq}(z)\, dz\right). \tag{4.23}$$

4.4 Analytical solution of the DGLAP equation

We will now solve the DGLAP equation following the method outlined in [19], for gluons in vacuum. The starting point is Eqn. (4.16), which is written with $\tilde{P}_{gg}(z) \equiv 2\, P_{gg}(z)$. The Mellin

transform and its inverse are defined as

$$\tilde{D}(\nu,t) = \int_0^1 dx\, x^{\nu-1}\, D(x,t) \quad , \quad D(x,t) = \int_{c-i\infty}^{c+i\infty} \frac{d\nu}{2\pi i}\, x^{-\nu}\, \tilde{D}(\nu,t). \tag{4.24}$$

Taking the Mellin transform of Eqn. (4.16) and then changing the integration limits $\int_0^1 dx \int_x^1 dz \to \int_0^1 dz \int_0^x dx$, and performing a change of variable $\xi = x/z \;\Rightarrow\; dx = z\, d\xi$ we obtain

$$\begin{aligned}
\frac{\partial}{\partial t}\int_0^1 dx\, x^{\nu-1} D(x,t) &= \int_0^1 dx\, x^{\nu-1} \int_x^1 dz\, \tilde{P}_{gg}(z)\, D(x/z,t) - \int_0^1 dx\, x^{\nu-1} \int_0^1 dz\, z\, \tilde{P}_{gg}(z)\, D(x,t) \\
\frac{\partial}{\partial t}\tilde{D}(\nu,t) &= \int_0^1 dz\, \tilde{P}_{gg}(z) \int_0^1 (z\, d\xi)\, (z\,\xi)^{\nu-1} D(\xi,t) - \int_0^1 dz\, z\, \tilde{P}_{gg}(z)\, \tilde{D}(\nu,t) \\
\frac{\partial}{\partial t}\tilde{D}(\nu,t) &= -\int_0^1 dz\, \tilde{P}_{gg}(z)\, (z - z^{\nu})\, \tilde{D}(\nu,t).
\end{aligned} \tag{4.25}$$

Inserting the simplified splitting function of Eqn. (4.9), we can write the evolution equation in Mellin space as

$$\frac{\partial}{\partial t}\tilde{D}(\nu,t) = -2C_A \int_0^1 dz \frac{1-z^{\nu-1}}{(1-z)} \tilde{D}(\nu,t). \tag{4.26}$$

Introducing the Digamma function

$$\psi(\nu) = \int_0^1 \frac{1-z^{\nu-1}}{1-z} dz - \gamma_E, \tag{4.27}$$

where γ_E is the *Euler-Mascheroni constant*, we can write Eqn. (4.26) as a simple differential equation

$$\frac{\partial}{\partial t}\tilde{D}(\nu,t) = -2C_A(\psi(\nu)+\gamma_E)\tilde{D}(\nu,t) \tag{4.28}$$

the solution is easily obtained with the initial condition $\tilde{D}(\nu,0) = 1$

$$\tilde{D}(\nu,t) = \exp\left[-2C_A(\psi(\nu)+\gamma_E)t\right]. \tag{4.29}$$

Now that the solution is obtained, we just have to transform back with the inverse Mellin transform

$$\begin{aligned}
D(x,t) &= \int_{c-i\infty}^{c+i\infty} \frac{d\nu}{2\pi i} x^{-\nu} \exp\left[-2C_A(\psi(\nu)+\gamma_E)t\right] \\
&= \int_{c-i\infty}^{c+i\infty} \frac{d\nu}{2\pi i} \exp\left[\ln 1/x^{\nu}\right] \exp\left[-2C_A(\psi(\nu)+\gamma_E)t\right] \\
&= \int_{c-i\infty}^{c+i\infty} \frac{d\nu}{2\pi i} \exp\left[-2C_A(\psi(\nu)+\gamma_E]t + \nu \ln\frac{1}{x}\right].
\end{aligned} \tag{4.30}$$

A solution to the equation an be obtained by utilizing the saddle-point approximation. Setting the argument of the exponential as $f(\nu) \equiv -2C_A(\psi(\nu)+\gamma_E)t + \nu \ln\frac{1}{x}$, then in a saddle point ν_s we should have

$$f(\nu) \approx f(\nu_S) + \frac{1}{2} f''(\nu_S)(\nu-\nu_S)^2. \tag{4.31}$$

$f(\nu)$ has a minimum value when

$$\psi'(\nu_s) = \frac{1}{2C_A}\frac{\ln(1/x)}{t} \tag{4.32}$$

which gives us, in the small x limit where $\ln(1/x) >> t$,

$$\psi(\nu) \approx -\nu^{-1} \quad \Rightarrow \quad \psi'(\nu) \approx \nu^{-2}. \tag{4.33}$$

and the value ν_s of the saddle point can therefore be found to be

$$\nu_s = \left(\frac{2C_A\, t}{\ln(1/x)}\right)^{1/2}. \tag{4.34}$$

We can then write Eqn. (4.30) by using the saddle point-approximation

$$D(x,t) \approx \exp\left(f(\nu_S)\right) \int_{c-i\infty}^{c+i\infty} \frac{d\nu}{2\pi i} \exp\left(\frac{1}{2} f''(\nu_s)(\nu-\nu_s)^2\right). \tag{4.35}$$

Performing a change of variable $\nu = ib$ to remove the complex numbers in the integral

$$D(x,t) \approx \exp\left(f(\nu_S)\right) \int_{-\infty}^{\infty} \frac{db}{2\pi} \exp\left(-\frac{1}{2} f''(\nu_s)(b+i\nu_s)^2\right) \tag{4.36}$$

and solving using Mathematica,

$$\int_{-\infty}^{\infty} \frac{db}{2\pi} \exp\left(-\frac{1}{2} f''(\nu_s)(b+i\nu_s)^2\right) = \frac{1}{2\sqrt{\pi/2}\sqrt{f''(\nu_s)}}. \tag{4.37}$$

Seeing that $f''(\nu_S) = 4C_A\, t\, \nu_S^{-3}$, we write our solution as

$$\begin{aligned}
D(x,t) &= exp\left(f(\nu_S)\right) \frac{1}{2\sqrt{(\pi/2)\, f''(\nu_S)}} \\
D(x,t) &= exp\left(2C_A\nu_S^{-1} - 2C_A\gamma_E t + \nu_S \ln\frac{1}{x}\right) \frac{1}{2} \frac{1}{\sqrt{2\pi C_A\, t\, \nu_S^{-3}}} \\
D(x,t) &= exp\left(2\sqrt{2C_A}\sqrt{t\ln\frac{1}{x}} - 2C_A\gamma_E\, t\right) \frac{1}{2} \left(\frac{2C_A\, t}{\pi^2 \ln^3(1/x)}\right)^{1/4}.
\end{aligned} \tag{4.38}$$

Eqn. (4.38) is therefore a solution of the DGLAP equation. Note that the factor $\sqrt{2C_A}$ comes from the symmetry factor and color factor of the $P_{gg}(z)$ splitting function. It is valid in the small x-limit such that $\ln\frac{1}{x} >> t$. In the double logarithmic limit, where we focus on the leading $\ln\frac{1}{x}$ behavior, the solution can be written as

$$\begin{aligned}
D_{DLL}(x,t) &\approx exp\left(2\sqrt{2C_A}\sqrt{t\ln\frac{1}{x}}\right) \\
&\approx \left(\frac{1}{x}\right)^{2\sqrt{2C_A}\sqrt{\frac{t}{\ln 1/x}}}.
\end{aligned} \tag{4.39}$$

5 Formalism of Parton Branching in Medium

This section will explore parton showers developing in a dense QCD medium. Most of the notation will be given in the same manner as [19]. The new medium showers will be described by a in-medium kinetic rate equation which has a similar structure to the DGLAP equation. After introducing the differences between vacuum and medium cascades, we will solve the evolution equation for gluons. Our treatment will begin by disregarding the broadening that can occur between splittings, and rather focus on how the cascade changes due to the large amount of soft gluon emission. At the end of the section, we will discuss how to account for the broadening of partons due to exchange of momenta with the medium.

We will be working exclusively with gluons throughout this section. Subsequent discussions on medium showers will also be purely gluonic.

5.1 Properties of medium cascades

Differences between vacuum and medium cascades

Before introducing the in-medium kinetic rate equation, a discussion is required for covering the main differences between medium and vacuum showers. In the vacuum discussion, the first point of interest was the evolution variable which was a dimensionless quantity used to conveniently write the evolution equations. For the medium showers this will be replaced by the characteristic time t_*, which has dimensions equal to the actual time $[GeV^{-1}]$ and is defined in Eqn. (5.1). The characteristic time, or stopping time, is the time it takes for a gluon of energy ω to radiate most of its energy into soft gluons

$$t_* \equiv \frac{1}{\bar{\alpha}} t_{\mathrm{br}}(E) = \frac{\pi}{\alpha_s N_C}\sqrt{\frac{E}{\hat{q}}} \tag{5.1}$$

here $t_{\mathrm{br}}(E)$ is the typical time, or branching time, introduced in Eqn. (2.5), which is the time it takes a gluon of energy E to branch into two gluons, and $\hat{q}$ is the *jet-quenching parameter*. Since we are exclusively working with gluons, we can set $C_A = N_C$, and define $\bar{\alpha} \equiv \alpha_s N_C/\pi$ and $\hat{q} = \hat{\bar{q}}\, C_A$, such that all color factors are absorbed into the branching time.

An important feature of the medium cascades is that the branching rate increases along the cascade, in contrast to the vacuum cascades, where the branching rate is constant along the cascade. This is apparent when looking at the characteristic time; as the energy ω of a given gluon decrease, the expected time for branching also decreases. This means that the branchings are accelerating, and it takes a finite time to transport a finite amount of energy from the leading particle to soft gluons. Energy is therefore effectively transported towards large angles, which contrasts the strong angular ordering of QCD cascades in vacuum. Both the increased branching rate and transport of energy towards large angles are natural consequences of medium induced soft gluon emissions. The spectrum of these radiated gluons is on the form

$$\omega \frac{dI}{d\omega} \approx \bar{\alpha}\sqrt{\frac{\omega_c}{\omega}} \tag{5.2}$$

where ω_c is the energy which gives one branching in the length of the traversed medium $t_{\mathrm{br}}(\omega_c) \sim L$, and can therefore be written as $\omega_c = \hat{q}L^2$. The spectrum in Eqn. (5.2) is called the BDMPS-Z

spectrum, named after Baier-Dokshitzer-Mueller-Peigne-Schiff and Zakharov. The first factor $\bar{\alpha}$ represents the standard bremsstrahlung spectrum for radiation by the parent gluon, while the second factor $\sqrt{\omega_c/\omega}$ is a correction factor. This factor needs to be cut off for a minimum frequency at which radiation is primarily produced by incoherent collisions. This cut-off ω_{BH} is where the branching time is of the order of the mean free path, $t_{\text{br}} \sim \ell$. The mechanisms and approximations required for large amounts of soft gluon emissions require the formation time to be much larger than the mean free path ℓ, but smaller than the size of the medium L, this gives us boundaries for the energy of the emitted gluons $\omega_{\text{BH}} << \omega < \omega_c$ [10].

Since this section is concerned with partons traversing a medium, it could also be insightful to rewrite the BDMPS-Z spectrum of Eqn. (5.2) in terms of dL, in order to indicate the branching rate when traversing a given length of medium. Simply inserting $\omega_c = \hat{q}L^2$, we can write

$$\frac{dI}{d\omega dL} = \frac{\bar{\alpha}}{\omega}\sqrt{\frac{\hat{q}}{\omega}}. \tag{5.3}$$

Scaling behavior

Another feature of the medium cascades is that they exhibit a scaling behavior in the number of partons occupying small values of x. This scaling stems from the solution of the BDMPS-Z spectrum which we will solve shortly, and is on the form

$$D(x,t) \approx \frac{t}{t_*\sqrt{x}} \exp\left[-\pi\left(\frac{t}{t_*}\right)^2\right]. \tag{5.4}$$

The scaling manifest itself when $t > t_*$, which means that most of the energy has been radiated into soft gluons $x < 0.1$. After this, the number of partons occupying a given element δx decreases in a uniform and shape-conserving way. A natural interpretation of this phenomenon would be a constant flow of energy towards small values of x, which can be related to the existence of a stationary solution of the energy distribution [19]. This scaling will be apparent later when we will create a Monte-Carlo program for simulating parton showers in medium, for different values of t.

Medium splitting functions

The splitting functions responsible for parton branchings in medium are somewhat different from their vacuum counterparts. From our discussion on the BDMPS-Z spectrum we would expect the splitting functions to be similar to the branching rate given by Eqn. (5.3). Since we have absorbed all color factors into the branching time, the gg splitting function given by [20] can be written as,

$$\mathcal{K}_{gg}(z) = \frac{1}{2}\,2\,\frac{[1-z(1-z)]^{5/2}}{[z(1-z)]^{3/2}}. \tag{5.5}$$

The factor $1/2$ come from the terms accounting for medium induced radiation, while the factor 2 comes from the symmetry of the gg splitting. Comparing with the vacuum counterpart we now have an additional term inside a square root. This appears due to partons interacting with the medium, leading to soft gluon emissions and making the medium splitting function more divergent. The parton distributions are therefore softened, or quenched, and is the only

measurable consequence of the quark energy-loss in the medium [21].

While this splitting function might seem quite different from its vacuum counterpart at first glance, the simple vacuum splittings functions can be easily identified such that Eqn. (5.5) can be written in terms the vacuum splitting function $P_{gg}(z)$. This form also accentuate the similarities of Eqn. (5.3) and the splitting function

$$\begin{aligned} C_A \mathcal{K}_{gg}(z) &= C_A \frac{[1-z(1-z)]^2}{z(1-z)} \sqrt{\frac{(1-z)+z^2}{z(1-z)}} \\ &= P_{gg}(z) \sqrt{\frac{1-z(1-z)}{z(1-z)}} \end{aligned} \tag{5.6}$$

The full splitting function has now been introduced. However, it will be sufficient - and more convenient - to work with a simplified splitting function which we will write as

$$\mathcal{K}(z) = \frac{1}{(z(1-z))^{3/2}}. \tag{5.7}$$

For the remainder of the chapter, Eqn. (5.7) will be used as our gg splitting function, and we will call it the reduced kernel.

5.2 The in-medium kinetic rate equation

The full in-medium kinetic rate equations

The necessary ingredients for constructing the in-medium kinetic rate equations have now been introduced. It is expected that the form of the evolution equations in medium, will be very similar to the vacuum version. For a derivation using generating functionals see [18], here we simply quote the results following the conventions of [19]. An important feature to note is that the in-medium kinetic rate equation is written in terms of the actual time t and characteristic time t_* (defined in Eqn. (5.1)). This means that angular ordering is not strictly imposed in these showers, which is to be expected as soft gluon emission at large angles occurs frequently due to medium interactions. For now we will write the characteristic time as a function of the energy $t_*(x) = t_*\sqrt{x}$. This gives an effective time scale for the branching of a gluon carrying a fraction x of the initial energy, which is one of the properties of the medium cascade. The evolution equations can be written

$$\begin{aligned} \frac{\partial}{\partial t} D_g(x,t) = &\int_x^1 dz \, \frac{1}{t_*(x/z)} \mathcal{K}_{gg}(z) \, D_g\left(\frac{x}{z}, t\right) - \frac{1}{2t_*(x)} \int_0^1 dz \, \mathcal{K}_{gg}(z) \, D_g\left(x,t\right) \\ &+ \int_x^1 dz \, \frac{1}{t_*(x/z)} \mathcal{K}_{gq}(z) \, D_g\left(\frac{x}{z}, t\right) - \frac{1}{t_*(x)} \int_0^1 dz \, \mathcal{K}_{gq}(z) \, D_g\left(x,t\right) \end{aligned} \tag{5.8}$$

$$\begin{aligned} \frac{\partial}{\partial t} D_q(x,t) = &\int_x^1 dz \, \frac{1}{t_*(x/z)} \mathcal{K}_{qq}(z) \, D_q\left(\frac{x}{z}, t\right) - \frac{1}{t_*(x)} \int_0^1 dz \, \mathcal{K}_{qq}(z) \, D_q\left(x,t\right) \\ &+ \int_x^1 dz \, \frac{1}{t_*(x/z)} \mathcal{K}_{qg}(z) \, D_g\left(\frac{x}{z}, t\right). \end{aligned} \tag{5.9}$$

The main difference between the in-medium kinetic rate equations, and the DGLAP equations should then be apparent. If we replace $\mathcal{K}_{ba}(z) \to \tilde{P}_{ba}(z)$ and $t_*(x) \to 1$, the in-medium kinetic rate equations reduces to the DGLAP equations.

The in-medium kinetic rate equation for gluons

We will be primarily focusing on cascades consisting exclusively of gluons. Since the splitting function $\mathcal{K}_{gg}(z)$ is perfectly symmetrical, we can again use that

$$\frac{1}{2}\int_{\epsilon}^{1-\epsilon} dz \mathcal{K}_{gg}(z) = \int_{\epsilon}^{1-\epsilon} dz\, z\, \mathcal{K}_{gg}(z) \tag{5.10}$$

and Eqn. (5.8) can be written,

$$\frac{\partial}{\partial t}D(x,t) = \int_x^1 dz\, \frac{1}{t_*(x/z)}\mathcal{K}_{gg}(z)\, D\left(\frac{x}{z},t\right) - \frac{1}{t_*(x)}\int_0^1 dz\, \mathcal{K}_{gg}(z)\, z\, D(x,t) \tag{5.11}$$

The evolution equation for gluons can also be written by noting that the splitting kernel is independent of time. The evolution equation can therefore be simplified by introducing a new variable τ which accounts for the energy dependence and time scale of the branchings

$$\tau = \frac{t}{t_*} = \bar{\alpha}\sqrt{\frac{\hat{q}}{E}}t \tag{5.12}$$

using this new variable the evolution equation for gluons can be written as

$$\frac{\partial}{\partial \tau}D(x,\tau) = \int_x^1 dz\, \mathcal{K}(z)\sqrt{\frac{z}{x}}D\left(\frac{x}{z},\tau\right) - \int_0^1 dz\, \mathcal{K}(z)\frac{z}{\sqrt{x}}D(x,t). \tag{5.13}$$

5.3 The Sudakov form factor in medium

We will now start with Eqn. (5.11), and rewrite it in terms of a Sudakov form factor

$$\Delta(t) = \exp\left(-\frac{t}{t_*(x)}\int_0^1 dz\, z\mathcal{K}(z)\right) \tag{5.14}$$

with the derivatives,

$$\begin{aligned}\frac{\partial}{\partial t}\Delta(t) &= -\frac{1}{t_*(x)}\int_0^1 dz\, z\mathcal{K}(z)\Delta(t)\\ \frac{\partial}{\partial t}\frac{1}{\Delta(t)} &= \frac{1}{t_*(x)}\int_0^1 dz\, z\mathcal{K}(z)\frac{1}{\Delta(t)}\end{aligned} \tag{5.15}$$

Starting by rewriting Eqn. (5.11)

$$\begin{aligned}
\frac{\partial}{\partial t}D(x,t) + \frac{D\,(x,t)}{t_*(x)}\int_0^1 dz\, z\,\mathcal{K}(z) &= \int_x^1 dz\,\mathcal{K}(z)\,\frac{D\left(\frac{x}{z},t\right)}{t_*(x/z)} \\
\frac{\partial}{\partial t}D(x,t) + D(x,t)\frac{\partial}{\partial t}\frac{1}{\Delta(t)} &= \int_x^1 dz\,\mathcal{K}(z)\,\frac{D\left(\frac{x}{z},t\right)}{t_*(x/z)} \\
\Delta(t)\frac{\partial}{\partial t}\left(\frac{D(x,t)}{\Delta(t)}\right) &= \int_x^1 dz\,\mathcal{K}(z)\,\frac{D\left(\frac{x}{z},t\right)}{t_*(x/z)} \\
\frac{\partial}{\partial t}\left(\frac{D(x,t)}{\Delta(t)}\right) &= \frac{1}{\Delta(t)}\int_x^1 dz\,\mathcal{K}(z)\,\frac{D\left(\frac{x}{z},t\right)}{t_*(x/z)} \qquad (5.16)
\end{aligned}$$

and integrating out the t integral,

$$\begin{aligned}
\frac{D(x,t)}{\Delta(t)} - \frac{D(x,t_0)}{\Delta(t_0)} &= \int_{t_0}^t \frac{dt'}{\Delta(t')}\int_x^1 dz\,\mathcal{K}(z)\,\frac{D\left(\frac{x}{z},t'\right)}{t_*(x/z)} \\
D(x,t) &= D(x,t_0)\,\frac{\Delta(t)}{\Delta(t_0)} + \int_{t_0}^t dt'\,\frac{\Delta(t)}{\Delta(t')}\int_x^1 dz\,\mathcal{K}(z)\,\frac{D\left(\frac{x}{z},t'\right)}{t_*(x/z)}. \qquad (5.17)
\end{aligned}$$

If we now consider the initial time $t_0 = 0$, then $\Delta(t_0) = 1$ and we obtain an equation which is the medium equivalent of Eqn. (4.21)

$$D(x,t) = D(x,t_0)\,\Delta(t) + \int_{t_0}^t dt'\,\frac{\Delta(t)}{\Delta(t')}\int_x^1 dz\,\mathcal{K}(z)\,\frac{D\left(\frac{x}{z},t'\right)}{t_*(x/z)}. \qquad (5.18)$$

5.4 Analytical solution of the in-medium kinetic rate equation

We will now solve the medium evolution equation for gluons, by closely following the method outlined in [19]. The starting point for solving the medium evolution equation is Eqn. (5.13), where $\mathcal{K}_{gg}(z)$ is the reduced kernel given in Eqn. (5.7), and τ is defined as in Eqn. (5.12).

The solution presented here is valid for values $x_c > 1$, which corresponds to a large medium $L > t_*$. This is a valid comparison with the Monte-Carlo program which is developed in Chapter III, as it assumes the shower is constantly evolving in a medium.

The first step is to perform a change of variable such that $\xi = \frac{x}{z}$ in the gain term and $\xi = xz$ in the loss term

$$\begin{aligned}
\mathbb{G} &= \int_x^1 dz\mathcal{K}(z)\sqrt{\frac{z}{x}}D\left(\frac{x}{z},\tau\right) \qquad , \quad \xi = \frac{x}{z} \\
&= \int_1^x d\xi\left(-\frac{x}{\xi^2}\right)\mathcal{K}\left(\frac{x}{\xi}\right)\sqrt{\frac{1}{\xi}}D(\xi,\tau) \\
&= \int_x^1 d\xi\,\frac{x}{\xi^{5/2}}\mathcal{K}\left(\frac{x}{\xi}\right)D(\xi,\tau) \qquad (5.19)
\end{aligned}$$

$$\begin{aligned}\mathbb{L} &= -\int_0^1 dz\mathcal{K}(z)\frac{z}{\sqrt{x}}D(x,\tau) \qquad , \quad \xi = xz \\ &= -\int_0^x d\xi \left(\frac{1}{x}\right)\mathcal{K}\left(\frac{\xi}{x}\right)\frac{\xi}{x(3/2)}D(x,\tau) \\ &= -\int_0^x d\xi \,\frac{\xi}{x^{5/2}}\mathcal{K}\left(\frac{\xi}{x}\right)D(x,\tau) \end{aligned} \tag{5.20}$$

in these equations a common splitting function can be identified as,

$$\begin{aligned} P(x,\xi) &= \frac{x}{\xi^{5/2}}\mathcal{K}\left(\frac{x}{\xi}\right) \\ &= \sqrt{\frac{\xi}{x}}\frac{1}{(\xi-x)^{3/2}} \end{aligned} \tag{5.21}$$

and Eqn. (5.13) can therefore be written as

$$\partial_\tau D(x,\tau) = \int_x^1 d\xi\, P(x,\xi)D(\xi,\tau) - \int_0^x d\xi\, P(\xi,x)D(x,\tau). \tag{5.22}$$

Note that $P(x,\xi) \neq P(\xi,x)$. Now that the gain and loss terms are written in a convenient and symmetrical way, **the second step** is to deal with the integral of the loss term

$$\int_0^x d\xi \sqrt{\frac{1}{\xi}}\frac{1}{(x-\xi+\epsilon)^{3/2}} = \frac{1}{\sqrt{\epsilon}}\frac{2x}{x+\epsilon} \approx \frac{2}{\sqrt{\epsilon}} - \frac{2\sqrt{\epsilon}}{x} + \mathcal{O}(\epsilon^{3/2}). \tag{5.23}$$

In the limit $\epsilon \to 0$, the first term is divergent, and all subleading terms vanish for any finite value of x. Therefore, the sole purpose of the loss term (in these variables) is to remove the singularity of the gain term. We can therefore replace the integral in the loss term with the following

$$\mathbb{L} = -D(x,\tau)\int_0^\infty \frac{dz}{z^{3/2}}. \tag{5.24}$$

Step three we introduce a re-scaling of the distribution $F(y,\tau) = \sqrt{x}D(x,\tau)$, where $y = 1-x$, by multiplying everything by $\sqrt{x}$ and inserting the new loss term, Eqn. (5.22) becomes

$$\begin{aligned} \partial_\tau\sqrt{x}D(x,\tau) &= \int_x^1 d\xi\,\frac{1}{(\xi-x)^{3/2}}\sqrt{\xi}\,D(\xi,\tau) - \sqrt{x}\,D(x,\tau)\int_0^\infty \frac{dz}{z^{3/2}}, \\ \partial_\tau F(y,\tau) &= \int_{1-y}^1 d\xi\,\frac{1}{[\xi-(1-y)]^{3/2}}\sqrt{\xi}\,D(\xi,\tau) \\ &\quad - \sqrt{(1-y)}\,D((1-y),\tau)\int_0^\infty \frac{dz}{z^{3/2}} \end{aligned}. \tag{5.25}$$

Then performing a change of variable $\tilde{\xi} = 1-\xi$, and using $F(y,\tau) = \sqrt{1-y}\,D(1-y,\tau)$

$$\begin{aligned} \partial_\tau F(y,\tau) &= \int_0^y d\tilde{\xi}\,\frac{1}{(y-\tilde{\xi})^{3/2}}\sqrt{1-\tilde{\xi}}\,D(1-\tilde{\xi},\tau) - F(y,\tau)\int_0^\infty \frac{dz}{z^{3/2}}, \\ &= \int_0^y d\tilde{\xi}\,\frac{1}{(y-\tilde{\xi})^{3/2}}F(\tilde{\xi},\tau) - F(y,\tau)\int_0^\infty \frac{dz}{z^{3/2}}. \end{aligned} \tag{5.26}$$

Step four is to extend the limits of the domain for $F(y,\tau)$ from $y \in [0,1] \to y \in [0,\infty]$, and

Laplace transform our evolution equation. Defining the Laplace transform as

$$\tilde{F}(\nu,\tau) = \int_0^\infty dy\, e^{-\nu y}\, F(y,\tau) \tag{5.27}$$

and performing the Laplace transform on Eqn. (5.26) gives

$$\begin{aligned}\partial_t \tilde{F}(\nu,\tau) &= \int_0^\infty dy\, e^{-\nu y} \int_0^y d\tilde{\xi}\, \frac{1}{(y-\tilde{\xi})^{3/2}} F(\tilde{\xi},\tau) - \int_0^\infty dy\, e^{-\nu y}\, F(y,\tau) \int_0^\infty \frac{dz}{z^{3/2}} \\ &= \int_0^\infty dy \int_0^y d\tilde{\xi}\, e^{-\nu y} \frac{1}{(y-\tilde{\xi})^{3/2}} F(\tilde{\xi},\tau) - \tilde{F}(y,\tau) \int_0^\infty \frac{dz}{z^{3/2}}.\end{aligned} \tag{5.28}$$

Since the loss term had one y dependence, the Laplace transform went very smoothly. When dealing with the gain term it is necessary to make some changes to the integration boundaries $\int_0^\infty dy \int_0^y d\tilde{\xi} \to \int_{\tilde{\xi}}^\infty dy \int_0^\infty d\tilde{\xi}$, and then introduce another change of variable $z = y - \tilde{\xi}$

$$\begin{aligned}\mathbb{G} &= \int_0^\infty d\tilde{\xi}\, F(\tilde{\xi},\tau) \int_{\tilde{\xi}}^\infty dy\, e^{-\nu y} \frac{1}{(y-\tilde{\xi})^{3/2}} \\ &= \int_0^\infty d\tilde{\xi}\, F(\tilde{\xi},\tau) \int_0^\infty dz\, \frac{e^{-\nu(z+\tilde{\xi})}}{z^{3/2}} \\ &= \int_0^\infty d\tilde{\xi} e^{-\nu\tilde{\xi}}\, F(\tilde{\xi},\tau) \int_0^\infty dz\, \frac{e^{-\nu z}}{z^{3/2}} \\ &= \tilde{F}(\nu,\tau) \int_0^\infty dz\, \frac{e^{-\nu z}}{z^{3/2}}.\end{aligned} \tag{5.29}$$

The results of our Laplace transform is apparent when the gain term transformed in Eqn. (5.29), is inserted back into the evolution equation of Eqn. (5.28)

$$\begin{aligned}\partial_t \tilde{F}(\nu,\tau) &= \tilde{F}(\nu,\tau) \int_0^\infty dz\, \frac{e^{-\nu z}}{z^{3/2}} - \tilde{F}(y,\tau) \int_0^\infty \frac{dz}{z^{3/2}} \\ &= \tilde{F}(\nu,\tau) \int_0^\infty dz\, \frac{(e^{-\nu z}-1)}{z^{3/2}} \\ &= \tilde{F}(\nu,\tau)\, (-2\sqrt{\pi\nu}).\end{aligned} \tag{5.30}$$

This is a simple differential equation. From energy conservation the initial condition is $\tilde{F}_0 = 1$ - more precisely is the initial condition a delta function which takes into account partons ending with precisely zero momentum - but the solution becomes

$$\tilde{F}(\nu,\tau) = e^{-2\sqrt{\pi\nu}\tau}. \tag{5.31}$$

Step five - the final step of this calculation - is to do the inverse Laplace transformation on Eqn. (5.31)

$$\begin{aligned}F(y,\tau) &= \int_{c-i\infty}^{c+i\infty} \frac{d\nu}{2\pi i} e^{\nu y}\, \tilde{F}(\nu,\tau) \\ &= \frac{\tau}{y^{3/2}}\, \exp\left(-\pi\frac{\tau^2}{y}\right)\end{aligned} \tag{5.32}$$

and reverting back $F(y,\tau) = \sqrt{x}\, D(x,\tau)$ and $y = 1 - x$, our final solution is

$$D(x,\tau) = \frac{\tau}{\sqrt{x}(1-x)^{3/2}} \exp\left(-\pi \frac{\tau^2}{1-x}\right). \tag{5.33}$$

At this point, it is worth taking a deep breath and reflect on what just happened. We started out with the medium evolution equation and wrote it in terms of a new variable ξ, this made it possible to solve the integral in the loss term. Another change of variables allowed us to perform a Laplace transform so that the gain and loss term obtained the same form, and the equation could therefore be solved as a differential equation in Laplace space. Finally, the inverse Laplace transform gave us the final expression in Eqn. (5.33).

The solution given in Eqn. (5.33) is the full solution for the in-medium kinetic rate equation, using the reduced kernel. Contrasting the solution to the DGLAP equation of Eqn. (4.38), which is valid only in the small x limit.

This general strategy was relatively similar to the solution of the DGLAP equation, as both aimed at writing the gain and loss terms in the same form by using some change of variable, and then performing a transformation in order to solve the equation, before transforming back to momentum space.

5.5 Medium broadening of parton showers

As mentioned at the start of the section we will now discuss how broadening can occur without inducing gluon radiation, and how to account for this in our evolution equations.

The evolution equations which we have presented for medium cascades so far, does not include any diffusion terms representing medium broadening happening between the individual splittings. This is represented by the partons in the distribution experiencing kicks form the medium, by the addition of a collision kernel $\mathcal{C}(\mathbf{l},\tau)$. If we were to include this broadening, the evolution equation for gluons could be written as [18, 22]

$$\begin{aligned}\frac{\partial}{\partial\tau} D(x,\mathbf{k},\tau) = &\int_{\mathbf{l}} \mathcal{C}(\mathbf{l},\tau)\, D(x,\mathbf{k}-\mathbf{l},\tau) \\ &+ \int_x^1 dz\, \frac{1}{z^2}\sqrt{\frac{z}{x}} \mathcal{K}(z) D\left(\frac{x}{z}, \frac{\mathbf{k}}{z}, \tau\right) - \int_0^1 dz\, \frac{z}{\sqrt{x}} \mathcal{K}(z) D(x,\mathbf{k},\tau)\end{aligned} \tag{5.34}$$

where $\mathcal{C}(\mathbf{l},t)$ is the elastic collision kernel, and τ is defined as in Eqn. (5.12). By integrating this equation over transverse momentum $\int_{\mathbf{k}} = \int \frac{d^2\mathbf{k}}{(2\pi)^2}$, and setting $D(x,t) = \int_{\mathbf{k}} D(x,\mathbf{k},t)$, we are left with

$$\begin{aligned}\int_{\mathbf{k}} \frac{\partial}{\partial\tau} D(x,\mathbf{k},\tau) = &\int_{\mathbf{k}}\int_{\mathbf{l}} \mathcal{C}(\mathbf{l},\tau)\, D(x,\mathbf{k}-\mathbf{l},\tau) \\ &+ \int_{\mathbf{k}}\int_x^1 dz\, \frac{1}{z^2}\sqrt{\frac{z}{x}} \mathcal{K}(z) D\left(\frac{x}{z}, \frac{\mathbf{k}}{z}, \tau\right) - \int_{\mathbf{k}}\int_0^1 dz\, \frac{z}{\sqrt{x}} \mathcal{K}(z) D(x,\mathbf{k},\tau)\end{aligned} \tag{5.35}$$

$$\begin{aligned}\frac{\partial}{\partial\tau} D(x,\tau) = &\int_{\mathbf{l}} \mathcal{C}(\mathbf{l},\tau)\, D(x,\tau) \\ &+ \int_x^1 dz \sqrt{\frac{z}{x}} \mathcal{K}(z) D\left(\frac{x}{z}, \tau\right) - \int_0^1 dz\, \frac{z}{\sqrt{x}} \mathcal{K}(z) D(x,\tau).\end{aligned} \tag{5.36}$$

Since $\int_{\mathbf{l}} \mathcal{C}(\mathbf{l},\tau) = 0$, this becomes simply,

$$\frac{\partial}{\partial\tau} D(x,\tau) = \int_x^1 dz \sqrt{\frac{z}{x}} \mathcal{K}(z) D\left(\frac{x}{z},\tau\right) - \int_0^1 dz \frac{z}{\sqrt{x}} \mathcal{K}(z) D(x,\tau). \tag{5.37}$$

Which is equivalent to Eqn. (5.13). We have therefore seen that when averaging over the final transverse momentum after the splitting process, the collision kernel can be disregarded. We are primarily concerned with the inclusive distribution integrated over transverse momentum, $D(x,t) = \int_{\mathbf{k}} D(x,\mathbf{k},t)$, and the broadening is therefore not relevant (in general) for our discussions.

Chapter III

Numerical

While the previous chapter introduced the formalism for parton branchings in vacuum and medium, we will now turn to a numerical treatment of the evolution equations. This will be done by using the results of the previous chapter to build a Monte-Carlo program for simulating parton showers, both for vacuum and medium cascades. Each section will be structured in the same manner, starting by determining how the cascade evolves relative to the branching probability, then developing methods for sampling random energy fractions from the splitting functions, and finally implementing this into Monte-Carlo programs. The results obtained from these programs will then be compared with the analytical results derived in Chapter II, and used to highlight different properties of the cascades.

6 Monte-Carlo for Parton Branching in Vacuum

Starting by creating the Monte-Carlo programs for the vacuum cascades, where we want to develop one for pure gluon cascades (only gg splittings), and one for both quarks and gluons. The former will be created using the simplified gg splitting function, which can then be compared to the analytical results of the DGLAP cascade. The latter will be done using the full splitting functions, sampled using the *Metropolis-Hastings algorithm* (MH), and will give us a more realistic picture of the branching process but no exact analytical solution to compare with.

6.1 Evolution interval

For our Monte-Carlo programs we need to determine the limits of the evolution variable t, such that we know when to terminate a given shower. Recalling the evolution variable defined in Eqn. (4.3), and that our jets evolve in angle from some initial jet radius R, down to the minimum angle $\theta_{\min} = Q_0/p_t$, with boundary values of the evolution variable given by Eqn. (4.7). A plot of the maximum value for t for a given range of p_t and R values is given by Figure 6.1. Here it is apparent that most values of t are below 0.4.

Knowing the boundaries we need to impose on the evolution variable for our Monte-Carlo, we can now move on to determining how to sample intervals of the evolution variable from the Sudakov form factor. As discussed in Chapter II, the Sudakov form factor gives us the probability of no branching to occur in a given interval, so it is the natural candidate for generating random values of Δt. Writing the Sudakov from Eqn. (4.17) in terms of the probability of splitting in the interval $\mathcal{P}(\Delta t)$, in a given interval Δt

$$\mathcal{P}(\Delta t) = \frac{\Delta(t)}{\Delta(t_0)} = \exp\left(-\Delta t \int_\epsilon^{1-\epsilon} dz\, P_{gg}(z)\right) \tag{6.1}$$

then it is trivial to rewrite the equation in terms of Δt, and generate a random number in the interval $\mathcal{P}(\Delta t) = \mathcal{R} \in [0, 1]$, to obtain a random interval in which we can expect a new splitting

$$\Delta t = -\frac{\ln(\mathcal{R})}{\int_\epsilon^{1-\epsilon} dz\, P_{gg}(z)}. \tag{6.2}$$

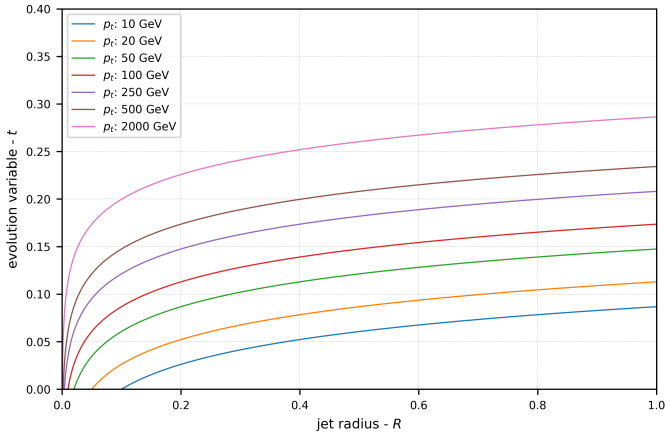

Figure 6.1: Maximum values of the evolution variable t for vacuum showers, plotted up to $p_t\, R > Q_0$. The strong coupling is set constant $\alpha_s = 0.1184$ and $Q_0 = 1GeV$. Not that most values of t are well below 0.4.

The expected splitting interval must be calculated for all the available partons. The parton which generates the smallest interval Δt is then expected to split first and will be the parton selected for splitting in our Monte-Carlo.

Algorithm 1 represents how our Monte-Carlo samples random evolution intervals, select a splitting parton, and imposes the boundary conditions of the evolution variable to determine when the terminate the shower. The general method outlined here is valid for all the vacuum programs, but Eqn. (6.2) is only valid for gg-branchings.

Algorithm 1 Evolution boundaries

1: calculate $t_{\max}$,

$$t_{\max} = \frac{\alpha_s}{\pi} \ln \frac{Rp_t}{Q_0}$$

2: **while** $t < t_{\max}$ **:**
3: **for** parton **in** AllPartons **:**
4: calculate expected splitting interval.

$$\Delta t = -\frac{ln(\mathcal{R})}{\int_\epsilon^{1-\epsilon} dz\, P_{gg}(z)}$$

5: select the parton with shortest interval, $\Delta t_{\min} = \min(\Delta t)$
6: evolve the angle $t = t + \Delta t_{\min}$.

6.2 Managing quarks and gluons

When creating a program with both quarks and gluons, the interval Δt must be advanced based on the type of parton being split. When splitting a gluon the interval will evolve according to the Sudakov given in Eqn. (4.22), and when splitting quarks the Sudakov is Eqn. (4.23). The

branching probabilities are then calculated from the following equations

$$\mathcal{P}_g(\Delta t) = \exp\left(-\Delta t \int_\epsilon^{1-\epsilon} \left[P_{qg}(z) + P_{gg}(z)\right]\, dz\right) \tag{6.3}$$

$$\mathcal{P}_q(\Delta t) = \exp\left(-\Delta t \int_\epsilon^{1-\epsilon} P_{qq}(z)\, dz\right). \tag{6.4}$$

The question that remains is how to determine the splitting vertex when this parton is a gluon, as it can split with two different vertices. This can be done by comparing the contribution of the two vertices have on the available phase space

$$W_{gg} = \frac{\int_\epsilon^{1-\epsilon} P_{gg}(z)\, dz}{\int_\epsilon^{1-\epsilon} \left[P_{qg}(z) + P_{gg}(z)\right]\, dz}. \tag{6.5}$$

If the splitting parton is a gluon, we need to roll a random number $\mathcal{R} \in [0, 1)$, if the value $\mathcal{R} < W_{gg}$, we will use the gg vertex, and if $\mathcal{R} \geq W_{gg}$ it will be the qg vertex. When setting $\epsilon = 10^{-3}$, the value is $W_{gg} \approx 0.96$, so the vast majority of gluon splittings will be done via the gg vertex.

A similar comparison could have been done for the relative contributions on the total phase space for quarks and gluons, but this is already implemented into the calculations for $\mathcal{P}_q(\Delta t)$, and $\mathcal{P}_g(\Delta t)$, so this is not necessary.

6.3 Sampling from the vacuum splitting functions

The process of evolving the evolution variable, and selecting which parton and what vertex to use for each splitting, has now been outlined. The final piece of the Monte-Carlo puzzle is to determine how to sample random energy fractions from the splitting functions. This can be done if we consider the probability density of obtaining a parton with momentum fraction z as

$$\mathcal{P} = \frac{P_{ba}(z)}{\int_\epsilon^{1-\epsilon} dz\, P_{ba}(z)}. \tag{6.6}$$

The probability $\mathcal{P}$ can then be replaced with a randomly generated number, and the momentum fraction of the branched parton can be calculated from

$$\mathcal{R} \int_\epsilon^{1-\epsilon} dz\, P_{ba}(z) = \int_\epsilon^{y} dz\, P_{ba}(z). \tag{6.7}$$

where $\mathcal{R} \in [0, 1]$ [15]. Note that since the splitting function is present on both sides of the equation, we can disregard any color and symmetry factors when calculating the splitting value, as they will not impact the final sample.

When trying to solve Eqn. (6.7) for the different splitting functions, we will find that not all of them can be solved for a general momentum-fraction y, and we need to introduce the Metropolis-Hastings algorithm for sampling them correctly [23]. The Metropolis-Hastings algorithm requires two different distributions,

1) A target distribution $P(x)$, which is the one we are trying to sample.

2) A proposal distribution $f(x)$ proportional to $\mathcal{P}(x)$.

The target distribution is naturally the full splitting function we are trying to sample. The proposal function will then be a *dummy* splitting function, which is similar in shape to the full splitting function. Once these are chosen the Metropolis-Hastings algorithm is executed according to Algorithm 2,

Algorithm 2 Metropolis-Hastings

1: sample a random value x' from $f(x)$.
2: calculate the acceptance probability,

$$A(x') = \min\left(1,\ \frac{P(x')}{f(x')}\right)$$

3: generate a random number $\mathcal{R} \in [0, 1]$.
4: **if** $\mathcal{R} \leq A(x')$ **:**
accept the value $x = x'$
5: **else if** $\mathcal{R} > A(x')$ **:**
reject the value x'

Sampling from the gg vertex

When trying to solve Eqn. (6.7) for the $P_{gg}(z)$ splitting function in Eqn. (3.19), it is difficult to obtain an exact value of y. It is therefore convenient to use the simplified splitting function of Eqn. (4.9) such that Metropolis-Hastings algorithm can be utilized. Excluding the color factor as it immediately cancels in the following calculation it can be written as

$$P_{gg}^{\text{dummy}}(z) = \frac{1}{z(1-z)} \tag{6.8}$$

and evaluating Eqn. (6.7) to obtain a way of sampling values from this simplified splitting function. The integral is straightforward to execute

$$\begin{aligned}
\mathcal{R}\int_{\epsilon}^{1-\epsilon} dz\,\frac{1}{z(1-z)} &= \int_{\epsilon}^{y}\frac{1}{z(1-z)} \\
\mathcal{R}\left[\ln\left(\frac{1-\epsilon}{\epsilon}\right)+\ln\left(\frac{1-\epsilon}{\epsilon}\right)\right] &= \ln\left(\frac{y}{1-y}\right)+\ln\left(\frac{1-\epsilon}{\epsilon}\right) \\
2\,\mathcal{R}\left[\ln\left(\frac{1-\epsilon}{\epsilon}\right)\right] &= \ln\left(\frac{y}{1-y}\frac{1-\epsilon}{\epsilon}\right)
\end{aligned} \tag{6.9}$$

exponentiating both sides of the equation

$$\begin{aligned}
\frac{y}{1-y}\frac{1-\epsilon}{\epsilon} &= \left(\frac{1-\epsilon}{\epsilon}\right)^{2\mathcal{R}} \\
\frac{y}{1-y} &= \left(\frac{1-\epsilon}{\epsilon}\right)^{2\mathcal{R}-1} \\
y &= \frac{\left(\frac{1-\epsilon}{\epsilon}\right)^{2\mathcal{R}-1}}{1+\left(\frac{1-\epsilon}{\epsilon}\right)^{2\mathcal{R}-1}}
\end{aligned} \tag{6.10}$$

and simplifying, gives an expression which can be used to randomly generate parton energy fractions from the simplified splitting function

$$y(\mathcal{R}) = \frac{\xi}{1+\xi} \qquad \text{for,} \quad \xi = \left(\frac{1-\epsilon}{\epsilon}\right)^{2\mathcal{R}-1}. \tag{6.11}$$

Applying the Metropolis-Hastings algorithm by sampling the dummy splitting function according to Eqn. (6.11), we can generate a plot of the original histogram, compared to the Metropolis-Hastings correction. This gives us a good idea of how the correction works and allows us to demonstrate how this simple algorithm allows us to sample more complex functions. The resulting plot is given in Figure 6.2.

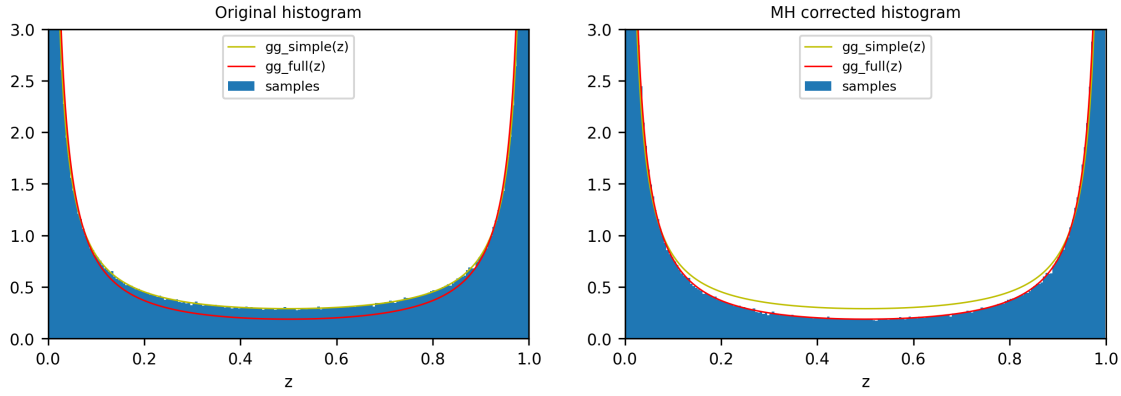

Figure 6.2: Probability density of the full $P_{gg}(z)$ splitting function and the dummy splitting function $P_{gg}^{\text{dummy}}(z)$. The left plot gives the values sampled from Eqn. (6.11),and the right plot is corrected using Metropolis-Hastings algorithm. Simulated with 10^6 samples, and a MH acceptance rate of 0.87.

Sampling from the qg vertex

Now we will find a way of sampling random values from the $P_{qg}(z)$ splitting function given by Eqn. (3.20). In contrast to the other splitting functions, this one is actually not divergent such that ϵ can be set equal zero. Solving Eqn. (6.7) for $P_{qg}(z)$,

$$\begin{aligned}
\mathcal{R}\int_0^1 P_{qg}(z)dz &= \int_0^y P_{qg}(z)dz \\
\frac{2}{3}\mathcal{R} &= \left[y - y^2 + \frac{2}{3}y^3\right] \\
\frac{2}{3}\mathcal{R} &= y - y^2 + \frac{2}{3}y^3 \\
0 &= \frac{2}{3}y^3 - y^2 + y - \frac{2\mathcal{R}}{3}
\end{aligned} \tag{6.12}$$

This is a cubic formula. Setting $d = \frac{2\mathcal{R}}{3}$, we can throw Eqn. (6.12) into WolframAlpha, and find the single real root to be,

$$y \approx 0.5 + 0.5\left[(36d^2 - 24d + 5)^{1/2} + 6d - 2\right]^{1/3} - \frac{0.5}{\left[(36d^2 - 24d + 5)^{1/2} + 6d - 2\right]^{1/3}} \tag{6.13}$$

It is therefore possible to sample randomly without using the Metropolis-Hastings algorithm. An argument could be made that it takes more time for python to calculate the value of this polynomial, than it would to generate a MH corrected value from a simpler function, but this allows for some interesting variation in how we determine our splitting values. The histogram of random samples generated, versus the exact splitting density given by Figure 6.3.

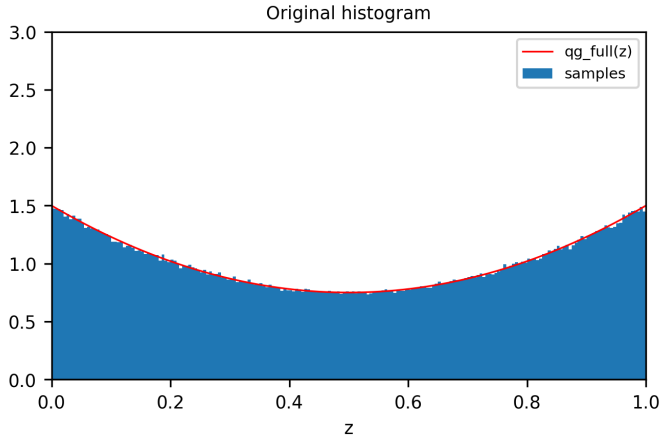

Figure 6.3: Probability density of the full $P_{qg}(z)$ splitting function, and the histogram of sampled values using Eqn. (6.13). Simulated with 10^6 samples.

Sampling from the qq vertex

Next up we will attempt to solve Eqn. (6.7) for the $P_{qq}(z)$ splitting function of Eqn. (3.21)

$$\begin{aligned}
\int dz \hat{P}_{qq}(z) &= \int \left(\frac{1+z^2}{1-z}\right) dz \\
&= \int -(z-1)\, dz - \int \frac{2z}{z-1}\, dz \\
&= \int (1-z)\, dz - \int \frac{2(u+1)}{u}\, du \qquad \text{, where } u = z-1 \\
&= -\int (z+1)\, dz - \int \frac{2}{u}\, du \\
&= -\frac{z^2}{2} - z - 2\ln(z-1)
\end{aligned} \tag{6.14}$$

since this integral has an exact solution, we can solve Eqn. (6.7) for this splitting function:

$$\frac{y^2}{2} + y + \ln\left(\frac{y-1}{\epsilon-1}\right)^2 = -\left(\mathcal{R}\frac{6\epsilon-3}{2} + \frac{-\epsilon^2-4\epsilon}{2}\right) - \ln\left(\frac{1-\epsilon}{\epsilon}\right)^{2\mathcal{R}}. \tag{6.15}$$

This equation is however difficult to solve, so we will need to use the Metropolis-Hastings algorithm once again. Attempting with a dummy function

$$P_{qq}^{\text{dummy}}(z) = \frac{-2}{z-1} \tag{6.16}$$

then Eqn. (6.7) becomes

$$\begin{aligned}
\mathcal{R}\left[-2\ln(z-1)\right]_{\epsilon}^{1-\epsilon} &= \left[-2\ln(z-1)\right]_{\epsilon}^{y} \\
\mathcal{R}\left(-2\ln((1-\epsilon)-1)+2\ln(\epsilon-1)\right) &= \left(-2\ln(y-1)+2\ln(\epsilon-1)\right) \\
\mathcal{R}\ln\left(\frac{1-\epsilon}{\epsilon}\right) &= -\ln(y-1)+\ln(\epsilon-1) \qquad (6.17)
\end{aligned}$$

rearranging terms and exponentiating both sides

$$\begin{aligned}
\ln(y-1) &= \ln(\epsilon-1) - \ln\left(\frac{1-\epsilon}{\epsilon}\right)^{\mathcal{R}} \\
y &= \frac{\epsilon-1}{(\frac{1-\epsilon}{\epsilon})^{\mathcal{R}}} + 1. \qquad (6.18)
\end{aligned}$$

Eqn. (6.18) can be used for sampling random values from the simple qq splitting function, and following the same procedure as in Section 6.3 we can implement Metropolis-Hastings algorithm for sampling random values from the full qq splitting function. The results of both the original samples, and the MH corrected histogram is given in Figure 6.4.

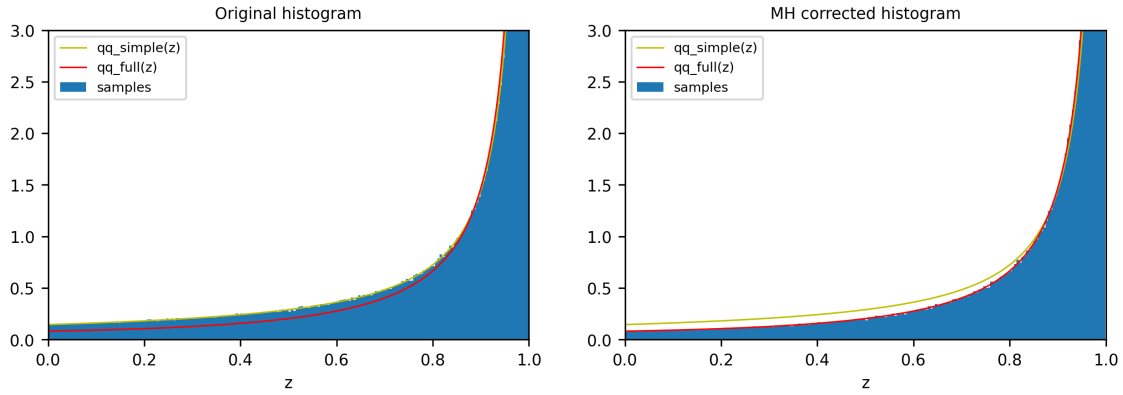

Figure 6.4: Probability density of the full $P_{qq}(z)$ splitting function and the dummy splitting function $P_{qq}^{\text{dummy}}(z)$. The left plot gives the values sampled from Eqn. (6.18),and the right plot is corrected using Metropolis-Hastings algorithm. Simulated with 10^6 samples, and a MH acceptance rate of 0.89.

6.4 Monte-Carlo implementation

This section serves to give a brief overview of the logical structure of the main *generate_shower* subprogram, which is the core of the parton-shower programs. This is where all of the actual physics is applied, while the rest of the program is for plotting, defining variables, and managing parent/daughter relations.

The full code for running the different parton shower programs, and Metropolis-Hastings algorithms is available on the authors GitHub [24]. The main loop running in the shower program is given here in Algorithm 3. Not all parameters are listed here, as to keep the representation as simple as possible.

Algorithm 3 generate_shower main loop

```
1: while len(SplittingPartons > 0 :
2:     SplittingParton, Δt = select_splitting_parton()
3:     t = t + Δt
4:     end_shower = loop_status(t, t_max)
5:     if end_shower :
6:         break
7:     SplittingPartons.remove(SplittingParton)
8:     FinalList.remove(SplittingParton)
9:     z = SplittingParton.split()
10:    for j in range(0,2) :
11:        if j==0 :
12:            NewParton = Parton(t, xz)
13:        else if j==1 :
14:            NewParton = Parton(t, x(1 − z))
15:    Shower0.FinalList.append(NewParton)
16:    if NewParton.InitialFrac > z_min ∼ 0.001 :
17:        SplittingPartons.append(NewParton)
18: return Shower
```

6.5 Results for vacuum showers

The mathematics and structure of the Monte-Carlo programs have now been presented, and we are therefore ready to examine the resulting distributions. For the vacuum programs, we are primarily interested in the inclusive parton, or inclusive energy distributions, given in terms of the momentum-fraction z_i of the different partons.

Results for gluon showers in vacuum

Starting by looking at the results for the parton shower with gluons in vacuum, where the inclusive energy distribution $D(x,t)$ is generated using using the simplified splitting function Eqn. (6.8). The results can be compared with the solution of the DGLAP equations which we obtained in Eqn. (4.38), valid in the small x limit, the resulting plot is given in Figure 6.5.

The Monte-Carlo generated distribution plotted in Figure 6.5 is in fairy good agreement with the analytical results for large values of the evolution variable t, and small values of the momentum x. This as expected as the solution is only valid for small values of x where $\ln \frac{1}{x} >> t$.

Results for quarks-, and gluons showers in vacuum

Turning to the Monte-Carlo for both quarks and gluons in vacuum, generated using the full splitting functions and sampled using the Metropolis-Hastings algorithm. This time there is no analytical results to compare with, but we can compare the inclusive parton distributions $f(x,t)$, of quark-initiated and gluon-initiated showers. The resulting plot is given in Figure 6.6. The final distributions contains both quarks and gluons, and the difference between them is simply the type of the initial parton. The hardest parton of each shower is also plotted using dotted lines, and it is simply determined by taking the parton with the highest momentum once the shower has terminated, and plotting its z value.

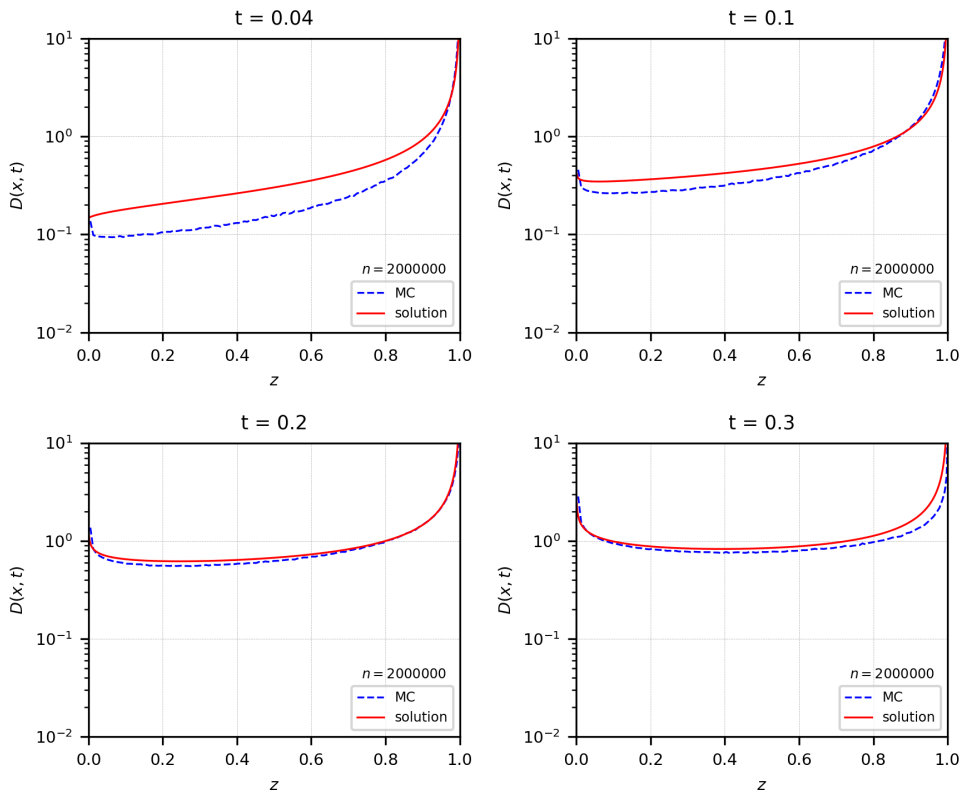

Figure 6.5: The inclusive energy distribution $D(x,t)$ for gluon showers in vacuum. The red line is the analytical solution obtained in Eqn. (4.38). The blue dotted line is the generated values by running $n = 2 \cdot 10^6$ showers in a Monte-Carlo program, using the dummy splitting function Eqn. (6.8). Parameters used are $\epsilon = 10^{-3}$ and $z_{\min} = 10^{-3}$

.

There are several observations to be made from Figure 6.6. Firstly the distribution of the hardest parton of each shower is the same as the inclusive distribution for values above $z < \frac{1}{2}$. This will be explored in more detail when we discuss leading partons in Chapter IV. Secondly, the impact the initial parton has on the distribution is significant, this is related to the expected branching intervals, and we will discuss it shortly.

An initial check of the validity of the program can be done by comparing with the results of [12, Figure 2.], in which the inclusive distribution has been plotted for fixed values of the evolution variable, $t = 0.04, 0.1, 0.2, 0.3$. While [12] discusses a slightly different approach, where the evolution goes from $R < \theta < 1$, meaning they obtain the total number of microjets within a given jet, as opposed to our treatment where we are looking for the parton distribution inside a jet with radius R such that, $Q_0/p_t < \theta < R$. The result can however be compared as long as the evolution goes over the same effective angle, as is the case when we are plotting with the same values of t. Our results are therefore in good agreement with [12].

More explicit calculations can be done for checking the validity of our results. From the DGLAP equation on integral form Eqn. (4.21), there is a term $\Delta(t)\, f(x, t_0)$, which represents the probability of no branching to occur at all for the initial parton during the interval $t \in [t_0, t_{max}]$. This can be calculated from Eqn. (6.1) for initial gluons, except now we know the value of Δt, and need to take into account the possibility of the gluon to branch into a gg-pair or a $q\bar{q}$-pair.

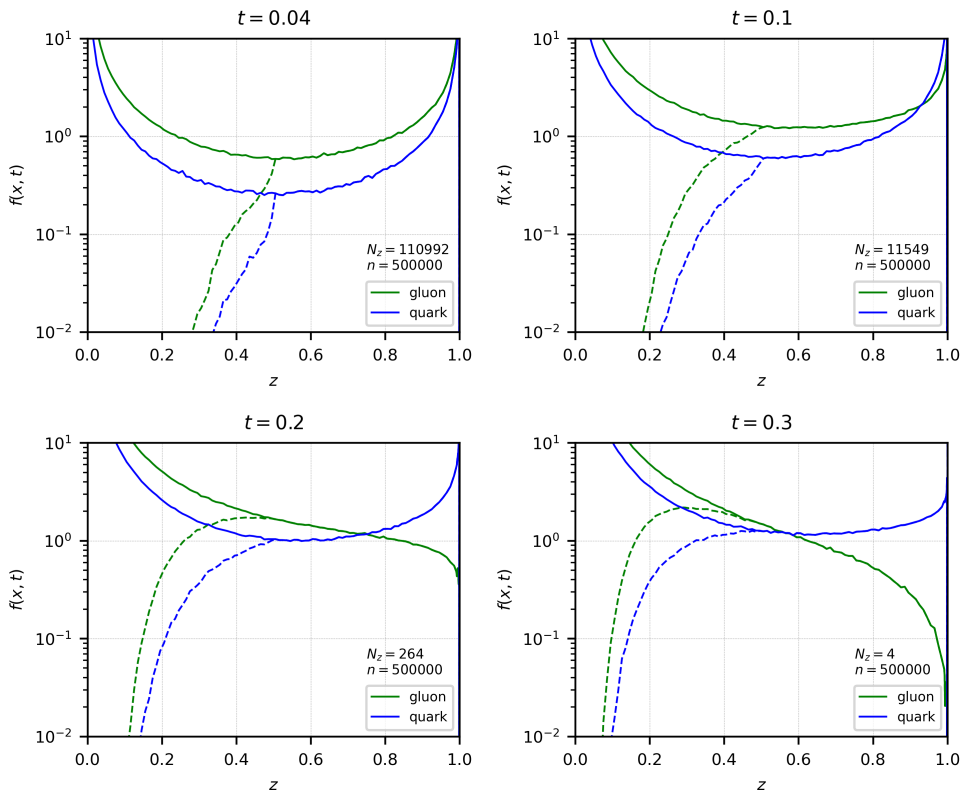

Figure 6.6: The inclusive parton distribution $f_i(x,t)$ for quarks and gluons in vacuum, generated by the Monte-Carlo program with both quarks and gluons in vacuum, using the full splitting functions. The solid lines show the inclusive parton distribution for initial quarks (blue) and initial gluons (green). The dashed lines show the hardest parton of each shower. Simulated with $n = 5 \cdot 10^5$ showers for both initial quark and initial gluon. Parameters used are $\epsilon = 10^{-3}$ and $z_{\min} = 10^{-3}$. The number of gluons N_z with $z = 1$ is printed on each of the plots.

The probability is then given as

$$\mathcal{P}(t) = \exp\left(-t \int_{\epsilon}^{1-\epsilon} dz \, (P_{gg}(z) + P_{qg}(z))\right). \tag{6.19}$$

Using the same values for t and ϵ as in the plot:

$$\begin{aligned} \mathcal{P}(0.04) &\approx 2.22 \cdot 10^{-1} \\ \mathcal{P}(0.1) &\approx 2.32 \cdot 10^{-2} \\ \mathcal{P}(0.2) &\approx 5.40 \cdot 10^{-4} \\ \mathcal{P}(0.3) &\approx 1.25 \cdot 10^{-5}. \end{aligned} \tag{6.20}$$

These probabilities should manifest themselves in our plot, and we can find them by simply counting the number of partons N_z with momentum $z = 1$ in the final distribution for each

value of t. The values for N_z is given in Figure 6.6, and correspond to the following probabilites:

$$\begin{aligned}
\mathcal{P}_{\text{MC}}(t=0.04) &= \frac{N_z(0.04)}{N} = \frac{110992}{510^5} \approx 2.22 \cdot 10^{-1} \\
\mathcal{P}_{\text{MC}}(t=0.1) &= \frac{N_z(0.1)}{N} = \frac{11549}{510^5} \approx 2.31 \cdot 10^{-2} \\
\mathcal{P}_{\text{MC}}(t=0.2) &= \frac{N_z(0.2)}{N} = \frac{264}{510^5} \approx 5.28 \cdot 10^{-4} \\
\mathcal{P}_{\text{MC}}(t=0.3) &= \frac{N_z(0.3)}{N} = \frac{4}{510^5} \approx 8 \cdot 10^{-6}.
\end{aligned} \tag{6.21}$$

We can see that the probabilities given from the calculation of the Sudakov in Eqn. (6.20) is in reasonable good agreement with the probabilities we find when running $5 \cdot 10^5$ showers and counting N_z in Eqn. (6.21) - which should be expected as the Sudakov form factor is used both for the calculation, and in the Monte-Carlo.

It could be argued that the results generated by the quarks and gluons cascade are more accurate than the gluon cascade, as there is no reason for a gluon not to branch into a $q\bar{q}$-pair[4]. It would therefore be interesting to compare the distribution of the pure gluon shower in vacuum as given in Figure 6.5, with the showers initiated by a gluon as given in Figure 6.6. The resulting plot is given in Figure 6.7.

The plot given here is a straight-up comparison of the two programs. It is therefore important to note that the splitting functions are not identical as the gluon showers is using the simplified splitting function which does not carry any color factors. This is apparent when examining the integrals over the different splitting functions, using $\epsilon = 10{-}3$:

$$\begin{aligned}
\int_\epsilon^{1-\epsilon} P_{gg}^{\text{simple}}(z)\, dz &\approx 13.8 \\
\int_\epsilon^{1-\epsilon} P_{gg}(z)\, dz &\approx 36.0 \\
\int_\epsilon^{1-\epsilon} P_{qg}(z)\, dz &\approx 1.7 \\
\int_\epsilon^{1-\epsilon} P_{qq}(z)\, dz &\approx 16.4.
\end{aligned} \tag{6.22}$$

Since the expected splitting intervals are inversely proportional to these integrals, it is to be expected that the gluon showers using the simplified P_{gg}^{simple} splitting function, would be going slower toward small momentum values. If we were to adjust the simplified splitting function such that the expected intervals of gg branchings were identical, then the gluon-only distribution would go faster towards low momentum values than the gluon initiated showers with both quarks and gluons.

There are two reasons for this. The first is that gluons can split using either the $P_{gg}(z)$ or $P_{qg}(z)$ splitting function, the second is that when we inevitably observe a qg splitting, those new quarks will split much slower than gluons. Both of these properties are direct consequences of how the branching intervals are calculated. We can check for this behavior by simply adding

[4] It is however significantly less likely for than $g \to gg$ branchings, for our program about $\sim 4\%$ of the gluon branchings are $g \to q\bar{q}$

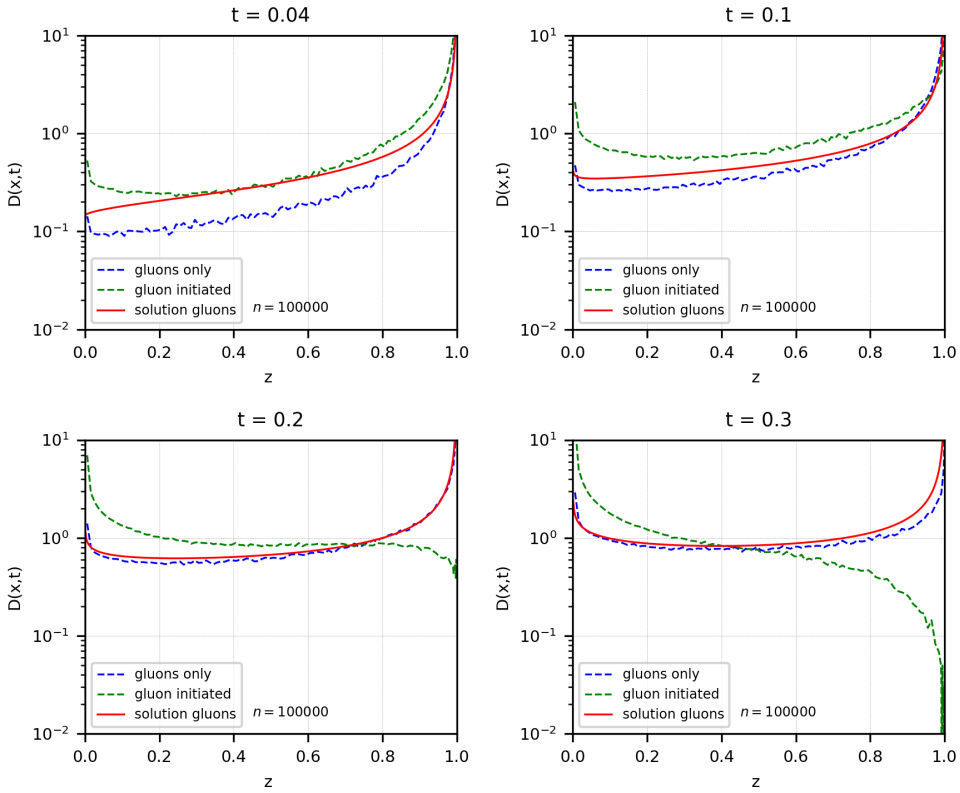

Figure 6.7: The inclusive energy distribution $D(x,t)$ generated by both Monte-Carlo programs: gluons in vacuum (blue), and quarks-and-gluons in vacuum, initiated by a gluon(green). The red line is the analytical solution of the DGLAP equation obtained in Eqn. (4.38) for gluons, which is only valid in the small x and large t limits. Simulated with $n = 10^5$ showers, using $\epsilon = 10^{-3}$ and $z_{\min} = 10^{-3}$.

a fictitious color factor $C \sim 2.6$ to the simplified splitting function such that

$$\int_{\epsilon}^{1-\epsilon} C P_{gg}^{\text{simple}}(z)dz \approx \int_{\epsilon}^{1-\epsilon} P_{gg}(z)dz. \tag{6.23}$$

The two distributions with this new factor is given in Figure 6.8. It is now apparent that the gluon showers is going faster towards small momentum values, as there are no quarks to slow down the splitting process. The difference in color factors does not affect the splitting values in the same manner, as those are calculated by two integrals over the splitting function, meaning the constant factors simply cancel each other out.

Validity of our Monte-Carlo in vacuum

The Monte-Carlo programs developed for vacuum cascades has now been under scrutiny, so lets quickly summarize the findings.

1. The results of the Monte-Carlo gluon cascade was compared with the analytical solution calculated in Section 4.4 and was in good agreement in the small x large t limit, as expected.

2. The inclusive distribution generated by gluon-initiated and quark-initiated showers, was visually compared with the results presented in [12], and we can see that the results were

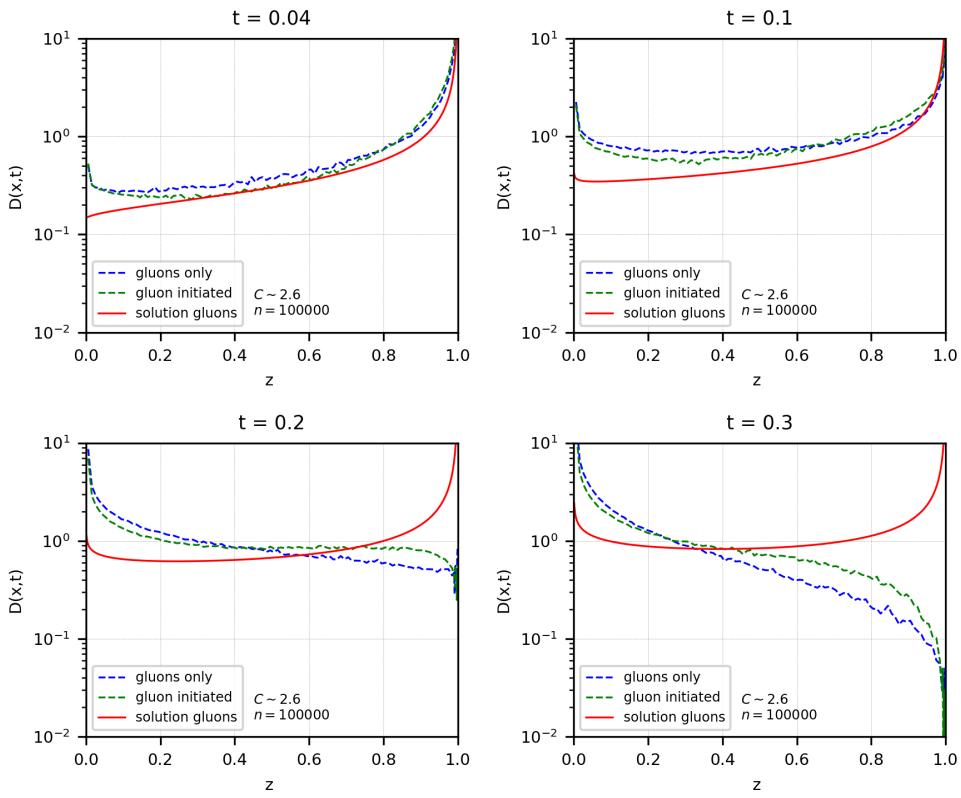

Figure 6.8: The inclusive energy distribution $D(x,t)$ generated by both Monte-Carlo programs. Blue: gluons in vacuum, but with a fictitious color factor $C \sim 2.6$ added to the simplified splitting function such that the expected branching interval of gluons are the same. Green: quarks-and-gluons in vacuum, initiated by a gluon. The red line is the analytical solution of the DGLAP equation obtained in Eqn. (4.38) for gluons, which is only valid for gluons and in the small x and large t limits. Simulated with $n = 10^5$ showers, using $\epsilon = 10^{-3}$ and $z_{\min} = 10^{-3}$.

visually identical.

3. The number of initial partons which do not branch in the interval $[t_{\min}, t_{\max}]$ was calculated from the Sudakov form factor for initial gluons, and compared with the Monte-Carlo for quarks and gluons. The numbers were of similar order.

4. The behaviour of the gluon cascade was compared with the quarks and gluons cascade. This was done by highlighting how adjusting for the expected branching intervals, still yielded different distributions. This was attributed to the addition of quarks in the shower, which generally makes it go slower towards small values.

While no formal comparison has been done with the results of well established event generators such as PYTHIA [25], the discussion presented here should spark confidence in our simple parton shower generator.

7 Monte-Carlo for Parton Branching in Medium

When developing a Monte-Carlo program for medium cascades, we will be restricting ourselves to gluons in medium, and use the simplified medium splitting function, or reduced kernel. This is done such that we can compare our results with the analytical solution for the in-medium kinetic rate equation, and examine the properties of leading-parton cascades. The process of creating a parton shower program for both quarks and gluons in medium, would follow the same structure as in the previous section, but we will limit ourselves to gluons in this thesis.

7.1 Evolution interval

As discussed in Section 5.2, the medium cascade evolves according to the actual time, and the characteristic time is simply the time it takes for the initial parton to radiate most of its energy into soft gluons. We will be evolving the cascades using the variable $\tau = t/t_*$, which was defined in Eqn. (5.12). It is therefore not a hard cutoff for the medium cascade but serves more as an indication of how long the cascades can evolve, and it is an important property that will affect our expectations for different values of τ. There is therefore no upper limit on the value of τ in our medium evolutions, but since most of the energy has disappeared into soft gluons ($z < 0,001$) at $\tau \sim 1$, we might as well set this as an approximate boundary,

$$0 < \tau \lessapprox 1. \tag{7.1}$$

Determining the probable branching interval Δt can again be done from the Sudakov form factor, introduced for the medium evolution in Eqn. (5.14), following the procedure presented in Section 6.1. Doing this in terms of τ, such that $\Delta\tau = \Delta t/t_*$, and $\Delta t/t_*(x) = \Delta t/t_*\sqrt{x} = \Delta\tau/\sqrt{x}$, the evolution probability takes the form

$$\mathcal{P}(\Delta\tau) = \frac{\Delta(\tau_0)}{\Delta(\tau)} = \exp\left(-\frac{\Delta\tau}{\sqrt{x}}\int_\epsilon^{1-\epsilon} dz\, z\mathcal{K}(z)\right). \tag{7.2}$$

Exchanging the probability with a randomly generated number $\mathcal{R} \in (0,1)$

$$\Delta\tau = -\frac{\sqrt{x}\,\ln(\mathcal{R})}{\int_\epsilon^{1-\epsilon} dz\, z\mathcal{K}(z)} \tag{7.3}$$

and from the symmetry of the reduced kernel, we have $\int_0^1 dz\, z\mathcal{K}(z) = \frac{1}{2}\int_0^1 dz\mathcal{K}(z)$, and the probable evolution interval an therefore be written as

$$\Delta\tau = -\frac{2\sqrt{x}\ln(\mathcal{R})}{\int_\epsilon^{1-\epsilon} dz\mathcal{K}(z)}. \tag{7.4}$$

7.2 Sampling from the medium splitting function

The full medium splitting functions was introduced in Section 5.1 but it will be sufficient for our treatment of medium showers to use the reduced $\mathcal{K}_{gg}(z)$ splitting kernel, as given in Eqn. (5.7). A way of sampling the full splitting functions is available for the interested reader in Appendix B.

Sampling from the reduced kernel

Sampling from the reduced kernel presented in Eqn. (5.7) follows the same procedure as when sampling the vacuum splitting functions where we solved Eqn. (6.7). The integral of the reduced kernel is

$$\int_a^b \frac{1}{(z(1-z))^{3/2}} dz = \left[\frac{4z-2}{\sqrt{-z(z-1)}} \right]_a^b \tag{7.5}$$

and Eqn. (6.7) is then

$$\begin{aligned} \mathcal{R} \int_\epsilon^{1-\epsilon} dz \, \frac{1}{(z(1-z))^{3/2}} &= \int_\epsilon^y \frac{1}{(z(1-z))^{3/2}} \\ \mathcal{R}\left(\frac{2-4\epsilon}{\sqrt{\epsilon(1-\epsilon)}} - \frac{4\epsilon-2}{\sqrt{\epsilon(1-\epsilon)}} \right) &= \frac{4y-2}{\sqrt{-y(y-1)}} - \frac{4\epsilon-2}{\sqrt{-\epsilon(\epsilon-1)}} \\ \mathcal{R}\left(\frac{4-8\epsilon}{\sqrt{\epsilon(1-\epsilon)}} \right) - \frac{2-4\epsilon}{\sqrt{\epsilon(1-\epsilon)}} &= \frac{4y-2}{\sqrt{-y(y-1)}}. \end{aligned} \tag{7.6}$$

The term on the l.h.s can be written in terms of the integral again and assigned to a variable a

$$a = \int_\epsilon^{1-\epsilon} dz \left(\mathcal{R} - \frac{1}{2} \right) = \mathcal{R}\left(\frac{4-8\epsilon}{\sqrt{\epsilon(1-\epsilon)}} \right) + \frac{2-4\epsilon}{\sqrt{\epsilon(1-\epsilon)}} \tag{7.7}$$

using this a, the remainder of the equation can be solved using Mathematica

$$\begin{aligned} y &= \frac{16 + a^2 \mp a\sqrt{16+a^2}}{2(16+a^2)} \\ y &= \frac{1}{2} \mp \frac{a\sqrt{16+a^2}}{2(16+a^2)} \\ y &= \frac{1}{2} \mp \frac{a}{2\sqrt{16+a^2}}. \end{aligned} \tag{7.8}$$

And we now have a method for randomly sampling from the reduced kernel. The histogram of the randomly sampled values compared to the exact splitting function is given in Figure 7.1.

7.3 Monte-Carlo implementation

Creating the Monte-Carlo program for the medium showers follows generally the same procedure as in Section 6.4. As already discussed, we will restrict ourselves to gluons and the reduced kernel. There are some obvious differences, as we now need to generate evolution intervals from the in-medium rate Sudakov form factor from Eqn. (7.4), and need to sample from the reduced kernel Eqn. (7.8).

The other parameters are very similar, but we will need a lower limit for how soft gluon can split. This is particularly important for the medium cascade, as very soft gluons will barely evolve τ at all, due to the x dependence in the generated evolution interval, meaning the program would be incredibly slow without a x-limit.. This limit is simply introduced by not appending gluons with a momentum fraction less than $z = 10^{-3}$ to the list of splitting gluons. When the plots are made it is then important to keep in mind that we don't have precise data below this limit.

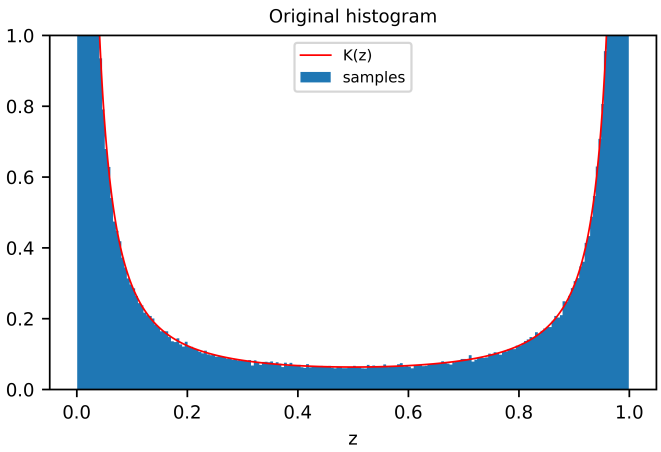

Figure 7.1: Probability density of the simplified $\mathcal{K}_{gg}(z)$ splitting kernel, and the histogram of sampled values using Eqn. (7.8). Simulated with 10^6 samples.

The final program is again available in the author's GitHub repository [24].

7.4 Results for gluon showers in medium

This section will be dedicated to verifying the results from our medium showers. Very similar to the vacuum programs we will compare the generated distributions with the analytical solution of the evolution equations, and other properties present will be highlighted using different plots.

We will now plot the inclusive energy distribution $D(x, \tau)$ from the Monte-Carlo parton shower, along with the analytical solution for the in-medium kinetic rate equation as obtained in Eqn. (5.33). It is important to keep in mind that this solution is only valid for the reduced kernel. The resulting plot is given with a linear scale in Figure 7.2. The Monte-Carlo results are in generally good agreement with the analytical solution.

For observing the scaling property of the medium evolution, we will plot the distribution for different values of τ, on a logarithmic scale. This is presented in Figure 7.3. The scaling properties of the medium evolution is apparent for large values of τ, as once the peak corresponding to the initial parton around $z = 1$ has disappeared, the flow of energy towards small x values seems to be constant. As we discussed in Section 5.1, the distribution changes in a uniform and shape-conserving way, once τ goes larger than $\tau \sim 1$.

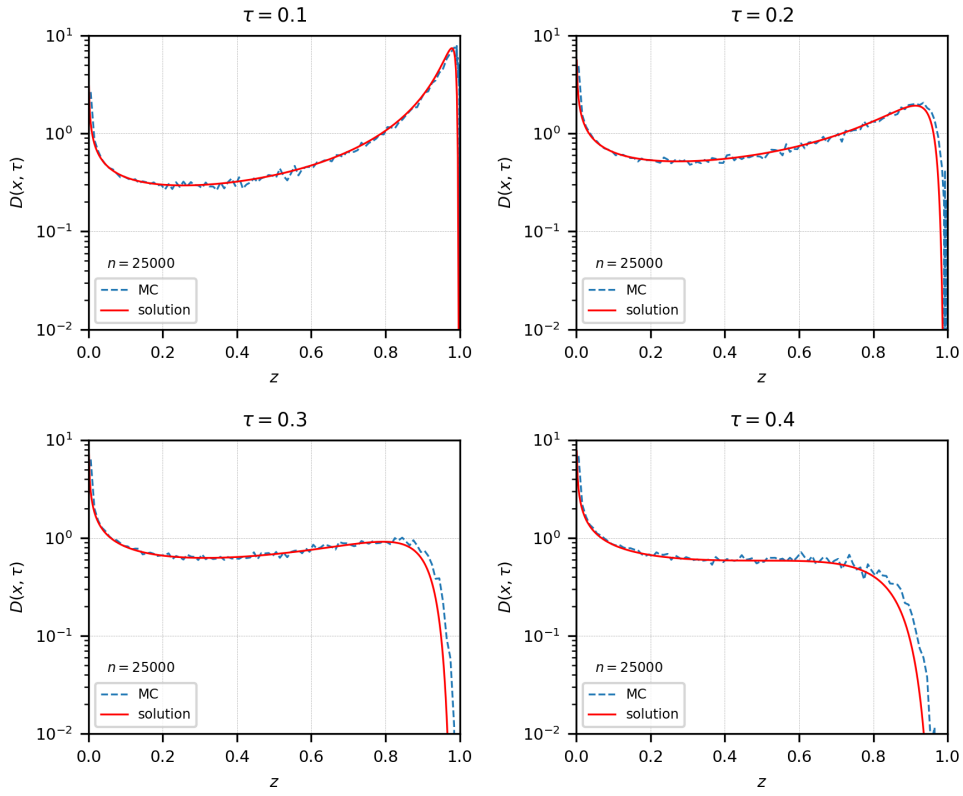

Figure 7.2: The inclusive energy distribution $D(x, \tau)$ as generated from the Monte-Carlo program for gluons in medium, using the reduced kernel. Simulated with $n = 2.5 \cdot 10^4$ showers, using $\epsilon = 10^{-3}$ and $z_{\text{min}} = 10^{-3}$. The distribution is compared with the analytical solution given in Eqn. (5.33).

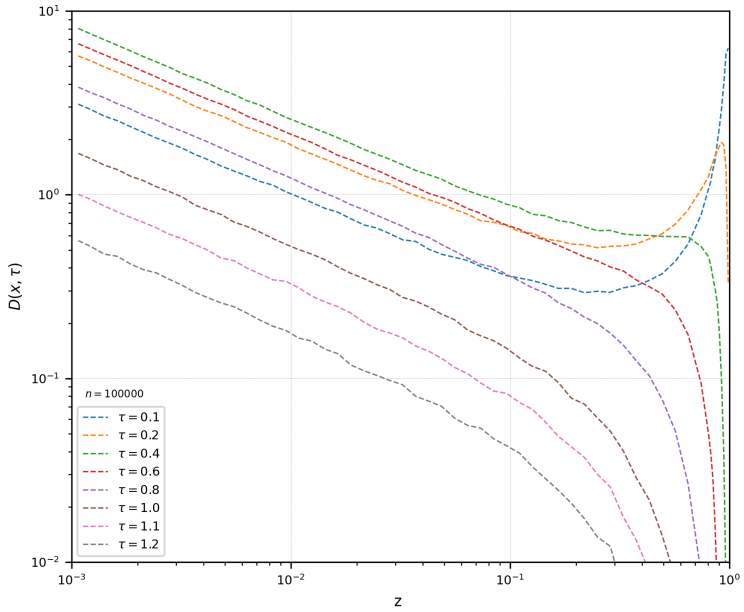

Figure 7.3: The inclusive energy distribution $D(x, \tau)$ as generated from the Monte-Carlo program for gluons in medium, using the reduced kernel. Simulated with $n = 10^5$ showers, using $\epsilon = 10^{-3}$ and $z_{\text{min}} = 10^{-3}$, for a wide range of values τ. The scaling property of the shower is apparent for values of $\tau > 1$.

Chapter IV

Leading Parton and Energy-Loss

While the preceding chapters had a natural flow where each new chapter built on the results of the previous one, this chapter will have a more stand-alone presentation. This is done so that the leading parton distribution, which to many is less familiar than the inclusive distribution, can have a more coherent and natural flowing discussion.

8 Leading Parton for Gluon Cascades

Starting by exploring a simple model of energy-loss, valid in the small x limit, and seeing how it compares to the leading parton distribution obtained from our Monte-Carlo program for gluons in medium. Then we will examine the behavior of the leading parton by using our Monte-Carlo to determine how often the leading parton remains on-branch in a given evolution. Finally we will attempt to derive an evolution equation for the leading parton, and solve it in Mellin space.

8.1 Energy-loss in the small x limit

We will now turn to the leading parton energy-loss for gluon cascades is medium. Rather than the shower depicted in Figure 2.3, we will now be following exclusively the leading parton of a given cascade, and consider all other partons simply as energy-loss ω_i. The softer partons may still branch independently and behave as usual, but we are only concerned with the leading parton. The energy fraction of the leading parton can therefore be stated as $x = \frac{E-\epsilon}{E} = 1 - \frac{\epsilon}{E}$, where the total energy-loss is $\epsilon = \sum_i \omega_i$. An illustration of this setup is given in Figure 8.1.

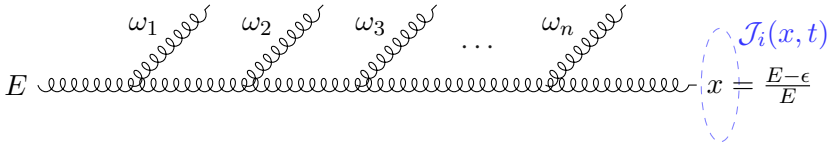

Figure 8.1: Illustration of the leading parton energy-loss, where all soft gluon radiation is treated as energy-loss.

The probability of emitting a total energy ϵ over an arbitrary number n of emissions, is given as [26–28]

$$D(\epsilon) = \sum_{n=0}^{\infty} \frac{1}{n!} \left[\Pi_{i=1}^{n} \int d\omega_i \frac{dI(\omega_i)}{d\omega} \right] \delta\left(\epsilon - \sum_{i=1}^{n} \omega_i \right) \exp\left(- \int_0^{\infty} d\omega \frac{dI}{d\omega} \right) \tag{8.1}$$

where n is the total number of emitted gluons, and $dI(\omega_i)/d\omega$ is the probability of emitting a single gluon with energy ω_i. The first term of Eqn. (8.1) is therefore the integral over all possible combinations of ω_i, such that $\epsilon = \sum_i^n \omega_i$, and then summed over the total number of emissions n. The second term is the integral over the medium-induced gluon spectrum $dI/d\omega$, defined in Eqn. (5.2), and serves to normalize the distribution as $\int_0^1 d\epsilon D(\epsilon) = 1$.

Eqn. (8.1) is valid when assuming the emission is soft $z << 1$, and that multiple emissions

happen independently. The solution of Eqn. (8.1) can be obtained in Mellin space, and is

$$D(\epsilon) \approx \frac{1}{\epsilon}\bar{\alpha}\sqrt{\frac{\omega_c}{2\epsilon}}\exp\left(-\pi\frac{\bar{\alpha}^2\omega_c}{\epsilon}\right) \tag{8.2}$$

where $\bar{\alpha} = \alpha_s N_C/\pi$. This is now an expression of the energy-loss, but we would like to write it in terms of the leading parton energy x, by replacing $\epsilon = E(1-x)$

$$D(x) \approx \bar{\alpha}\sqrt{\frac{\omega_c}{E^3(1-x)^3}}\exp\left(-\pi\frac{\bar{\alpha}^2\omega_c}{E(1-x)}\right). \tag{8.3}$$

Introducing τ as defined in Eqn. (5.12), variable, but setting the time equal the length of the medium, $t = L$, such that

$$\tau = \bar{\alpha}\sqrt{\frac{\hat{q}}{E}}\,L = \bar{\alpha}\sqrt{\frac{\omega_c}{E}} \tag{8.4}$$

then the solution can be written as,

$$D(x) \approx \frac{1}{E}\frac{\tau}{(1-x)^{3/2}}\exp\left(-\pi\frac{\tau^2}{1-x}\right). \tag{8.5}$$

This equation is strikingly similar to the solution of the in-medium kinetic rate equation for gluons obtained in Eqn. (5.33). The difference is that a factor $\sqrt{x}$ has been replaced by a factor E.

This solution may be plotted alongside the leading parton distribution obtained by our Monte-Carlo program for gluons in medium, using the reduced kernel, along with the solution of the in-medium kinetic rate equation presented in Section 5.4. The resulting plot is given in Figure 8.2,

From Figure 8.2 we can see that the solution given by Eqn. (8.5) is a very good agreement for values of $x > 0,8$, and decent for values $x > 0,5$. This is expected as the energy-loss distribution Eqn. (8.1) assumes all emissions to be soft. It should however motivate us to find model for the energy-loss distribution able to deal with harder gluon emissions.

8.2 Leading branches

Before attempting to modify the current evolution equations, or crating a whole new set of equations for describing the leading parton evolution, we must know more about how the distribution behaves. A key question is whether the leading branch in a given splitting, generally yields the hardest parton at the end of the cascade. The simplest model imaginable is illustrated in Figure 8.3 where the leading parton remains on the same branch for the entire evolution. In this scenario we could disregard the softest branch in every splitting, and just focus on the hardest branch.

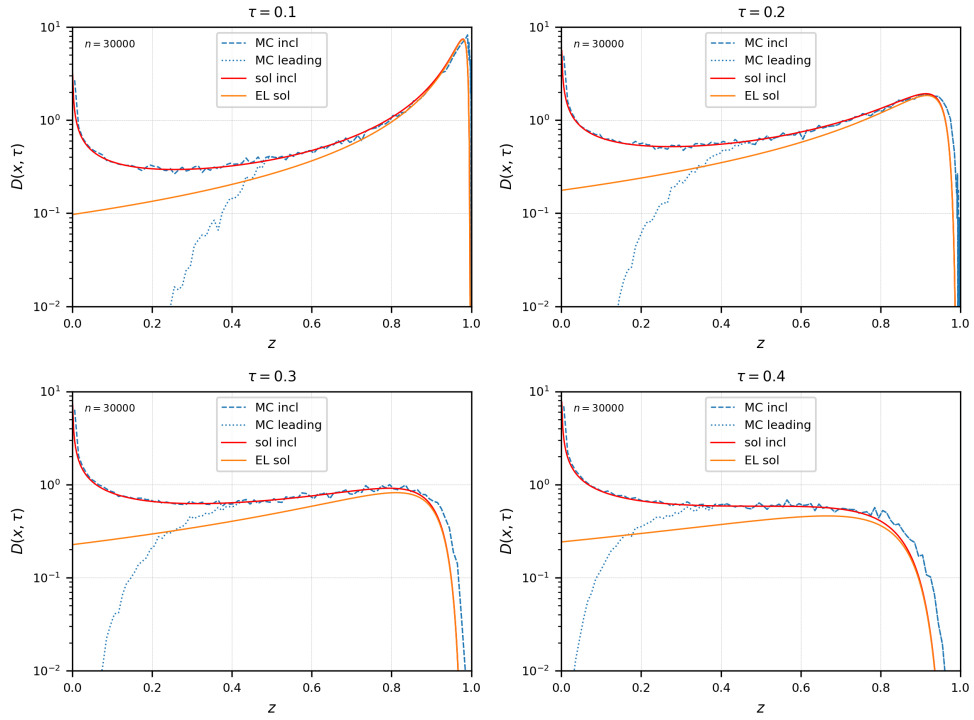

Figure 8.2: The inclusive energy distribution $D(x, \tau)$ as generated by the Monte-Carlo program for gluons in medium. The dotted line indicates the leading parton of each shower. Plotted alongside the analytical solution of the kinetic rate equation Eqn. (5.33), and the leading parton solution Eqn. (8.5). Simulated with $n = 3 \cdot 10^4$ showers, using $\epsilon = 10^{-3}$ and $z_{\min} = 10^{-3}$.

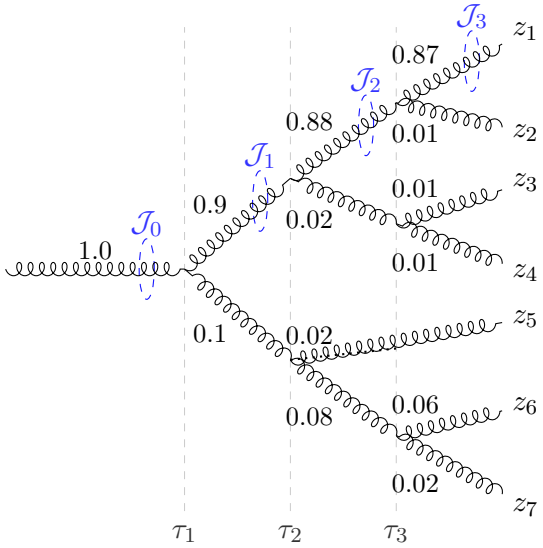

Figure 8.3: Illustration of the leading parton $\mathcal{J}_{\tau_i}$ remaining on the same branch for the entire evolution. The leading parton is therefore on-branch.

The other scenario is illustrated in Figure 8.4, where the leading parton at one time, is on a different branch than the leading parton at a later time. If this is how the evolution goes, it is important to keep track of every single branch following a splitting, to find the hardest parton. When the leading parton remains on the same branch throughout the cascade, we will call it

on-branch, when it changes branches we will call it *off-branch*.

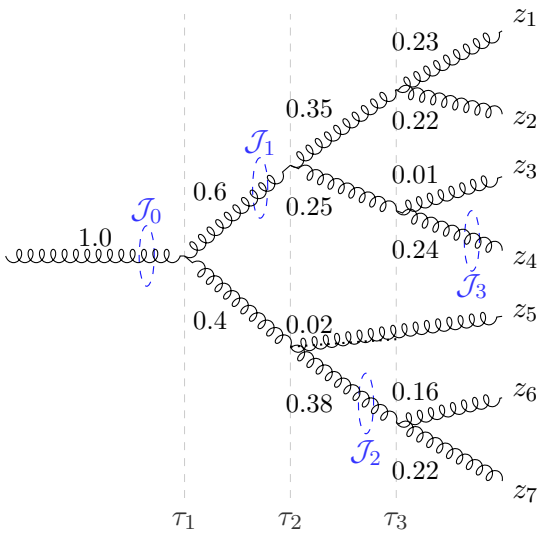

Figure 8.4: Illustration of the leading parton $\mathcal{J}_{\tau_i}$ changing what branch it on during the evolution, due to splittings where $z \to 0.5$. The leading is parton at the end of the evolution is therefore off-branch.

There is no precise formulation for how often the leading parton is off-branch, so it could be interesting to determine this by using our Monte-Carlo program for gluons in medium. This is implemented by picking the hardest parton at the end of the shower, and then iterating backwards through the evolution, to check that the hardest parton is the hardest leg of each splitting. The resulting plot for several different values of τ, where the leading on-branch partons are plotted separately from the leading off-branch partons, is given in Figure 8.5.

There are several notable results in Figure 8.5. Firstly, the off-branch leading partons are all confined to $z \lessapprox 0,5$. This is expected, since the shower requires either a splitting $z \sim 0,5$ for the leading parton to change branches during the evolution, or a very long evolution such that all partons are moving towards small values of x. The second property to note is how the percentage of leading on-branch partons, changes with the values of τ. This can be made more explicit my creating a plot of the fraction of on-branch leading partons, for a shower with given τ, as presented in Figure 8.6 with a second degree polynomial fit.

It is therefore important to take into account how often off-branch leading partons is expected when creating a new model for the evolution of the leading parton distribution. For small values of τ, where off-branch leading partons is rare, it can be viable to exclusively follow the leading parton in each vertex. For larger evolutions it is however necessary to take into account these off-branch leading partons.

8.3 Leading parton evolution equations in vacuum

When looking at Figure 6.6 which was generated for quarks and gluons in the vacuum cascade, there is an interesting observation to be made. The distribution of the leading parton is identical to the inclusive distribution for values of $z > 0.5$. This implies that the information we are looking for is already contained within the evolution equations - which makes sense as they are

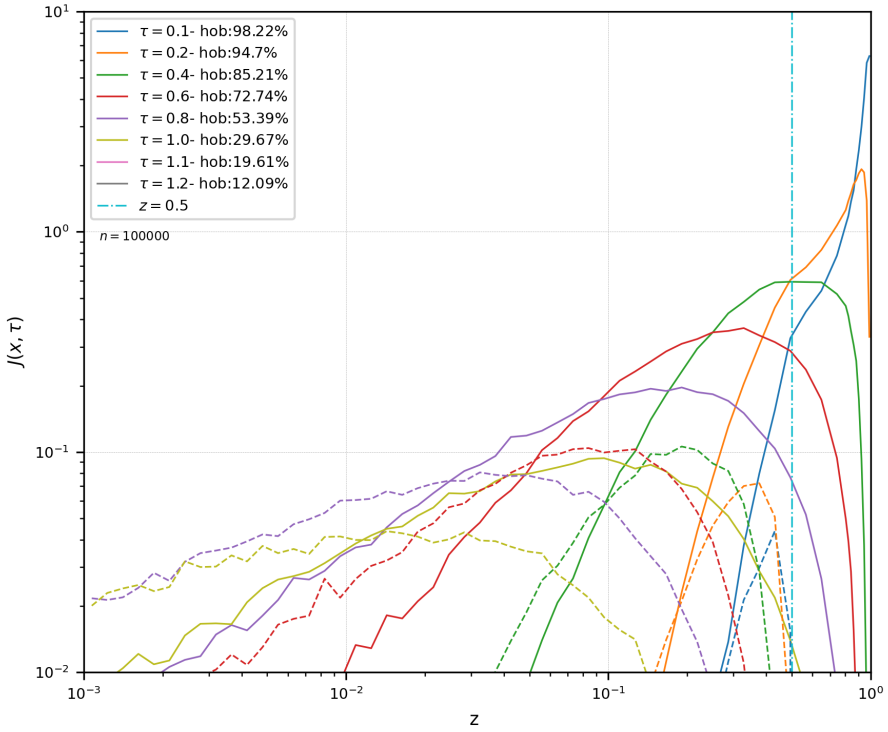

Figure 8.5: Leading partons of the medium cascade. The solid lines indicate that the leading parton is on-branch, while the dashed lines indicate that the leading parton is off-branch. Percentages of total number of leading partons on-branch for each value of τ is given in the legend. Simulated with $n = 10^5$ showers, using $\epsilon = 10^{-3}$ and $z_{\text{min}} = 10^{-3}$.Some of the values for τ are excluded from the plot, to make it more readable, but the percentages of hob (hardest on branch) is still given in the legend.

resumming all splittings which may occur. This should motivate us to make some adjustments to the current evolution equations, such that they follow exclusively the leading parton.

Derivation

In Section 8.2 we saw that the leading parton is predominantly on-branch up to values of $\tau \sim 0.5$. Keeping this in mind, we can attempt to find an alternate formulation of the evolution equations in vacuum, where we follow exclusively the leading parton in each vertex, and be confident of where these results should be valid.

The equations can be constructed in a manner similar to the DGLAP equation which we constructed in Appendix A, using generating functionals. We start with the functional $\mathcal{Z}(p, t = 0) = u(p)$, with the property $\frac{\delta u(p)}{\delta u(k)} = u(1 - \frac{k}{p})$, and normalization $\mathcal{Z}(p)|_{u=1} = 1$

$$\frac{\partial}{\partial t}\mathcal{Z}(p,t) = \int_0^1 dz\, P(z)\mathcal{Z}(zp)\mathcal{Z}((1-z)p) - \int_0^1 dz\, P(z)\mathcal{Z}(p) \tag{8.6}$$

but now we wish to adjust this to account for the leading partons, by changing the integration limits $0 \to 1/2$ and $1/2 \to 1$. The real term of Eqn. (8.6) can then be written as

$$\mathbb{R} = \int_0^{1/2} dz\, P(z)\mathcal{Z}(zp)\mathcal{Z}((1-z)p) + \int_{1/2}^1 dz\, P(z)\mathcal{Z}(zp)\mathcal{Z}((1-z)p) \tag{8.7}$$

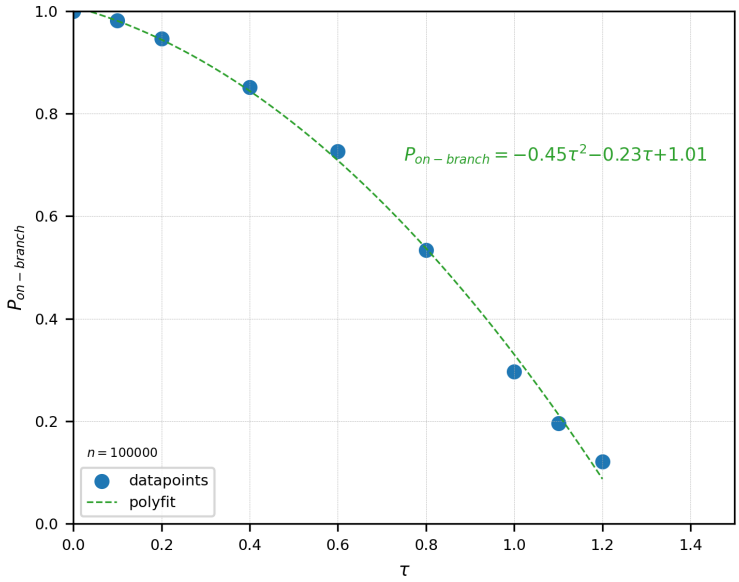

Figure 8.6: Polyfit of the fraction of leading partons which are on-branch, for a shower with a given τ value. The dataset used is the same as for Figure 8.5; simulated with $n = 10^5$ showers, using $\epsilon = 10^{-3}$ and $z_{\min} = 10^{-3}$.

and we are only interested in retaining the leading particle with $z > 1/2$,

$$\mathbb{R} = \int_0^{1/2} dz\, P(z) u(zp) \mathcal{Z}((1-z)p) + \int_{1/2}^{1} dz\, P(z) \mathcal{Z}(zp) u((1-z)p). \tag{8.8}$$

Since we are still working with gluons we can use $P_{gg}(z) = P_{gg}(1-z)$, and use a change of variable $z' = 1-$, to write

$$\begin{aligned} \mathbb{R} &= \int_0^{1/2} dz\, P(z) u(zp) \mathcal{Z}((1-z)p) - \int_{1/2}^{0} dz\, P(z') \mathcal{Z}((1-z')p) u(z'p) \\ &= 2 \int_0^{1/2} dz\, P(z) u(zp) \mathcal{Z}((1-z)p) \end{aligned} \tag{8.9}$$

then taking the functional derivative,

$$\begin{aligned} \frac{\delta \mathbb{R}}{\delta u(k)}|_{u=1} &= 2 \int_0^{1/2} dz\, P(z) \left[\frac{\delta u(zp)}{\delta u(k)}|_{u=1} \mathcal{Z}((1-z)p)|_{u=1} + u(zp)|_{u=1} \frac{\delta \mathcal{Z}((1-z)p)}{\delta u(k)}|_{u=1} \right] \\ &= 2 \int_0^{1/2} dz\, P(z) \left[\delta(1 - \frac{x}{z}) + D(\frac{x}{1-z}, t) \right]. \end{aligned} \tag{8.10}$$

Being careful with the limits in the second term as we are requiring that $x < 1 - z \to z < 1 - x$ in the distribution, as well as $z < 1/2$ from the integral. Bringing both of these explicitly into the integral, and again introducing $\tilde{P}(z) = 2P(z)$ we can write

$$\frac{\delta \mathbb{R}}{\delta u(k)}|_{u=1} = \int_0^{1/2} dz\, \tilde{P}(z) \delta(1 - \frac{x}{z}) + \int_0^{\min(\frac{1}{2}, 1-x)} dz\, \tilde{P}(z) D(\frac{x}{1-z}, t). \tag{8.11}$$

In the first term there is a criteria from the delta function that $x = z$, that means the real term

can be rewritten using a step function $\Theta(x < \frac{1}{2})$,

$$\frac{\delta \mathbb{R}}{\delta u(k)}|_{u=1} = \Theta(x < \frac{1}{2}) x\tilde{P}(x) + \int_0^{\min(\frac{1}{2}, 1-x)} dz\, \tilde{P}(z) D(\frac{x}{1-z}, t) \tag{8.12}$$

and a similar treatment can be given for the virtual term,

$$\begin{aligned} \frac{\delta \mathbb{V}}{\delta u(k)}|_{u=1} &= -\int_0^{1/2} dz\, \tilde{P}(z) \frac{\delta \mathcal{Z}(p)}{\delta u(k)}|_{u=1} \\ &= -\int_0^{1/2} dz\, \tilde{P}(z) D(x,t). \end{aligned} \tag{8.13}$$

Using Eqn. (8.12) and Eqn. (8.13), we can write Eqn. (8.6) as

$$\frac{\partial}{\partial t} D(x,t) = \Theta(x < \frac{1}{2}) x\tilde{P}(x) + \int_0^{\min(\frac{1}{2}, 1-x)} dz\, \tilde{P}(z) D(\frac{x}{1-z}, t) - \int_0^{1/2} dz\, \tilde{P}(z) D(x,t). \tag{8.14}$$

Eqn. (8.14) is therefore now a proposed evolution equation for the leading parton of pure gluon cascades in medium, where the leading parton is assumed to be on-branch.

Writing the equation in Mellin space

We will now attempt to solve Eqn. (8.14). Starting by making a change of variables $z' = 1 - z$ in the gain term

$$\begin{aligned} \frac{\partial}{\partial t} D(x,t) = \Theta(x < \frac{1}{2}) x\tilde{P}(x) \\ + \int_{\min(\frac{1}{2}, x)}^1 dz'\, \tilde{P}(z') D(\frac{x}{z'}, t) - \int_{1/2}^1 dz'\, \tilde{P}(z') D(x,t). \end{aligned} \tag{8.15}$$

and the z's can for simplicity be written as z. Performing the Mellin transform defined in Eqn. (4.24)

$$\begin{aligned} \frac{\partial}{\partial t} \tilde{D}(\nu,t) = \int_0^1 dx\, x^{\nu-1} \Theta(x < \frac{1}{2}) x\tilde{P}(x) \\ + \int_0^1 dx\, x^{\nu-1} \int_{\min(\frac{1}{2}, x)}^1 dz\, \tilde{P}(z) D(\frac{x}{z}, t) - \int_{1/2}^1 dz\, \tilde{P}(z) \tilde{D}(\nu,t) \end{aligned} \tag{8.16}$$

and splitting up the integrals in the gain term for values of $x < 1/2$ and $x > 1/2$,

$$\begin{aligned} \frac{\partial}{\partial t} \tilde{D}(\nu,t) = \int_0^{1/2} dx\, x^{\nu-1} x\tilde{P}(x) \\ + \int_0^{1/2} dx\, x^{\nu-1} \int_{1/2}^1 dz\, \tilde{P}(z) D(\frac{x}{z}, t) - \int_{1/2}^1 dz\, \tilde{P}(z) \tilde{D}(\nu,t) \\ + \int_{1/2}^1 dx\, x^{\nu-1} \int_x^1 dz\, \tilde{P}(z) D(\frac{x}{z}, t). \end{aligned} \tag{8.17}$$

Changing the integration limits in the third line such that $\int_{1/2}^{1} dx \int_{x}^{1} dz \Rightarrow \int_{1/2}^{1} dz \int_{1/2}^{z} dx$

$$\begin{aligned}\frac{\partial}{\partial t}\tilde{D}(\nu,t) = &\int_0^{1/2} dx\, x^{\nu-1} x\tilde{P}(x) \\ &+ \int_0^{1/2} dx\, x^{\nu-1} \int_{1/2}^{1} dz\, \tilde{P}(z) D(\frac{x}{z},t) - \int_{1/2}^{1} dz\, \tilde{P}(z)\tilde{D}(\nu,t) \\ &+ \int_{1/2}^{1} dz\, \tilde{P}(z) \int_{1/2}^{z} dx\, x^{\nu-1} D(\frac{x}{z},t)\end{aligned} \tag{8.18}$$

and then performing a change of variable in the gain terms such that $\xi = x/z \quad \Rightarrow \quad dx = z d\xi$

$$\begin{aligned}\frac{\partial}{\partial t}\tilde{D}(\nu,t) = &\int_0^{1/2} dx\, x^{\nu-1} x\tilde{P}(x) \\ &+ \int_{1/2}^{1} dz\, \tilde{P}(z) \int_0^{1/2z} (z d\xi)\, (z\xi)^{\nu-1} D(\xi,t) - \int_{1/2}^{1} dz\, \tilde{P}(z)\tilde{D}(\nu,t) \\ &+ \int_{1/2}^{1} dz\, \tilde{P}(z) \int_{1/2z}^{1} (z d\xi)\, (z\xi)^{\nu-1} D(\xi,t).\end{aligned} \tag{8.19}$$

It is then possible to merge the integration limits with respect to $d\xi$ again and perform the Mellin transform on $D(\xi,t)$

$$\begin{aligned}\frac{\partial}{\partial t}\tilde{D}(\nu,t) = &\int_0^{1/2} dx\, x^{\nu-1} x\tilde{P}(x) \\ &+ \int_{1/2}^{1} dz\, \tilde{P}(z) z^{\nu} \tilde{D}(\nu,t) - \int_{1/2}^{1} dz\, \tilde{P}(z)\tilde{D}(\nu,t)\end{aligned} \tag{8.20}$$

which can be written as a non-homogeneous differential equation

$$\frac{\partial}{\partial t}\tilde{D}(\nu,t) = 2\int_0^{1/2} dx\, \frac{x^{\nu-1}}{(1-x)} + 2\int_{1/2}^{1} dz\, \left(\frac{z^{\nu}-1}{z(1-z)}\right) \tilde{D}(\nu,t). \tag{8.21}$$

For simplicity we can introducing the incomplete beta function $\mathrm{B}_{\frac{1}{2}}(\nu,0)$

$$\frac{\partial}{\partial t}\tilde{D}(\nu,t) = 2\,\mathrm{B}_{\frac{1}{2}}(\nu,0) + 2\int_{1/2}^{1} dz\, \left(\frac{z^{\nu}-1}{z(1-z)}\right) \tilde{D}(\nu,t). \tag{8.22}$$

Solving the equation in Mellin space

We will now solve Eqn. (8.22), with the initial condition $\tilde{D}(\nu,0) = 1$. Writing the equation in a general form

$$s'(\nu,t) - p(\nu)s(\nu,t) = f(\nu) \tag{8.23}$$

where

$$\begin{aligned} s(\nu,t) &= \tilde{D}(\nu,t) \\ s'(\nu,t) &= \frac{\partial}{\partial t}\,\tilde{D}(\nu,t) \\ p(\nu) &= 2\int_{1/2}^{1} dz\,\left(\frac{z^{\nu}-1}{z(1-z)}\right) \\ f(\nu) &= 2\,\mathrm{B}_{\frac{1}{2}}(\nu,0), \end{aligned} \tag{8.24}$$

then the solution of the corresponding homogeneous system $h'(\nu,t) - p(\nu)h(\nu,t) = 0$, with with the initial condition $h(\nu,0) = 1$,

$$h(\nu,t) = -\frac{f(\nu)}{p(\nu)}\,\exp\left(p(\nu)\,t\right). \tag{8.25}$$

By variation of parameters we are looking for a solution $s(\nu,t)$ of the non-homogeneous system

$$s(\nu,t) = v(t)\,h(\nu,t), \tag{8.26}$$

which is obtained by finding a function $v(t)$ such that $v'(t)h(\nu,t) = f(\nu)$.

$$v(t) = \int \frac{f(\nu)}{h(\nu,t)}dt = \exp\left(-p(\nu)\,t\right) + C \tag{8.27}$$

and the solution $s(\nu,t)$ is therefore

$$s(\nu,t) = v(t)\,h(\nu,t) = -C\,\frac{f(\nu)}{p(\nu)}\,\exp(p(\nu)t) - \frac{f(\nu)}{p(\nu)}. \tag{8.28}$$

determining C from the initial condition we get the final solution

$$s(\nu,t) = \frac{f(\nu)+p(\nu)}{p(\nu)}\,\exp(p(\nu)t) - \frac{f(\nu)}{p(\nu)}, \tag{8.29}$$

which can be verified by inserting Eqn. (8.29) into Eqn. (8.23). Inserting the full functions defined in Eqn. (8.24) we obtain,

$$\begin{aligned} \tilde{D}(\nu,t) = &\frac{\mathrm{B}_{\frac{1}{2}}(\nu,0) + \int_{1/2}^{1} dz\,\left(\frac{z^{\nu}-1}{z(1-z)}\right)}{\int_{1/2}^{1} dz\,\left(\frac{z^{\nu}-1}{z(1-z)}\right)}\,\exp\left(2\int_{1/2}^{1} dz\,\left(\frac{z^{\nu}-1}{z(1-z)}\right)\,t\right) \\ &- \frac{\mathrm{B}_{\frac{1}{2}}(\nu,0)}{\int_{1/2}^{1} dz\,\left(\frac{z^{\nu}-1}{z(1-z)}\right)} \end{aligned} \tag{8.30}$$

Discussing the solution in Mellin space

Performing the inverse Mellin transform on the solution obtained in Eqn. (8.30) is not straightforward. To gain a clearer picture of why, we can plot the solution of the leading parton distribution, against the solution of the DGLAP equation Eqn. (4.29), in Mellin space. Note that this is not the final solution of the DGLAP equation, but the one obtained in Mellin space, before transforming back to momentum space. The resulting plot is given in Figure 8.7

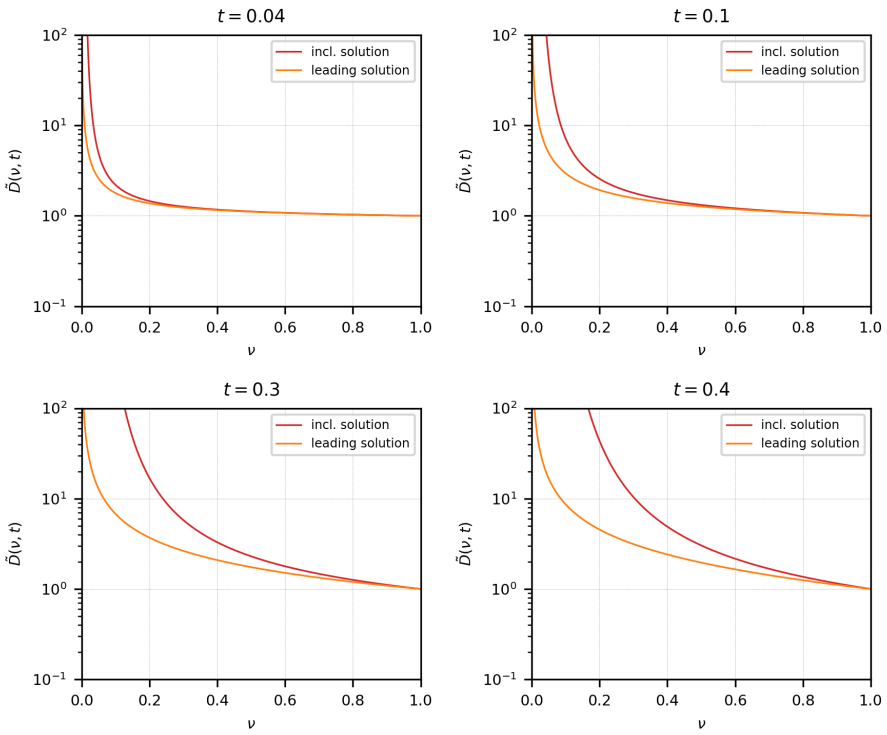

Figure 8.7: The solution of the leading parton evolution equations, for gluons in vacuum, in Mellin space as given by Eqn. (8.30) (orange), and the solution of the DGLAP equation as obtained in Mellin space as given by Eqn. (4.29) (red). The behavior at small ν values is compared in the plot. For $\nu > 1$ they behave in the same manner.

When examining the plot it is worth noting that the general form is remarkably similar for values $\nu < 1$, and if the limits of the plot were expanded we would see that the behavior at $\nu > 1$ is identical. This is roughly what we would expect, as our proposed leading parton evolution equations are very similar in form to the DGLAP equation, with some modifications to the z limits.

It should then be made explicit that the solution presented in Eqn. (8.30) is a function of ν in Mellin space, and it needs to be transformed to momentum space to have proper interpretation. This may be possible by employing the Mellin transforms relation to other transformations such as the Laplace or Fourier transforms. Otherwise, an altogether different set of transformations and change of variables may be able to find a solution in momentum space.

Summary and Outlook

Motivation

The motivation of the thesis was to investigate how the distribution of leading partons behave inside of a QCD jet, and whether it can be described and solved analytically. Since the most energetic parton in a shower is (presumably) less sensitive to medium fluctuations, it could serve as a cleaner probe of the QGP, and therefore improve studies of jet quenching and QGP. To thoroughly acquaint ourselves with the required analytical and numerical methods of parton showers, we had to start by examining the inclusive parton distribution which is well studied. The presented methods could then be verified by comparing the numerical results and the analytical solutions with one another.

Discussion and results

In Chapter II we showed how the inclusive distribution in vacuum is described by the DGLAP evolution equations. Our treatment focused on the leading order behavior. A suitable evolution variable was introduced to simplify the evolution equations and impose angular ordering in our showers. Writing them as integral equations allowed us to interpret the Sudakov form factor as a branching probability in a given interval. Solving the DGLAP equations was possible by considering gluon showers in the small x limit. This was done by performing a Mellin-transformation and then using the saddle-point approximation to find a solution that can be transformed back into momentum space.

When discussing jet evolutions in medium, we chose to start at the BDMPS-Z spectrum which describes the induced soft gluon radiation of jets. When incorporating these soft emissions into the evolution equations we obtain the in-medium kinetic rate equations, which is the medium counterpart to the DGLAP equations. Focusing on gluons, and using the reduced splitting kernel, the evolution equation was solved in Laplace space. The solution obtained required no further assumptions or constraints and is therefore a valid solution for how a medium cascades consisting exclusively of gluons evolve with the reduced kernel.

Implementing the vacuum and medium evolution equations into Monte-Carlo programs was done in Chapter III. The general procedure was the same for both evolutions. By generating expected branching intervals from the Sudakov form-factor, the evolution boundaries can be implemented, and when a parton is selected for branching we can sample a random splitting value by using the Metropolis-Hastings algorithm.

Plotting the results of the Monte-Carlo programs alongside the analytical results allowed us to discuss the properties of the cascades, and highlight differences and discrepancies. For gluon cascades in vacuum, Figure 6.5 showed how the solution of the DGLAP equation is in good agreement with the Monte-Carlo in the small x and large t limit, as expected. The behavior of vacuum cascades with both quarks and gluons was presented in Figure 6.6 for showers where the initial parton was either a quark or a gluon. This was also the first indication of how the leading parton distribution behaves, clearly showing in Figure 6.6 that the leading and inclusive distributions are identical for values of $x > 0,5$.

The Monte-Carlo generated distribution for gluon cascades in vacuum was plotted alongside

the analytical solution of the in-medium kinetic rate equation in Figure 7.2. The two graphs were in good agreement for all values of τ and x. In Figure 7.3 the Monte-Carlo was run to high values of τ to display the scaling property of the BDMPS-Z spectrum.

Finally, having built a deeper understanding of parton showers, both analytically and numerically, we moved on to the leading parton distribution in Chapter IV. Using a known model for the energy-loss of the leading parton we calculated a solution valid in the small x limit. The resulting plot in Figure 8.2 confirmed that it is a good fit for values $x > 0,8$. In order to suggest a better model for the energy-loss, which should be valid for harder gluon emissions, we must know the validity range of the model. We attempted to address this issue by proposing the concept of on and off-branch leading partons, and then investigating how often the leading parton remains on-branch. The results showed that up to values of $\tau \sim 0.5$, the majority ($\sim 80\%$) of the leading partons are on-branch.

The method of generating functionals was used to formulate the evolution equations for the leading parton distribution in vacuum, valid for on-branch leading partons. The key difference from the inclusive distribution is that we must assume that the emitted parton has a momentum $z < 1/2$, such that the parton we are following is always the hardest. When only branching from the leading parton we are also keeping it on-branch, which is where the on-branch discussion becomes relevant. The evolution equations were then written in Mellin space and solved. Unfortunately returning to momentum space is challenging, and further development has not been made.

Outlook

The list of points which could be improved for our Monte-Carlo programs is long. Examples include using the full splitting functions in medium, and including both quarks and gluons in medium. But improving the Monte-Carlo is altogether not all that interesting as it has already been done for event-generators such as PYTHIA. The reason for us to develop them from the ground up was to illustrate how the solution to the evolution equations, while difficult to solve analytically, practically appears out of nowhere when applying a Monte-Carlo approach. Another approach which might be able to validate the leading parton evolution equations, is to implement them into a leading parton Monte-Carlo shower, and compare the results with the leading parton distribution of the other shower programs.

There are several results for the leading parton distribution we would have liked to obtain in Chapter IV. The most obvious one is that the solution obtained in Mellin space for the leading parton evolution equation is difficult to transform back to momentum space. The consequence is that the evolution equation can not be compared directly with the results of our Monte-Carlo parton showers.

Another issue, which is a bit more subtle, is that we would ideally have wanted an evolution equation for the leading parton in medium, as this allows us to compare with the current energy-loss distribution. This challenge is closely related to a general search for a more precise formulation of the energy-loss of a parton traversing a medium. Such an expression would pave the way for improved calculations of the nuclear modification form factor. Further work could also extend the formalism to include heavy quarks.

Acknowledgements

First and foremost, I would like to express my deepest gratitude to my supervisor Konrad Tywoniuk, Researcher at the University of Bergen, for excellent guidance throughout these last two semesters. I was always welcome to ask for help, and Konrad would never hesitate to go through long and tedious derivations in order to explain a particular concept. Without Konrad's guidance, this thesis would not have been possible, and I am grateful for all that I have learned from him during this process.

I would also like to express my gratitude to the heavy-ion group for interesting seminars and journal clubs over the last two years. Thanks should also go to Adam Takacs, Ph.D. Candidate, for teaching me about the Sudakov form factor.

I would like to extend sincere thanks to my fellow master's students for partaking in this journey. In particular, Mathias and Sigurd for fruitful discussions, sharing a reading room, and consistently allowing me to prod their shoulders whenever I have had questions.

Finally, I would like to give a special thank you to Silje, for always reminding me of the world outside of theoretical physics.

Appendix A Constructing the DGLAP Equation

The DGLAP equation can be constructed using generating functionals. This is done in [18] for gluons in medium, a simpler approach with gluons in vacuum is presented here. For vacuum cascades where an initial gluon at time t_0 with momentum p, a generating functional can be defined as

$$\mathcal{Z}(p, t = 0) = u(p). \tag{A.1}$$

where $u \equiv u(p)$ indicates a 100% probability of finding a single gluon with momentum p at the given time. Similarly $u(k)$ gives a gluon with momentum $k = xp$. From normalization we have $\mathcal{Z}(p)|_{u=1} = 1$. Defining the relation of the functions $u(p)$ and $u(k)$ as

$$\frac{\delta u(p)}{\delta u(k)} = \delta\left(1 - \frac{k}{p}\right). \tag{A.2}$$

Since we are considering vacuum cascades, the only effect that can happen in an interval dt is a splitting. The generating functional then changes as,

$$\frac{\partial}{\partial t}\mathcal{Z}(p, t) = \int_0^1 dz\, P(z)\mathcal{Z}(zp)\mathcal{Z}((1-z)p) - \int_0^1 dz\, P(z)\mathcal{Z}(p) \tag{A.3}$$

where the first term on the right represents a splitting, and the second term is a correction corresponding to a virtual loop, where no splittings occur. The inclusive energy distribution is then found from the generating functional as $D(x, t) = x\frac{dN}{dx} = \frac{\delta\mathcal{Z}[p]}{\delta u(p)}|_{u=1}$, which implies

$$\frac{\delta\mathcal{Z}\,(p)}{\delta u\,(k)}|_{u=1} = D\left(\frac{k}{p}, t\right) = D(x, t) \tag{A.4}$$

$$\frac{\delta\mathcal{Z}\,(zp)}{\delta u(k)}|_{u=1} = D\left(\frac{k}{zp}, t\right) = D\left(\frac{x}{z}, t\right) \tag{A.5}$$

therefore Eqn. (A.3) becomes,

$$\begin{aligned}
\frac{\partial}{\partial t}\frac{\delta\mathcal{Z}(p)}{\delta u(k)}|_{u=1} &= \int_0^1 dz\, P(z)\left[\frac{\delta\mathcal{Z}(zp)}{\delta u(k)}|_{u=1}\mathcal{Z}\left((1-z)p\right)|_{u=1} + \mathcal{Z}(zp)|_{u=1}\frac{\delta\mathcal{Z}\left((1-z)p\right)}{\delta u(k)}|_{u=1}\right] \\
&\quad - \int_0^1 dz\, P(z)\frac{\delta\mathcal{Z}(p)}{\delta u(k)}|_{u=1} \\
\frac{\partial}{\partial t}D(x, t) &= \int_0^1 dz\, P(z)\left[D\left(\frac{x}{z}, t\right)H(z > x) + D\left(\frac{x}{1-z}, t\right)H(1 - z > x)\right] \\
&\quad - \int_0^1 dz\, P(z)D(x, t)
\end{aligned}$$

working with gluons only we can use $P_{gg}(z) = P_{gg}(1-z)$, $\int_0^1 dz\, P_{gg}(z) = \frac{1}{2}\int_0^1 dz\, zP_{gg}(z)$, and $\tilde{P}(z) = 2P(z)$, to write this as

$$\frac{\partial}{\partial t}D(x, t) = \int_x^1 dz\, \tilde{P}(z)\left(\frac{x}{z}, t\right) - \int_0^1 dz\, z\tilde{P}(z)D(x, t) \tag{A.6}$$

which is the DGLAP equation for gluon-only cascades.

Appendix B Sampling the Full Medium Splitting Functions

This appendix will give the procedures for sampling random values from the full medium splitting functions by use of Metropolis-Hastings algorithm. The splitting functions for the three vertices are given to leading logarithmic accuracy by [20]

$$\mathcal{K}_{gg}(z) = \frac{1}{2} 2C_A \, \frac{[1-z(1-z)]^2}{z(1-z)} \sqrt{\frac{(1-z)C_A + z^2 C_A}{z(1-z)}} \tag{B.1}$$

$$\mathcal{K}_{qg}(z) = \frac{1}{2} 2N_f \, T_F \, \left(z^2 + (1-z)^2\right) \sqrt{\frac{C_F - z(1-z)C_A}{z(1-z)}} \tag{B.2}$$

$$\mathcal{K}_{qq}(z) = \frac{1}{2} C_F \, \frac{1+z^2}{(1-z)} \sqrt{\frac{zC_A + (1-z)^2 C_F}{z(1-z)}}. \tag{B.3}$$

The color factors on the outside of the square roots will be disregarded in the calculations, as these will cancel out, but we will keep the color factors inside the square roots (which we usually absorb into $\hat{q}$, as they have some impacts on the shape of the distributions. We could set $C_A = C_F = 1$, and the algorithms presented here would still sample correctly, but the shape would be slightly different.

The gg vertex

The full ggg splitting kernel is given by Eqn. (B.1). To generate a random value from this function, we need to go back to the Metropolis-Hastings algorithm. For this we need a proportional dummy-function, we can use the simplified kernel given by Eqn. (5.7), the integral can be generally shown to be,

$$\int \mathcal{K}_{gg}^{\text{dummy}}(z)\, dz = \int \frac{2}{(z(1-z))^{3/2}}\, dz = 2\, \frac{4z-2}{\sqrt{-z(z-1)}}. \tag{B.4}$$

Sampling random momentum fractions for the distribution is again done by solving Eqn. (6.7)

$$\begin{aligned}
\mathcal{R} \int_\epsilon^{1-\epsilon} \mathcal{K}_{gg}^{\text{dummy}}(z)\, dz &= \int_\epsilon^{y} \mathcal{K}_{gg}^{\text{dummy}}(z)\, dz \\
\mathcal{R} \int_\epsilon^{1-\epsilon} \mathcal{K}_{gg}^{\text{dummy}}(z)\, dz &= 2\, \frac{4y-2}{\sqrt{-y(y-1)}} - 2\, \frac{4\epsilon-2}{\sqrt{-\epsilon(\epsilon-1)}} \\
\frac{\mathcal{R}}{2} \int_\epsilon^{1-\epsilon} \mathcal{K}_{gg}^{\text{dummy}}(z)\, dz + \frac{4\epsilon-2}{\sqrt{\epsilon(1-\epsilon)}} &= \frac{4y-2}{\sqrt{y(1-y)}} \\
\frac{1}{2} \int_\epsilon^{1-\epsilon} \mathcal{K}_{gg}^{\text{dummy}}(z)\, dz \left(\mathcal{R} - \frac{1}{2}\right) &= \frac{4y-2}{\sqrt{y(1-y)}}.
\end{aligned} \tag{B.5}$$

Reinserting the initial factors of the integral, by setting $a = \frac{1}{2}\int_{\epsilon}^{1-\epsilon} \mathcal{K}_{gg}^{\text{dummy}}(z)\,dz\,\left(\mathcal{R} - \frac{1}{2}\right)$, this equation can be solved using Mathematica,

$$\begin{aligned} y &= \frac{16 + a^2 \mp a\sqrt{16 + a^2}}{2(16 + a^2)} \\ y &= \frac{1}{2} \mp \frac{a\sqrt{16 + a^2}}{2(16 + a^2)} \\ y &= \frac{1}{2} \mp \frac{a}{2\sqrt{16 + a^2}}. \end{aligned} \tag{B.6}$$

We now have a method for randomly drawing a sample from the dummy splitting function, and can follow the procedure of Section 6.3 to implement Eqn. (B.6) into a MH algorithm to draw samples from the full splitting function. The plots of the original histogram, and MH corrected histogram is given in Figure B.1.

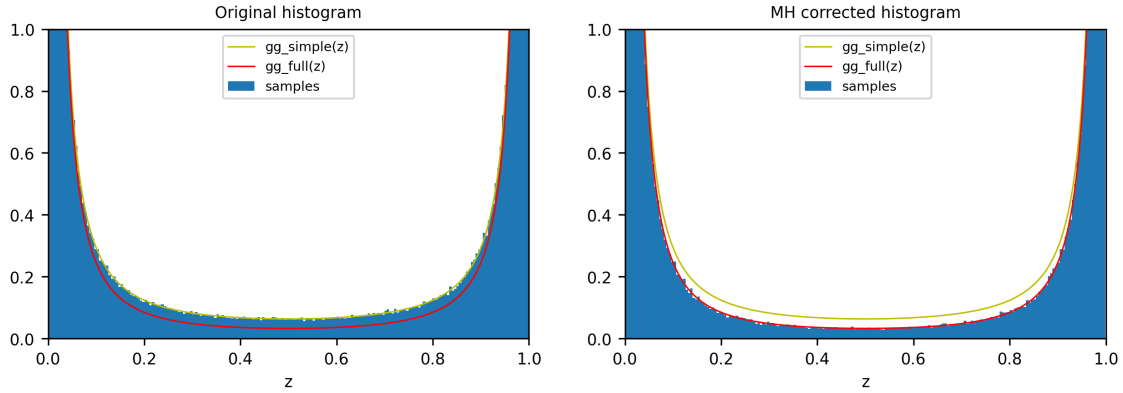

Figure B.1: Probability density of the medium $\mathcal{K}_{gg}$ splitting function, compared to the histogram of the dummy splitting function, and the Metropolis-Hastings corrected results. Simulated with $1,000,000$ points, and an acceptance rate of 0.82.

The qg vertex

Continuing now with the qg splitting function, Eqn. (B.2). With some inspiration from the previous section, we can propose the following dummy function

$$\mathcal{K}_{qg}^{\text{dummy}}(z) = \frac{1}{\sqrt{z(1-z)}} \tag{B.7}$$

whose integral can be shown to be,

$$\int \mathcal{K}_{qg}^{\text{dummy}}(z)\,dz = \int \frac{1}{\sqrt{z(1-z)}}\,dz = -2\sin^{-1}(\sqrt{1-z}). \tag{B.8}$$

When evaluating Eqn. (6.7) we get

$$\mathcal{R}\int_{\epsilon}^{1-\epsilon}\mathcal{K}_{qg}^{\text{dummy}}(z)\,dz = \int_{\epsilon}^{y}\mathcal{K}_{qg}^{\text{dummy}}(z)\,dz$$
$$\mathcal{R}\int_{\epsilon}^{1-\epsilon}\mathcal{K}_{qg}^{\text{dummy}}(z)\,dz = -2\sin^{-1}(\sqrt{1-y}) + 2\sin^{-1}(\sqrt{1-\epsilon})$$
$$-\mathcal{R}\int_{\epsilon}^{1-\epsilon}\mathcal{K}_{qg}^{\text{dummy}}(z)\,dz + 2\sin^{-1}(\sqrt{1-\epsilon}) = 2\sin^{-1}(\sqrt{1-y}) \tag{B.9}$$

setting $a = -\mathcal{R}\int_{\epsilon}^{1-\epsilon}\mathcal{K}_{qg}^{\text{dummy}}(z)\,dz + 2\sin^{-1}(\sqrt{1-\epsilon})$, and finally solving for y

$$a = 2\sin^{-1}(\sqrt{1-y})$$
$$y = 1 - \left(\sin\left(\frac{a}{2}\right)\right)^2. \tag{B.10}$$

Using Eqn. (B.10) to sample values for the dummy function, we can run the MH algorithm as in previous sections and obtain Figure B.2.

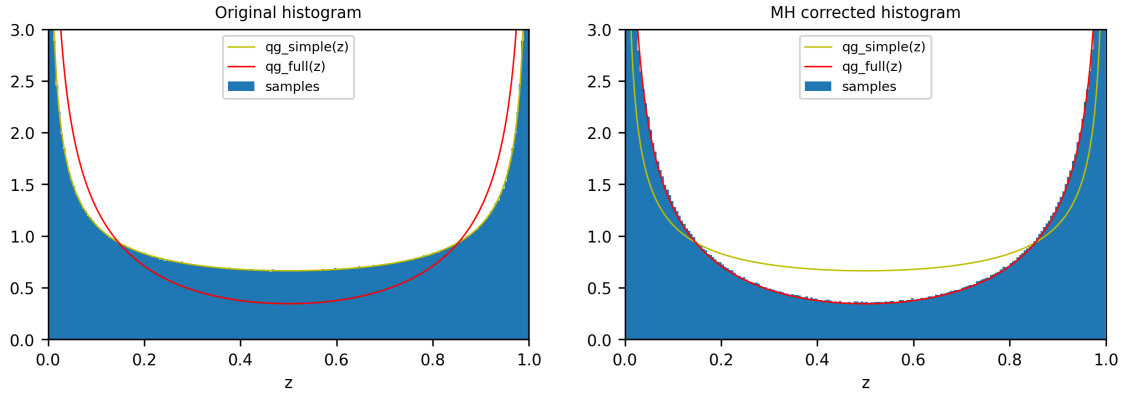

Figure B.2: Probability density of the medium $\mathcal{K}_{qg}$ splitting function, compared to the histogram of the dummy splitting function, and the Metropolis-Hastings corrected results. Simulated with $5,000,000$ points, and an acceptance rate of 0.71.

The qq vertex

Finally we have the gq vertex, of Eqn. (B.3). From this we might try a dummy function such as

$$\mathcal{K}_{qq}^{\text{dummy}}(z) = \frac{4}{z^{1/2}(1-z)^{3/2}} \tag{B.11}$$

whose integral is

$$\int \mathcal{K}_{qq}^{\text{dummy}}(z)\,dz = \int \frac{4}{z^{1/2}(1-z)^{3/2}}\,dz = \frac{8\sqrt{z}}{\sqrt{1-z}}. \tag{B.12}$$

And we can solve Eqn. (6.7)

$$\begin{aligned}
\mathcal{R}\int_{\epsilon}^{1-\epsilon}\mathcal{K}_{qq}^{\text{dummy}}(z)\,dz &= \int_{\epsilon}^{y}\mathcal{K}_{qq}^{\text{dummy}}(z)\,dz \\
\mathcal{R}\int_{\epsilon}^{1-\epsilon}\mathcal{K}_{qq}^{\text{dummy}}(z)\,dz &= \frac{8\sqrt{y}}{\sqrt{1-y}} - \frac{8\sqrt{\epsilon}}{\sqrt{1-\epsilon}} \\
\frac{\mathcal{R}}{8}\int_{\epsilon}^{1-\epsilon}\mathcal{K}_{qq}^{\text{dummy}}(z)\,dz + \frac{\sqrt{\epsilon}}{\sqrt{1-\epsilon}} &= \frac{\sqrt{y}}{\sqrt{1-y}}
\end{aligned} \tag{B.13}$$

setting $a = \frac{\mathcal{R}}{8}\int_{\epsilon}^{1-\epsilon}\mathcal{K}_{qq}^{\text{dummy}}(z)\,dz + \frac{\sqrt{\epsilon}}{\sqrt{1-\epsilon}}$, we can again solve for y,

$$y = \frac{a^2}{1+a^2}. \tag{B.14}$$

Implementing Eqn. (B.14) into the MH algorithm, we will obtain the distribution given in Figure B.3.

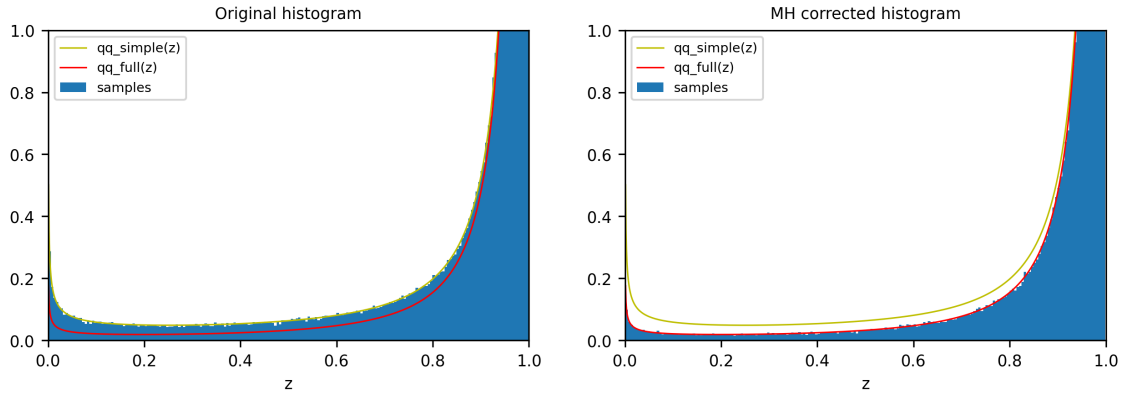

Figure B.3: Probability density of the medium $\mathcal{K}_{qq}$ splitting function, compared to the histogram of the dummy splitting function, and the Metropolis-Hastings corrected results. Simulated with $1,000,000$ points, and an acceptance rate of 0.82.

References

[1] H. Fritzsch. "The history of QCD". In: *CERN Courier* 52.8 (Oct. 2012), pp. 21–24.

[2] M. Schwartz. *Quantum Field Theory and the Standard Model*. Cambridge University Press, 2014.

[3] M. E. Peskin and D. V. Schroeder. *An Introduction to Quantum Field Theory*. Westview Press, 1995.

[4] F. Mandl and G. Shaw. *Quantum Field Theory*. A Wiley-Interscience publication. Wiley, 2010.

[5] P. Caucal. "Jet evolution in a dense QCD medium". Ph.D. thesis, Université Paris-Saclay. Oct. 2020. arXiv: 2010.02874 [hep-ph].

[6] W. Florkowski. *Phenomenology Of Ultra-relativistic Heavy-ion Collisions*. World Scientific Publishing Company, 2010.

[7] C. S. Fischer. "QCD at finite temperature and chemical potential from Dyson–Schwinger equations". In: *Prog. Part. Nucl. Phys.* 105 (2019), pp. 1–60. DOI: 10.1016/j.ppnp.2019.01.002. arXiv: 1810.12938 [hep-ph].

[8] Y. L. Dokshitzer et al. *Basics of perturbative QCD*. Editions Frontieres, 1991.

[9] R. Scharenberg et al. "Hot Dense Matter: Deconfinement and Clustering of Color Sources in Nuclear Collisions". In: *Universe* 4 (Sept. 2018), p. 96. DOI: 10.3390/universe4090096.

[10] J.-P. Blaizot et al. "Medium-induced gluon branching". In: *JHEP* 01 (2013), p. 143. DOI: 10.1007/JHEP01(2013)143. arXiv: 1209.4585 [hep-ph].

[11] J.-P. Blaizot and Y. Mehtar-Tani. "Jet Structure in Heavy Ion Collisions". In: *Int. J. Mod. Phys. E* 24.11 (2015), p. 1530012. DOI: 10.1142/S021830131530012X. arXiv: 1503.05958 [hep-ph].

[12] M. Dasgupta et al. "Small-radius jets to all orders in QCD". In: *JHEP* 04 (2015), p. 039. DOI: 10.1007/JHEP04(2015)039. arXiv: 1411.5182 [hep-ph].

[13] D. Neill, F. Ringer, and N. Sato. "Leading jets and energy loss". In: *JHEP* 07 (2021), p. 041. DOI: 10.1007/JHEP07(2021)041. arXiv: 2103.16573 [hep-ph].

[14] G. Altarelli and G. Parisi. "Asymptotic Freedom in Parton Language". In: *Nucl. Phys. B* 126 (1977), pp. 298–318. DOI: 10.1016/0550-3213(77)90384-4.

[15] R. K. Ellis, W. J. Stirling, and B. R. Webber. *QCD and collider physics*. Vol. 8. Cambridge University Press, Feb. 2011. DOI: 10.1017/CBO9780511628788.

[16] G. Altarelli et al. "Resummation". English (US). In: *1st Workshop on the Implications of HERA for LHC Physics*. HERA-LHC 2005. Apr. 2005, pp. 160–180.

[17] T. Gehrmann, T. Luebbert, and L. L. Yang. "Calculation of the transverse parton distribution functions at next-to-next-to-leading order". In: *JHEP* 06 (2014), p. 155. DOI: 10.1007/JHEP06(2014)155. arXiv: 1403.6451 [hep-ph].

[18] J.-P. Blaizot et al. "Probabilistic picture for medium-induced jet evolution". In: *JHEP* 06 (2014), p. 075. DOI: 10.1007/JHEP06(2014)075. arXiv: 1311.5823 [hep-ph].

[19] J.-P. Blaizot and Y. Mehtar-Tani. "Energy flow along the medium-induced parton cascade". In: *Annals Phys.* 368 (2016), pp. 148–176. DOI: 10.1016/j.aop.2016.01.002. arXiv: 1501.03443 [hep-ph].

[20] Y. Mehtar-Tani and S. Schlichting. "Universal quark to gluon ratio in medium-induced parton cascade". In: *JHEP* 09 (2018), p. 144. DOI: 10.1007/JHEP09(2018)144. arXiv: 1807.06181 [hep-ph].

[21] X.-N. Wang and X.-f. Guo. "Multiple parton scattering in nuclei: Parton energy loss". In: *Nucl. Phys. A* 696 (2001), pp. 788–832. DOI: 10.1016/S0375-9474(01)01130-7. arXiv: hep-ph/0102230.

[22] E. Blanco et al. "System of evolution equations for quark and gluon jet quenching with broadening". In: *Eur. Phys. J. C* 82.4 (2022), p. 355. DOI: 10.1140/epjc/s10052-022-10311-2. arXiv: 2109.05918 [hep-ph].

[23] C. Andrieu et al. "An Introduction to MCMC for Machine Learning". In: *Machine Learning* 50 (Jan. 2003), pp. 5–43. DOI: 10.1023/A:1020281327116.

[24] K. Skjelanger. *QCD Parton Fragmentation in Vacuum and Medium with Leading Jet Energy-Loss*. GitHub. 2022. URL: https://github.com/skjelanger/thesis.

[25] C. Bierlich et al. "A comprehensive guide to the physics and usage of PYTHIA 8.3". In: (Mar. 2022). arXiv: 2203.11601 [hep-ph].

[26] F. Arleo. "Tomography of cold and hot QCD matter: Tools and diagnosis". In: *JHEP* 11 (2002), p. 044. DOI: 10.1088/1126-6708/2002/11/044. arXiv: hep-ph/0210104.

[27] Y. Mehtar-Tani, J. G. Milhano, and K. Tywoniuk. "Jet physics in heavy-ion collisions". In: *Int. J. Mod. Phys. A* 28 (2013), p. 1340013. DOI: 10.1142/S0217751X13400137. arXiv: 1302.2579 [hep-ph].

[28] R. Baier et al. "Quenching of hadron spectra in media". In: *JHEP* 09 (2001), p. 033. DOI: 10.1088/1126-6708/2001/09/033. arXiv: hep-ph/0106347.